Metabolic Regulation of Longevity by Flavin-containing Monooxygenase 2

by

Christopher Ian Choi

A dissertation submitted in partial fulfillment
of the requirements for the degree of
Doctor of Philosophy
(Molecular and Integrative Physiology)
in the University of Michigan
2022

Doctoral Committee:

Professor Daniel A. Beard, Co-Chair
Assistant Professor Scott F. Leiser, Co-Chair
Associate Professor Bruce Palfey
Professor Scott D. Pletcher

Christopher Ian Choi

choihp@umich.edu

ORCID iD: 0000-0002-2063-695X

Acknowledgements

I would like to first thank my mentor, Dr. Scott Leiser, for everything he has done for my scientific training. Dr. Leiser constantly gave me encouragement and feedback on my writing, presentation, and work ethics, which helped me tremendously to improve in these areas. Whenever I sought out help, Dr. Leiser would provide it without hesitation. Whenever I had a research idea, he would allow me the freedom to pursue it. Most importantly, Dr. Leiser created a lab environment where everyone, including myself, felt comfortable and enjoyable working in. It would not be an exaggeration to say that none my achievements in graduate school would have been possible without Dr. Leiser's mentorship.

I would also like to thank my co-mentor, Dr. Dan Beard, for his support and words of encouragement over the years. During our regular meetings, Dr. Beard always checked to make sure that I was not feeling too stressed out and gave me pep talks when I needed them the most. He was also one of my biggest supporters when I decided to pursue medical education after finishing my graduate training. I feel bad about not picking up new hobbies like he suggested, so I will try to do so in medical school (but no promises). I would also like to thank the rest of my committee members, Drs. Bruce Palfey and Scott Pletcher, for their thoughtful suggestions and letters of

recommendation. The support and encouragement I received from my committee made me look forward to each committee meeting with delight.

Much of the work in this thesis was not possible without the help from the members of the Leiser Lab. I would like to first thank Dr. Ajay Bhat and Marshall Howington for all their technical help with my research as well as many hours of scientific discussions and non-scientific banters over the years. I thank Dr. Safa Beydoun for recruiting me on one of her projects that is now a chapter of my thesis and for her generous support in the lab. I also thank Dr. Hillary Warrington for her training and support through many aspects of graduate school. Even though she may disagree, I consider her to be my unofficial third mentor. I also thank the rest of the current and former members of the lab, including Dr. Shijiao Huang, Dr. Rebecca Cox, Meg Schaller, Elizabeth Dean, Angela Tuckowski, Brie Fretz, Dr. Joe Kruempel and Dr. Marjana Sarker for their helpful suggestions, support and for being an awesome group of people who treat each other like family.

I would like to also thank the members of the Department of Molecular and Integrative Physiology. First, I would like to thank Drs. Sue Moenter, Dan Michele, and Sue Brooks for their support as the Program Chair. I would also like to thank Michele Boggs and Jane Coffey for their administrative support. I also thank my cohort members for their solidarity and support, and for attending most, if not all, of my talks at the university even though they have heard it many times before.

Last and most importantly, I would like to thank my parents for all the sacrifice and effort that they made raising me in a foreign country and for their continued love and support over the years. If I were to acknowledge them here fully, this section would be as long as my entire thesis, so I will wrap up by simply stating that this journey would have been impossible without them. Thank you.

Table of Contents

List of Figures

List of Tables

Abstract

Aging is the greatest risk factor for multiple leading causes of death, such as heart diseases, multiple types of cancer, and Alzheimer's disease. Aging is thus a growing economic and health concern worldwide as the number of people over the age of 65 continues to increase. Multiple genetic and environmental pathways that slow aging have been discovered using animal models. However, the mechanisms by which these pathways extend lifespan remain largely unclear. Metabolism is a major regulator of longevity whose perturbation can slow aging and promote healthspan and longevity. Previous studies implicate metabolism in multiple longevity pathways, such as insulin signaling, nutrient sensing, and dietary restriction, across multiple organisms, including *C. elegans*. These findings make understanding the mechanisms of metabolic regulation of longevity a crucial next step.

A major challenge to studying metabolism in *C. elegans* is its reliance on a live bacterial food source. Bacteria have their own metabolic activity that confounds the metabolic changes in *C. elegans*. While methods of killing bacteria to stop their metabolic activity exist, they make the bacteria inedible, present additional confounding variables or are not practical to use. Using paraformaldehyde (PFA), a crosslinking chemical, we developed a viable method of killing bacteria and stopping their metabolic activity that 1) is edible for the worms, 2) can be used in a high-throughput manner, and 3) does not

substantially affect longevity phenotypes. Thus, PFA treatment is a viable way of preventing bacterial metabolism to study *C. elegans* metabolism.

The PFA treatment allowed us to determine the metabolic changes that occur following the expression of *fmo-2*, a member of the highly conserved enzyme family flavin-containing monooxygenase and a major longevity regulator downstream of multiple pathways, including dietary restriction. Using metabolomics and RNAi knockdown, we determine that *fmo-2* interacts with one carbon metabolism (OCM) to influence longevity and stress resistance. OCM is a metabolic network that has been implicated in multiple longevity pathways and is a crucial intermediate network for processes necessary for survival, including nucleotide synthesis, the transsulfuration pathway, and methylation. Using computational modeling, we identify the flux through methylation processes to be reduced in *fmo-2* overexpression animals, suggesting that *fmo-2* and reduced methylation flux are in the same functional pathway. Our data also identify tryptophan as an endogenous substrate of FMO-2 and implicate the kynurenine pathway as a target of FMO-2 that is likely linked to changes OCM.

A potential downstream consequence of the changes in OCM following *fmo-2* expression is the induction of endoplasmic reticulum unfolded protein response (UPR^{ER}), which is involved in proteostasis and longevity regulation. A reduction in methylation flux can lead to the reduction of phosphatidylcholine (PC) synthesis, which in turn can activate the UPR^{ER}. Our data thus far are consistent with a model where

FMO-2 reduces PC synthesis to activate the UPR^{ER}, thereby promoting longevity and health.

My thesis work furthers our understanding of a highly conserved enzyme family whose member serves as a critical convergence point for multiple longevity pathways. In addition, it also furthers our understanding of the metabolic regulation of the aging process and identifies key regulators that can potentially serve as therapeutic targets to slow aging to promote health and longevity.

Chapter I

Introduction

Significance of Aging Research

Aging poses serious health and economic challenges as the global life expectancy continues to increase. It is estimated that the US population over the age of 65 will double by 2050 to nearly 100 million[1]. Currently, age-related diseases, such as cancer, Alzheimer's disease, and cardiovascular disease, are the leading causes of death worldwide (information taken from World Health Organization's 2020 top 10 causes of death fact sheet). As the general population gets older, the healthcare cost of treating elderly patients will continue to rise. One way to address this issue is to figure out a cure for each of these diseases individually. However, this method is inefficient as curing one of these diseases will not prevent the onset or progression of other age-related diseases, thus diminishing the health and lifespan benefits of the cure. Considering that aging is a common risk factor, it is more efficient to target the aging process itself to simultaneously slow down the onset and progression of these diseases. It is important that the research be focused on extending not only the lifespan of the population, but also its healthspan, or the period of life where an individual is not suffering from age-related diseases or disorders, to ensure that people can live free of age-related

diseases for a greater period of time[2]. Therefore, the goal of aging research is to identify interventions that extend both lifespan and healthspan to promote healthy aging.

Studying the molecular mechanisms of aging is critical for figuring out how to slow down the aging process. Aging is a physiological process that affects nearly all organisms[3] and thus can be considered as an evolutionarily-conserved process. There have been many hypotheses as to why organisms age, but the more recent hypotheses share a similar idea: organisms age due to the accumulation of deleterious damage and/or molecules, including DNA mutations[4], free radicals[5], and damaged proteins[6], possibly as a consequence of the decline in the function of molecular machineries that are necessary to respond to these insults[6]. These hypotheses suggest that specific molecules and molecular machineries can be targeted and manipulated to slow down the aging process. Therefore, identifying and understanding the molecular mechanisms underlying the aging process will be important to manipulate these targets to slow down the onset of or prevent multiple chronic diseases at once, thus improving our long-term health.

C. elegans as a Model Organism for Aging Research

Considering that average human lifespan is several decades long and that there are ethical concerns surrounding human testing, model organisms are used to study the molecular mechanisms of the aging process. One of the major model organisms used in aging research, including this work, is the nematode *Caenorhabditis elegans*. As

described below, there are several aspects of *C. elegans* that make them useful models for aging research.

1) Development

C. elegans is a free-living nematode that feeds on microorganisms on rotting fruits and vegetables[7,8]. Adult animals are roughly 1 mm long, with transparent bodies and are hermaphrodites that self-fertilize two hours after reaching adulthood under optimal conditions at 20 ^{o}C[9–11]. A single worm typically lays around 250 eggs over a period of several days[9–11]. *C. elegans* undergo a developmental cycle of four larval stages (L1-L4) and go from eggs to reproductive adults within 2-3 days[9–11]. Under stressful conditions, such as starvation, *C. elegans* can enter dauer diapause, an alternative larval stage after the L1 stage[9–11]. Going into the dauer stage arrests the worms developmentally and allows them to survive until the environmental conditions improve[12]. Once the conditions do improve, worms can progress to the L4 larval stage to resume normal developmental cycle[12].

2) Genetics and aging phenotypes

C. elegans are well-characterized organisms whose genomes are highly conserved to humans. The complete *C. elegans* genome has been sequenced, and around 80% of their genes have known human homologs[13]. Similar to humans, *C. elegans* exhibit age-associated anatomical deterioration and functional decline. These phenotypes include frailty in movement, decline in reproductive capacity, neurodegeneration, loss of muscle integrity, and decline in proteostasis[14–20].

3) Manipulation

In addition, *C. elegans* are a convenient organism to use in experiments. As mentioned before, *C. elegans* have short lifespan and high fecundity, which allows relatively short survival experiments with high sample size as well as high-throughput screenings using drugs and RNAi gene knockdown approach. Knocking down genes using RNAi is more convenient in worms than other animals. Genes can be knocked down in worms by simply feeding them with bacteria expressing dsRNA of the gene of interest[21–23]. The RNAi libraries are well-established and cover around 90% of the genes in worms[24] and thus in most cases, RNAi can be used to study a gene of interest. Moreover, the transparent nature of *C. elegans* allows gene and protein expressions to be visualized using fluorescent markers, which makes it relatively easy to generate and use transgenic animals compared to other model organisms[25]. In sum, the ease of maintenance, their short lifespan, high fecundity, high degree of conservation and characterization, and ease of doing genetic manipulation make *C. elegans* an excellent model organism to be used for aging research.

4) Limitations

However, while *C. elegans* are useful, they have limitations compared to other models. One limitation is their lack of anatomical structures, such as major organs, including the brain and liver, and blood transport system[26]. On a molecular level, *C. elegans* lack DNA methylation, which is a crucial epigenetic marker in higher organisms[27]. Therefore, it is important to be cognizant of these limitations when

designing experiments and interpreting results that are desired to be translated to humans and other mammals.

Longevity Pathways in C. elegans

Longevity pathways are a series of molecular interactions that regulate the aging process, whereby a perturbation in one of the components of the pathway (e.g., genes, proteins, and metabolites) changes the rate of aging in organisms[28]. As previously mentioned, understanding the molecular mechanisms of the aging process is important for developing longevity interventions to promote healthy aging, and studying these pathways allows us to determine the key regulators of longevity. Given the evolutionarily-conserved nature of the aging process, many of these pathways are also conserved across taxa[29], highlighting the translational potential of aging research in model organisms.

As mentioned above, *C. elegans* is a powerful tool for studying the molecular mechanisms of aging. It is therefore not surprising that many discoveries have been made using this model organism to study the mechanisms of longevity pathways. Some of the major longevity pathways studied in *C. elegans* are discussed below:

1) Reduced Insulin/IGF-1 Signaling

   Suppressing insulin signaling extends *C. elegans* lifespan[30]. This finding has been translated to other organisms, including flies and mice[31–33], demonstrating

the conserved nature of longevity pathways and serving as a proof of principle for using *C. elegans* as a model for aging research.

DAF-2 (abnormal dauer formation protein-2) is an insulin receptor tyrosine kinase homolog that was initially discovered through a genetic screen for genes that regulate the dauer formation in *C. elegans*[34]. A loss-of-function mutant of the *daf-2* gene extends worm lifespan[30]. This lifespan extension requires the presence of DAF-16, a homolog of mammalian forkhead box O (FOXO) transcription factor[35,36]. The activation of DAF-2 leads to a PI3K (phosphoinositide 3 kinase) activity, which in turn leads to the phosphorylation of DAF-16 that prevents its nuclear translocation[36]. This kinase cascade involves AGE-1, an ortholog of the p110 catalytic subunit of mammalian PI3K[37], which is also the first longevity-regulation gene discovered in *C. elegans*[38]. *Age-1* acts downstream of DAF-2 and upstream of DAF-16[39–41]. The suppression of insulin signaling via mutations in either *daf-2* or *age-1* leads to the translocation of DAF-16 into the nucleus, which induces the expression of multiple genes that are involved longevity regulation and stress response[42]. As such, the phenotypes observed in *daf-2* and *age-1* mutants can be rescued by *daf-16* mutation[43–45]. In parallel to DAF-16, reduced insulin signaling can enhance *C. elegans* longevity through the NF-E2-related factor (NRF2) ortholog skinhead-1 (SKN-1), which is a key regulator of oxidative stress response[46]. SKN-1 is both necessary for the lifespan extension through the insulin signaling pathway and sufficient to increase worm lifespan by itself when it is genetically overexpressed[47].

2) Nutrient Sensing Pathways

Inhibiting mTOR (mechanistic target of rapamycin) activity is also beneficial to longevity and this effect was initially shown in *C. elegans* through RNAi knockdown of mTOR ortholog *let-363* and the mTORC1 component raptor ortholog *daf-15*[48,49]. Rapamycin, the drug inhibitor of mTOR, extends lifespan across taxa[50–53], establishing mTOR inhibition as a conserved longevity intervention. mTOR signaling is activated under high nutrient conditions and regulates multiple cellular process including growth, proliferation, protein synthesis, autophagy and transcription[54]. mTOR inhibition extends lifespan through multiple mechanisms. One of them is by increasing autophagy, thereby improving proteostasis, through the activation of FOXA transcription factor ortholog PHA-4[55]. Another mechanism is by reducing protein translation through the suppression of p70 ribosomal S6 kinase (S6K) activity[56]. Knocking down or knocking out *C. elegans* S6K homolog *rsks-1* is sufficient to extend lifespan[57,58]. AMP-activated protein kinase (AMPK) signaling pathway acts in an antagonistic manner to mTOR signaling. AMPK is activated during starvation conditions to inhibit mTOR activity[59]. Overexpression of *aak-2*, which encodes for AMPK ortholog in *C. elegans*, extends worm lifespan and requires DAF-16[59].

3) Dietary Restriction (DR)

In 1935, it was discovered that reducing animals' food intake without malnutrition extends their lifespan[60]. Since then, multiple studies report the beneficial role of

dietary restriction on health and longevity across taxa[61]. Dietary restriction further extends the lifespan of *daf-2* mutants, suggesting that DR and insulin signaling function independently[62]. In *C. elegans*, *eat-2* mutants, a genetic mimetic of DR that has defective pharyngeal pumping, also show lifespan extension under *daf-2* mutation[63]. PHA-4, which was mentioned previously as an important regulator of autophagy, is also an important regulator of DR-mediated longevity response[64]. PHA-4 is required the for the lifespan extension under DR, but not under the suppression of insulin signaling[65]. In addition, methionine restriction also shows longevity benefits through the mTOR pathway, suggesting that restricting specific nutrient sources can modulate the aging process[66]. This last finding suggests that a perturbation of a single nutrient source can cause a dramatic physiological change in a similar manner to a transcription factor.

More recently, our lab has identified flavin-containing monoxygenase-2 (*fmo-2*) as an important regulator of longevity in *C. elegans,* whose expression is induced by multiple life-extending interventions, including dietary restriction and hypoxia[67]. Knocking out *fmo-2* abrogates the lifespan and health benefits of these longevity pathways[67]*.* In addition, our lab found that the induction of *fmo-2* expression alone is sufficient to confer longevity and health benefits in worms[67], establishing *fmo-2* as a necessary and sufficient regulator of the aging process. Overexpressing *fmo-2* also increases stress resistance against multiple stressors, including tunicamycin, heat, and oxidative stress[67]. Recent studies also show that *fmo-2* is induced under exposure to pathogenic bacteria and is

involved in mitochondrial unfolded protein response as well[68,69]. In the case of pathogen exposure, *fmo-2* expression is necessary for the animal's survival[69]. Taken together, the data show that *fmo-2* is involved in multiple longevity and stress response pathways, consistent with the hypothesis that *fmo-2* is a key regulator of longevity.

Flavin-containing Monooxygenases

Flavin-containing monooxygenases (FMOs) are a family of enzymes that oxygenate substrates with nucleophilic centers, such as nitrogen and sulfur[70]. They were first discovered 50 years ago by the Ziegler Lab and have been studied extensively under the context of xenobiotic and drug metabolism[70]. FMO proteins form a stable hydroperoxyflavin intermediate complex with $NADP^+$ in the presence of its cofactor FAD[71]. This complex is primed to oxygenate substrates that access its active site[72], a characteristic that distinguishes FMOs from other families of oxygenases, such as cytochrome P450s, that require substrates to initiate catalytic activity[73]. Once a substrate accesses the active site, the intermediate complex then binds with a dioxygen (O_2) molecule to transfer an oxygen atom to its substrate, producing water and NADP+ as byproducts[74]. FMOs have also been shown to catalyze an NADPH-dependent oxygenation of water to hydrogen peroxide *in vitro*[75].

FMOs are promiscuous enzymes that are able to not only oxygenate substrates, but can also catalyze other reactions, such as decarboxylation, demethylation, and disulfide bond formation[73,76–78]. FMOs are classically known to catalyze reactions involving

xenobiotic compounds to increase their solubility through the plasma membrane both in and out of the cell[72]. Some of the known xenobiotic substrates of FMOs include imipramine, nicotine, clozapine, tamoxifen, and amphetamine[73]. While the endogenous role of FMOs have not been studied as extensively, FMOs are also known to metabolize endogenous substrates, such as methionine, cysteine, cysteamine, lipoic acid, and selenocysteine[72,76,78].

The FMO protein family is highly conserved both genetically and structurally from bacteria to humans[74,79]. In addition, full length amino acid alignment comparing the sequence identities of *C. elegans* FMO-2 and mouse FMO1–5 show high conservation for the catalytic residues between these species, suggesting a conserved enzymatic activity and function between the two species[80]. Humans have five functional FMO proteins (hFMO1-5) that are homologous to mouse FMOs of the same name (mFMO1-5)[81]. While *C. elegans* also have five FMOs (CeFMO-1-5), they are arbitrarily named and are not orthologous to the mammalian FMOs of the same name[82].

Considering the conserved nature of FMOs, it is plausible that they share an endogenous, more ancient physiological role than detoxifying xenobiotics. There is emerging evidence that FMOs play a role beyond xenobiotic metabolism in mammals. Initial reports linking FMOs to the aging process came from the Swindell and Miller labs, who each reported induction of *Fmo* genes in long-lived mouse models, such as dietary-restricted mice[83,84]. A more functional study of the endogenous role of FMOs came from the Shephard lab, who showed metabolic changes when *Fmos* are knocked out in mice,

specifically in those involved in maintaining cholesterol, lipid, and glucose homeostasis[82,85–88]. However, it is unclear whether these changes are beneficial to the animals' health and longevity. In mammals, FMO3 is required for weight gain on high-fat diet[89]. Moreover, FMO3 is consistently elevated in the multiple long-lived mouse models including Snell dwarf mice and dietary restricted mice[83]. Previous studies hypothesize that FMO3 affects metabolism by converting one of the few known endogenous metabolites, trimethylamine (TMA), to trimethylamine oxide (TMAO)[82,87]. A recent study, however, showed that FMO3 knockout mice do not gain weight on high fat diet, but TMAO supplementation fails to reverse this phenotype, suggesting that FMOs affect endogenous metabolism through other unknown endogenous metabolites[84]. The most well-known disease phenotype associated with FMOs is trimethylaminuria (TMAU), colloquially known as "fish odor syndrome." In TMAU patients, hFMO3 is unable to metabolize TMA to TMAO[73,82,87,89]. As a result, TMA is excreted through the skin and gives off fish-like odor, which the disease is known for[73]. More recently, our lab has shown that multiple mouse FMOs alter multiple endogenous metabolic pathways and confer multiplex stress resistance[80]. While all these findings suggest that FMOs can act as regulators of endogenous metabolic processes, the mechanism by which they may regulate the aging process is not yet known.

As mentioned above, *C. elegans fmo-2* is necessary and sufficient to confer longevity and health benefits downstream of multiple longevity pathways, including DR and hypoxia[67]. Similarly, *C. elegans fmo-1* is induced under dietary restriction[90] and *fmo-4* is induced under hypoxia[91], potentiating their role in regulating the aging process. These

findings, in conjunction with the power of *C. elegans* as a tool to study the aging process, the ability of FMOs to regulate endogenous metabolic processes, and the conserved catalytic and functional nature of FMOs, make studying the endogenous metabolic mechanism of longevity regulation by FMOs with the goal of ultimately translating these findings to humans worthwhile.

Metabolic Pathways of Aging

Metabolism is an important aspect of the aging process. Metabolism is the set of cellular processes by which cells produce and regulate energy and metabolites (e.g., nucleic acids, proteins, carbohydrates, and lipids) from nutrient sources, and manage waste[92]. Metabolic functions generally slow down as organisms age, and specific metabolic pathways, including insulin and energy metabolism, are altered in response to aging[93]. Metabolism also plays an important role in regulating longevity as metabolic pathways are involved in all three of the longevity pathways discussed above[94]. In addition, supplementation of individual metabolites, some of which I will discuss in this section, influence longevity and health in various organisms.

Metabolism is arguably the most complex system in biology, as there are more metabolites than there are genes and proteins[95]. Therefore, studying metabolism requires cutting-edge experimental tools, like metabolomics, to obtain and interpret data. As mentioned before, metabolism is an important aspect of studying the biology of aging, and metabolomics allows the measurement of individual metabolites and assessment of important metabolic pathways under different environmental and genetic

conditions. Broadly, there are two types of metabolomics approaches: untargeted and targeted metabolomics. As its name suggests, untargeted metabolomics is used to identify and characterize a large number of metabolites in an untargeted or unbiased manner. The resulting data from the untargeted approach can be analyzed to identify interesting metabolic pathways and to formulate hypotheses about metabolic changes. Once a hypothesis is generated using the untargeted approach, targeted metabolomics can be used to test this hypothesis by measuring and quantifying known metabolites of interest. The metabolites measured using this approach are typically involved in a related biochemical pathway, as the purpose of running a targeted approach is to test a specific hypothesis on what a metabolic pathway is doing under a given condition[96]. Therefore, when used in combination, metabolomics allows for both the unbiased hypothesis generation and the testing of the resulting hypothesis. Given its large progeny number and small body size, *C. elegans* allows metabolomics analysis at the organismal level with large sample size to determine systemic metabolic changes.

While *C. elegans* is a useful organism to study metabolism, one of the aspects of *C. elegans* maintenance presents a major experimental challenge: bacterial food source. *C. elegans* are typically grown on *E. coli*. As they themselves are living organisms, *E. coli* have their own metabolic activity. This presents a challenge for metabolomics as live bacterial metabolism confounds the metabolic changes occurring in *C. elegans*. This also presents similar challenges for other metabolic studies, such as drug screening and respiration measurements[97]. Therefore, a way of suppressing or stopping bacterial metabolism is useful for metabolic studies in *C. elegans*. Several methods

have been developed to attempt to mitigate this problem, albeit unsuccessfully. The three most well-known methods are heat-killing, antibiotic treatment, and ultraviolet (UV) irradiation. Heat-killing destroys nutrients and alters the bacterial texture to become inedible to worms, preventing worm development[98]. Antibiotic treatments present even more confounding variables, altering worm development and metabolism[99]. UV-irradiation is typically done by UV treating the plates seeded with live bacteria. This method inconsistently kills bacteria both reproductively and metabolically, necessitating the need to test each plate to ensure death, which makes the process laborious and impractical[97]. Therefore, a more reliable and high-throughput method of killing bacteria is needed to study worm metabolism. I have developed such a way and will discuss it in Chapter II.

While the metabolomics approach provides useful information about metabolite concentrations at a given time point, the measurements are static and do not provide direct information about metabolic fluxes, or how the metabolite concentrations change over time. Computational modeling can be used to simulate changes in metabolic flux under different conditions. In many applications systems of ordinary differential equations (ODEs) are used to simulate metabolic kinetics. Applications of this approach require knowledge of initial concentrations, different kinetic parameters, and reaction rate equations to simulate metabolic flux for given metabolic pathways. Thus a major limitation of this approach is that it requires experimental data that may not be available in some situations. An alternative approach is to use a constraint-based stoichiometric model. In this type of model, the stoichiometric reactions of the metabolic pathway of

interest are converted into a series of linear algebraic constraints under the assumption of a steady-state. Unlike the dynamic model, which gives a unique solution based on the initial metabolite concentrations, a constraint-based approach typically give an infinite number of feasible solutions due to its underdetermined nature (i.e. there are fewer equations than variables to solve for). Therefore, the solution-space needs to be further constrained using experimental data and/or assumptions to find an optimal solution[100].

For the remainder of this section, I will provide a background on the major metabolic pathways that I have encountered during my thesis project to determine the downstream mechanisms of FMO-2-mediated longevity regulation. Given that multiple discoveries of their role in the aging process have been made and that they are actively studied in the aging field, figuring out how FMO-2 regulates these processes will be important in understanding the mechanisms of the aging process.

1) One Carbon Metabolism

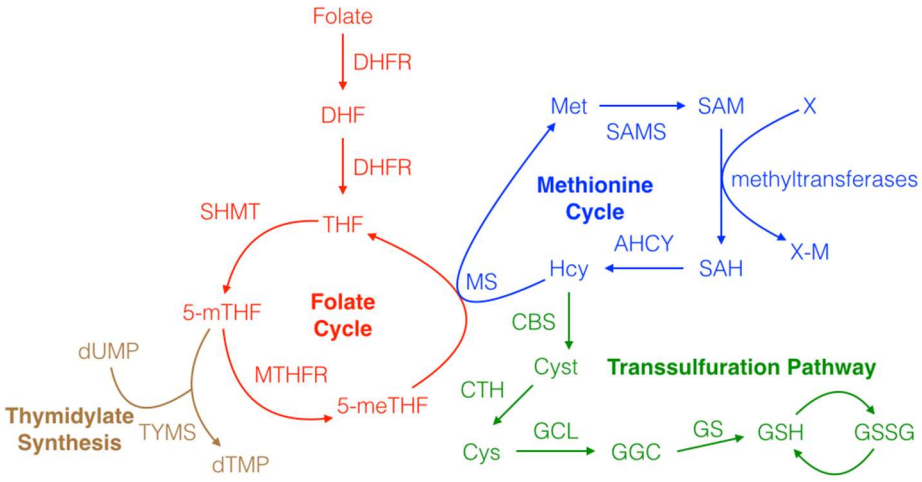

Figure 1.1: Diagram of one-carbon metabolism. DHF = dihydrofolate, THF = tetrahydrofolate, 5-mTHF = 5,10-methylene-THF, 5-meTHF = 5-methyl-THF, dUMP = deoxyuridylate, dTMP = deoxythymidylate, Met = methionine, SAM = s-adenosylmethionine, SAH = s-adenosylhomocysteine, X = substrate of methyltransferase, X-M = methylated product of methyltransferase, Hcy = homocysteine, Cyst = cystathionine, Cys = cysteine, GGC = glutamylcysteine, GSH = reduced glutathione, GSSG = oxidized glutathione, DHFR = dihydrofolate reductase, SHMT = serine hydroxymethyltransferase, MTHFR = methylene-THF-reductase, TYMS = thymidylate synthase, MS = methionine synthase, SAMS = s-adenosylmethionine synthase, AHCY = s-adenosylhomocysteine hydrolase, CBS = cystathionine beta synthase, CTH = cystathionine γ-lyase, GCL = glutamate cysteine ligase, and GS = glutathione synthase.

One carbon metabolism (OCM) is an important intermediate metabolic pathway that is formed by a two-cycle metabolic network of the folate cycle and the methionine cycle[101]. OCM takes nutrient inputs and converts them into metabolic intermediates to be used to promote growth and survival, including nucleotide metabolism, the transsulfuration and transmethylation pathways[102–104].

One of the key nutrient inputs for OCM is folate. Folate is a precursor molecule for the folate cycle. In this process, folate is first converted to dihydrofolate (DHF) and then to tetrahydrofolate (THF) by DHF reductase (DHFR) using nicotinamide adenine dinucleotide phosphate (NADPH). THF is then converted to 5,10-methylene-THF (5-mTHF) by serine hydroxymethyltransferase (SHMT1/MEL-32), which requires vitamin B6 and serine. 5-mTHF can be used by thymidylate synthase (TYMS) for *de novo* thymidylate synthesis by converting deoxyuridylate (dUMP) into deoxythymidylate (dTMP). 5-mTHF can also be converted instead into 5-methyl-THF (5-meTHF) by methylene-THF-reductase (MTHFR) using NADPH[105].

Methionine serves as the major substrate for the methionine cycle portion of OCM. Methionine is first converted into S-adenosylmethionine (SAM), a major methyl donor for methylation reactions, by methionine adenosyltransferase (MAT), also known as S-adenosylmethionine synthase (SAMS), in an ATP-dependent reaction. The loss of methyl group converts SAM into S-adenosylhomocysteine (SAH). SAH is then converted into homocysteine (HCY) by S-adenosylhomocysteine hydrolase (AHCY). Methionine synthase connects and completes the methionine and folate cycles by transferring a carbon unit from 5-meTHF to HCY, leading to the regeneration of THF and methionine[105].

Below are the components of OCM and what is known about their influence on longevity:

A) Folate Cycle

Folate metabolism is associated with the aging process, but its role is contradictory between invertebrates and mammals. Older mammals exhibit a lower plasma folate level that is correlated with age-associated phenotypes[106]. Similarly, restricting folate in the diet of mice recapitulates these phenotypes, including circadian rhythm impairment, short-term memory impairment, and metabolic and epigenetic changes[107,108]. Consistent with these findings, supplementing folate leads to increased lifespan in mice[109]. In *C. elegans*, however, folate metabolism seems to have an opposite effect on longevity and health. Inhibition of folate synthesis in worm's bacterial food source using genetic mutants or metformin extends worm

lifespan[102,110]. Knocking down DHFR in worms also results in lifespan extension[111]. Exogenous supplementation of 5-meTHF blunts the lifespan extension mediated by multiple longevity pathways, including insulin signaling, dietary restriction, and mitochondrial impairments[111]. While this suggests that multiple longevity pathways converge on folate metabolism to regulate lifespan in worms, further studies are required to reconcile the differences observed in *C. elegans* and mammals following perturbations in the folate cycle.

B) Methionine Cycle

As mentioned previously, methionine restriction increases lifespan in multiple organisms, including yeast, worms, flies, and mice[112]. Genetic mimetics of methionine restriction also have similar effects in these animals[105]. In addition to intracellular methionine levels, SAM availability is also reportedly an important regulator of methionine restriction-mediated phenotypes. In *Drosophila melanogaster,* increasing SAM catabolism by overexpressing glycine-N-methltransferase (GNMT), a necessary enzyme for insulin signaling-mediated longevity benefits, increases lifespan[113]. In worms, genetic inhibition of SAM synthase (*sams-1* and *sams-5*), which would decrease SAM availability, increases lifespan[114,115]. Genetic suppression of specific methyltransferases in nonmammalian species, including yeast, worms, and flies tends to improve longevity[112]. While not studied as extensively as methionine and folate mechanistically, increased plasma levels of homocysteine is considered a risk factor for age-associated cardiovascular

diseases and decline in cognitive function in humans and thus further investigation into its role in longevity regulation is warranted[116].

C) Transsulfuration Pathway

Excess homocysteine that is not consumed in the regeneration of THF and methionine enters the transsulfuration pathway to generate cysteine and glutathione. Cystathionine beta synthase (CBS) converts HCY into cystathionine using serine in a vitamin B6-dependent reaction, which is then converted to cysteine by cystathionine γ-lyase (CSE)[117]. CBS is a necessary component of DR-mediated lifespan extension in flies and its overexpression is sufficient to increase lifespan in flies and worms[103,118]. CBS can also convert cysteine into hydrogen sulfide (H_2S)[117]. In *C. elegans*, exogenous supplementation of H_2S increases lifespan through SKN-1 activation[119]. H_2S is required for the DR-mediated lifespan extension in yeast, worms, flies, and mice and is implicated in insulin and nutrient sensing pathways that are described above[120]. Once synthesized by CSE, cysteine can be converted into glutamylcysteine by glutamate cysteine ligase using glutamate[117]. Finally, glutathione synthase (GS) converts glutamylcysteine into glutathione (GSH) by adding glycine[117]. GSH is a critical redox buffer that mediates the removal of peroxides through reduction[105]. This redox buffer system regulates the level of reactive oxygen species (ROS), which can act as signaling molecules[121]. This is important for longevity regulation as a transient increase in ROS levels during development leads to improved lifespan and health in worms by modulating H3K4me3 levels[121]. In addition, GSH and its oxidized form GSSG are important for

regulating protein folding, where they promote cleavage and formation of disulfide bonds, respectively[122].

2) Kynurenine Pathway

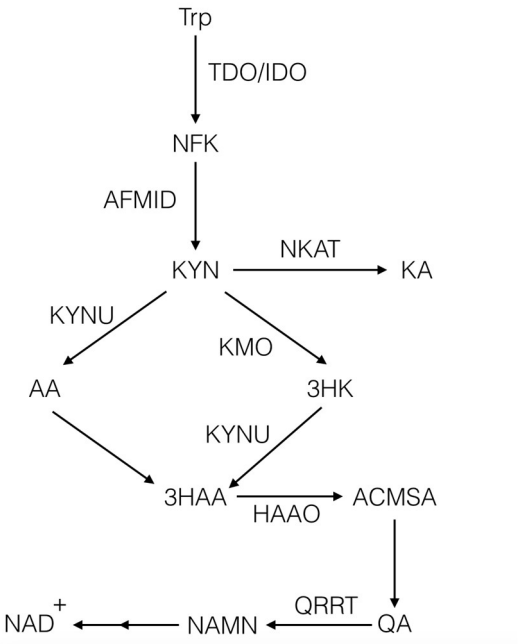

Figure 1.2: Diagram of the kynurenine pathway. Trp = tryptophan, NFK = n-formylkynurenine, KYN = kynurenine, KA = kynurenic acid, AA = anthranilic acid, 3HK = 3-hydroxykynurenine, 3HAA = 3-hydroxyanthranilic acid, ACMSA = 2-amino-3-carboxymuconic semialdehyde, QA = quinolinic acid, NAMN = nicotinic acid mononucleotide, NAD^+ = nicotinamide adenine dinucleotide, TDO = tryptophan 2,3-dioxygenase, IDO = indoleamine 2,3 dioxygenase, AFMID = arylformamidase, NKAT = kynurenine aminotransferase, KYNU = kynureninase, KMO = kynurenine 3-monooxygenase, HAAO = 3HAA dioxygenase, and QRRT = QA phosphoribosyl transferase.

The kynurenine pathway is a conserved tryptophan catabolism pathway, whose two key products are NAD+ and kynurenic acid. In this pathway, tryptophan is converted into N-formylkynurenine by either indoleamine 2,3 dioxygenase-1, 2 (IDO-1, 2) or tryptophan 2,3-dioxygenase (TDO-2)[123]. N-formylkynurenine is converted to

kynurenine by arylformamidase (AFMID/AMFD-1)[123] and releases formate, a major carbon source for OCM, as a byproduct[124]. Kynurenine can either be converted to 1) kynurenic acid by kynurenine aminotransferase (NKAT) or glutamic-oxaloacetic transaminase 2 (GOT-2), forming one of the two key products of the pathway, 2) anthranilic acid by kynureninase (KYNU), or 3) 3-hydroxykynurenine (3HK) by kynurenine 3-monooxygenase (KMO). 3HK and anthranilic acid are then converted 3-hydroxyanthranilic acid (3HAA) by either KYNU or via non-enzymatic reaction, respectively. 3HAA is then converted to 2-amino-3-carboxymuconic semialdehyde (ACMSA) by 3HAA dioxygenase (HAAO), which then converts to quinolinic acid (QA) spontaneously. QA phosphoribosyl transferase (QPRT) converts QA into nicotinic acid mononucleotide (NAMN), which can then be converted into NAD+[123,125].

In *C. elegans*, inhibition of multiple genes within the kynurenine pathway, including *tdo-2* (TDO), *kynu-1* (KYNU), and *acsd-1* (ACMSD) all increase lifespan[126–128]. However, the mechanisms by which they extend lifespan are unclear. Knockdown of *tdo-2* is thought to increase lifespan by increasing intracellular tryptophan level because 1) intracellular tryptophan level is increased upon *tdo-2* knockdown[127] and 2) exogenous supplementation of tryptophan increases worm lifespan[129]. Lifespan extension by *acsd-1* knockdown is hypothesized to be due to increased NAD+ production, whose longevity benefits are already known[128]. However, knocking down *kynu-1* does not increase tryptophan level and given its position in the kynurenine pathway, suppressing *kynu-1* expression should not increase NAD+ production[126],

thus suggesting that these enzymes extend lifespan through an as yet unknown mechanism.

3) Phospholipid Metabolism and Downstream UPR^{ER} Activation

Phospholipid metabolism plays a key role in the activation of the endoplasmic reticulum unfolded protein response (UPR^{ER}) that is independent of proteostasis-related stress. As organisms age, their proteostasis, or protein homeostatic balance, declines[130]. Therefore, maintaining and prolonging proteostasis is an important goal of longevity intervention. The UPR^{ER} is a stress response mechanism by which cells reduce the amount of misfolded proteins under stressful conditions, such as environmental and metabolic insults[130]. IRE-1, PERK, and ATF-6 are the key regulators of the UPR^{ER}[130]. In *C. elegans*, the UPR pathways of these proteins are conserved and are well-known[131,132]. However, I will mainly focus on IRE1-mediated UPR^{ER} here because 1) it regulates majority of the transcriptional induction during the UPR^{ER}[133]. and 2) it is relevant to my thesis project and will be further discussed in Chapter IV.

The activation of inositol-requiring enzyme-1 (IRE-1)-mediated UPR^{ER} begins with the canonical tyrosine kinase activation. Under ER stress, the luminal domain of IRE-1 dimerizes, leading to ATP-dependent transautophorylation on the cytosolic domain, which induces RNAse activity. The RNAse activity of IRE-1 allows the splicing of the intronic region from *xbp-1* (X-box binding protein-1) mRNA. The spliced form of *xbp-1* is translated into XBP-1 transcription factor (XBP-1s), which is

then translocated into the nucleus to induce the expression of genes involved in protein repair and autophagy[134].

IRE-1-mediated activation of the UPR^{ER} is a necessary and sufficient component of multiple longevity pathways. In *C. elegans*, *ire-1* is required for the lifespan extension under *daf-2* mutants, genetic DR mimetic *eat-2* mutants, and mitochondrial respiration-suppressed *isp-1* mutants[135]. In addition, constitutive activation of the neuronal XBP-1s improves age-associated decline in ER proteostasis, extends lifespan, improves stress resistance, and activates the UPR^{ER} in other tissues via cell-nonautonomous signaling[136]. IRE-1 also regulates the animal's response to DR. *ire-1* mutants fail to induce *fil-1* and *fil-2*, which are key enzymes involved in lipolysis during starvation, and thereby impact the worm's ability to utilize fat storage for energy[137]. Similar to *eat-2* mutants, DR also requires *ire-1* to extend lifespan, where knocking out *ire-1* abrogates its lifespan benefits[138].

In *C. elegans*, reduction in phosphatidylcholine synthesis leads to the activation of the UPR^{ER}. Mutation or knockdown of MDT-15 (Mediator subunit) and SCD (stearoyl-CoA-desaturases), which are involved in fatty acid metabolism, reduces phosphatidylcholine synthesis and activates the UPR^{ER}. Similarly, the knockdown of *sams-1*, which encodes for SAM synthase that is responsible for producing the lipid methyl donor SAM, also activates the UPR^{ER}. Under normal conditions, *pmt-1* (phosphoethanolamine N-methyltransferase-1) catalyzes the reaction between SAM and phosphatidylethanolamine to produce phosphocholine, which is then converted

to phosphatidylcholine further down the pathway. Supplementation of choline, which is a substrate for SAM-independent phosphatidylcholine synthesis pathway through *ckb-2* (choline kinase B), abrogates the induction of the UPR^{ER} in *sams-1* knockdown animals. Consistent with these findings, the UPR^{ER} is reported to be induced under low level of phosphatidylcholine level. In all of these conditions, the UPR^{ER} is activated in the absence of misfolded proteins, suggesting that the UPR^{ER} can be activated by lipid imbalance independent of proteostasis[139].

Goals of Thesis

The main goal of my thesis is to determine the mechanisms by which FMO-2 regulates longevity and health in *C. elegans*. As mentioned earlier in the chapter, aging is a serious global health and economic issue that necessitates the understanding of its molecular mechanisms to identify therapeutic targets to slow down the aging process. *C. elegans* is a useful model for studying the aging process due to its ease of maintenance, short lifespan, and physiological and molecular conservation to humans. DR is one of the most well-studied longevity interventions and requires the induction of *fmo-2* to improve lifespan and health in *C. elegans*. Despite recent reports (including our own) defining *Fmos* as regulators of endogenous processes, the mechanisms for FMO-mediated regulation of metabolism and longevity are unclear. This information, combined with the knowledge that *fmo* genes are well-conserved across taxa, make understanding the mechanisms of FMO-2-mediated life extension a crucial next step. Moreover, many longevity interventions, including dietary restriction, suppression of mTOR activity, and reduced insulin/IGF signaling, affect lifespan in both worms and

mammals, suggesting that what we learn about longevity regulation by FMOs in worms may also be conserved in mammals.

To understand how *fmo-2* confers longevity and health benefits, my dissertation focuses on two critical questions:

1. What are the endogenous targets of FMO-2?
2. Which genes affected by FMO-2 are necessary and sufficient to promote healthy aging?

This work has the potential to define therapeutic agents for longevity in the form of "druggable" small molecules and/or gene and protein targets. While the last 50 years of FMO research have been mostly limited to drug metabolism, recent progress defining the critical role of *fmo-2* in regulating health and longevity and the high conservation of FMOs across taxa lead to the proposed mechanistic study of FMOs in the context of longevity regulation in pursuit of improving human health.

Structure of Thesis

The work is divided into five chapters focusing on different parts of the project:

Chapter I introduces the significance of aging research on improving human health, background of using *C. elegans* as a model organism, relevant metabolic longevity pathways in *C. elegans*, including DR that led to the discovery of FMO as a regulator of longevity, background on FMOs, and potential metabolic targets of FMOs. In sum, this

information serves as a rationale for studying *fmo-2* in *C. elegans* under the context of metabolic regulation of aging to understand the metabolic processes by which we can improve human health.

Chapter II focuses on the development of a novel food preparation methodology for *C. elegans* for metabolic experiments to remove bacterial metabolism as a confounding variable. The work presented in this chapter is published in a peer-reviewed journal, as cited in references for the chapter.

Chapter III is the crux of my dissertation, where I determine the endogenous metabolic role of FMO-2 in regulating lifespan and health through its interaction with OCM and tryptophan metabolism, potentially leading to a reduction in flux through methylation processes. This work is currently under review at *Nature Communications*.

Chapter IV introduces lipid metabolism, phosphatidylcholine metabolism in particular, as a potential mediator of longevity downstream of FMO-2 induction. The experiments in this chapter are not finalized as a manuscript, but given the interaction between lipid metabolism and the UPR that is discussed in Chapter I, the work presented in this chapter serves as an important knowledge base for those interested in studying the mechanisms of FMOs in the context of aging.

Chapter V summarizes the main findings of my dissertation and presents ideas for future directions for the study.

References

1. Miller HA, Dean ES, Pletcher SD, Leiser SF. Cell non-autonomous regulation of health and longevity. *Elife*. 2020;9. doi:10.7554/eLife.62659

2. Kaeberlein M. Longevity and aging. *F1000Prime Rep*. 2013;5. doi:10.12703/P5-5

3. Petralia RS, Mattson MP, Yao PJ. Aging and longevity in the simplest animals and the quest for immortality. *Ageing Res Rev*. 2014;16(1):66-82. doi:10.1016/j.arr.2014.05.003

4. MORLEY A. Somatic Mutation and Aging. *Ann N Y Acad Sci*. 1998;854(1 TOWARDS PROLO):20-22. doi:10.1111/j.1749-6632.1998.tb09888.x

5. Harman D. Aging: A Theory Based on Free Radical and Radiation Chemistry. *J Gerontol*. 1956;11(3):298-300. doi:10.1093/geronj/11.3.298

6. Terman A, Brunk UT. Aging as a catabolic malfunction. *Int J Biochem Cell Biol*. 2004;36(12):2365-2375. doi:10.1016/j.biocel.2004.03.009

7. Brenner S. THE GENETICS OF CAENORHABDITIS ELEGANS. *Genetics*. 1974;77(1):71-94. doi:10.1093/genetics/77.1.71

8. Félix MA, Braendle C. The natural history of Caenorhabditis elegans. *Curr Biol*. 2010;20(22):R965-R969. doi:10.1016/j.cub.2010.09.050

9. Schaffitzel E, Hertweck M. Recent aging research in Caenorhabditis elegans. *Exp Gerontol*. 2006;41(6):557-563. doi:10.1016/j.exger.2006.02.008

10. Golden TR, Melov S. Gene expression changes associated with aging in C. elegans. *WormBook*. 2007:1-12. doi:10.1895/wormbook.1.127.2

11. Hertweck M, Hoppe T, Baumeister R. C. elegans, a model for aging with high-throughput capacity. *Exp Gerontol*. 2003;38(3):345-346. doi:10.1016/S0531-5565(02)00208-5

12. Chen Y, Scarcelli V, Legouis R. Approaches for studying autophagy in caenorhabditis elegans. *Cells*. 2017;6(3). doi:10.3390/cells6030027

13. Lai CH, Chou CY, Ch'ang LY, Liu CS, Lin WC. Identification of novel human genes evolutionarily conserved in Caenorhabditis elegans by comparative proteomics. *Genome Res*. 2000;10(5):703-713. doi:10.1101/gr.10.5.703

14. Chew YL, Walker DS, Towlson EK, et al. Recordings of Caenorhabditis elegans locomotor behaviour following targeted ablation of single motorneurons. *Sci Data*. 2017;4. doi:10.1038/sdata.2017.156

15. Olsen A, Vantipalli MC, Lithgow GJ. Using Caenorhabditis elegans as a model for aging and age-related diseases. In: *Annals of the New York Academy of Sciences*. Vol 1067. Blackwell Publishing Inc.; 2006:120-128. doi:10.1196/annals.1354.015

16. Garigan D, Hsu AL, Fraser AG, Kamath RS, Abringet J, Kenyon C. Genetic analysis of tissue aging in Caenorhabditis elegans: A role for heat-shock factor and bacterial proliferation. *Genetics*. 2002.

17. Chen CH, Chen YC, Jiang HC, Chen CK, Pan CL. Neuronal aging: Learning from C. elegans. *J Mol Signal*. 2013;8(1). doi:10.1186/1750-2187-8-14

18. Liu J, Zhang B, Lei H, et al. Functional aging in the nervous system contributes to age-dependent motor activity decline in C. elegans. *Cell Metab*. 2013;18(3):392-402. doi:10.1016/j.cmet.2013.08.007

19. Pickett CL, Dietrich N, Chen J, Xiong C, Kornfeld K. Mated progeny production is a biomarker of aging in caenorhabditis elegans. *G3 Genes, Genomes, Genet*. 2013;3(12):2219-2232. doi:10.1534/g3.113.008664

20. Podshivalova K, Kerr RA, Kenyon C. How a Mutation that Slows Aging Can Also Disproportionately Extend End-of-Life Decrepitude. *Cell Rep*. 2017. doi:10.1016/j.celrep.2017.03.062

21. Timmons L, Court DL, Fire A. Ingestion of bacterially expressed dsRNAs can produce specific and potent genetic interference in Caenorhabditis elegans. *Gene*. 2001;263(1-2):103-112. doi:10.1016/S0378-1119(00)00579-5

22. Kamath RS, Martinez-Campos M, Zipperlen P, Fraser AG, Ahringer J. Effectiveness of specific RNA-mediated interference through ingested double-stranded RNA in Caenorhabditis elegans. *Genome Biol*. 2000;2(1):research0002.1. doi:10.1186/gb-2000-2-1-research0002

23. Rual JF, Ceron J, Koreth J, et al. Toward improving Caenorhabditis elegans phenome mapping with an ORFeome-based RNAi library. *Genome Res*. 2004;14(10 B):2162-2168. doi:10.1101/gr.2505604

24. Zhuang JJ, Hunter CP. RNA interference in Caenorhabditis elegans: Uptake, mechanism, and regulation. *Parasitology*. 2012;139(5):560-573. doi:10.1017/S0031182011001788

25. Boulin T, Etchberger JF, Hobert O. Reporter gene fusions. *WormBook*. 2006:1-23. doi:10.1895/wormbook.1.106.1

26. Corsi AK, Wightman B, Chalfie M. A Transparent window into biology: A primer on Caenorhabditis elegans (June 18, 2015), WormBook, ed. The C. elegans Research Community. *WormBook*. 2015. doi:doi/10.1895/wormbook.1.177.1

27. Weinhouse C, Truong L, Meyer JN, Allard P. Caenorhabditis elegans as an emerging model system in environmental epigenetics. *Environ Mol Mutagen*. 2018;59(7):560-575. doi:10.1002/em.22203

28. Bareja A, Lee DE, White JP. Maximizing Longevity and Healthspan: Multiple Approaches All Converging on Autophagy. *Front Cell Dev Biol*. 2019;7:183. doi:10.3389/fcell.2019.00183

29. Gkikas I, Petratou D, Tavernarakis N. Longevity pathways and memory aging. *Front Genet*. 2014;5(JUN):155. doi:10.3389/fgene.2014.00155

30. Kenyon C, Chang J, Gensch E, Rudner A, Tabtiang R. A C. elegans mutant that lives twice as long as wild type. *Nature*. 1993;366(6454):461-464. doi:10.1038/366461a0

31. Clancy DJ, Gems D, Harshman LG, et al. Extension of life-span by loss of CHICO, a Drosophila insulin receptor substrate protein. *Science (80-)*. 2001;292(5514):104-106. doi:10.1126/science.1057991

32. Tatar M, Kopelman A, Epstein D, Tu MP, Yin CM, Garofalo RS. A mutant Drosophila insulin receptor homolog that extends life-span and impairs neuroendocrine function. *Science (80-)*. 2001;292(5514):107-110. doi:10.1126/science.1057987

33. Blüher M, Kahn BB, Kahn CR. Extended longevity in mice lacking the insulin receptor in adipose tissue. *Science (80-)*. 2003;299(5606):572-574. doi:10.1126/science.1078223

34. Kimura KD, Tissenbaum HA, Liu Y, Ruvkun G. Daf-2, an insulin receptor-like gene that regulates longevity and diapause in Caenorhabditis elegans. *Science (80-)*. 1997;277(5328):942-946. doi:10.1126/science.277.5328.942

35. Ogg S, Paradis S, Gottlieb S, et al. The fork head transcription factor DAF-16 transduces insulin-like metabolic and longevity signals in C. elegans. *Nature*. 1997;389(6654):994-999. doi:10.1038/40194

36. Lin K, Hsin H, Libina N, Kenyon C. Regulation of the Caenorhabditis elegans longevity protein DAF-16 by insulin/IGF-1 and germline signaling. *Nat Genet*. 2001;28(2):139-145. doi:10.1038/88850

37. Morris JZ, Tissenbaum HA, Ruvkun G. A phosphatidylinositol-3-OH kinase family member regulating longevity and diapause in Caenorhabditis elegans. *Nature*. 1996;382(6591):536-539. doi:10.1038/382536a0

38. Friedman DB, Johnson TE. A mutation in the age-1 gene in Caenorhabditis elegans lengthens life and reduces hermaphrodite fertility. *Genetics*. 1988;118(1):75-86. doi:10.1093/genetics/118.1.75

39. Dorman JB, Albinder B, Shroyer T, Kenyon C. The age-1 and daf-2 genes function in a common pathway to control the lifespan of Caenorhabditis elegans. *Genetics*. 1995;141(4):1399-1406. doi:10.1093/genetics/141.4.1399

40. Paradis S, Ailion M, Toker A, Thomas JH, Ruvkun G. A PDK1 homolog is necessary and sufficient to transduce AGE-1 PI3 kinase signals that regulate diapause in Caenorhabditis elegans. *Genes Dev*. 1999;13(11):1438-1452. doi:10.1101/gad.13.11.1438

41. Paradis S, Ruvkun G. Caenorhabditis elegans Akt/PKB transduces insulin receptor-like signals from age-1 PI3 kinase to the DAF-16 transcription factor. *Genes Dev*. 1998;12(16):2488-2498. doi:10.1101/gad.12.16.2488

42. Murphy CT, McCarroll SA, Bargmann CI, et al. Genes that act downstream of DAF-16 to influence the lifespan of Caenorhabditis elegans. *Nature*. 2003;424(6946):277-284. doi:10.1038/nature01789

43. Mukhopadhyay A, Oh SW, Tissenbaum HA. Worming pathways to and from DAF-16/FOXO. *Exp Gerontol*. 2006;41(10):928-934. doi:10.1016/j.exger.2006.05.020

44. Maddocks ODK, Labuschagne CF, Adams PD, Vousden KH. Serine Metabolism Supports the Methionine Cycle and DNA/RNA Methylation through De Novo ATP Synthesis in Cancer Cells. *Mol Cell*. 2016;61(2):210-221. doi:10.1016/j.molcel.2015.12.014

45. Lin K, Dorman JB, Rodan A, Kenyon C. daf-16: An HNF-3/forkhead family member that can function to double the life-span of Caenorhabditis elegans. *Science (80-)*. 1997;278(5341):1319-1322. doi:10.1126/science.278.5341.1319

46. Ewald CY, Landis JN, Abate JP, Murphy CT, Blackwell TK. Dauer-independent insulin/IGF-1-signalling implicates collagen remodelling in longevity. *Nature*. 2015;519(7541):97-101. doi:10.1038/nature14021

47. Tullet JMA, Hertweck M, An JH, et al. Direct Inhibition of the Longevity-Promoting Factor SKN-1 by Insulin-like Signaling in C. elegans. *Cell*. 2008;132(6):1025-1038. doi:10.1016/j.cell.2008.01.030

48. Jia K, Chen D, Riddle DL. The TOR pathway interacts with the insulin signaling pathway to regulate C. elegans larval development, metabolism and life span. *Development*. 2004;131(16):3897-3906. doi:10.1242/dev.01255

49. Vellai T, Takacs-Vellai K, Zhang Y, Kovacs AL, Orosz L, Müller F. Influence of TOR kinase on lifespan in C. elegans. *Nature*. 2003;426(6967):620. doi:10.1038/426620a

50. Bjedov I, Toivonen JM, Kerr F, et al. Mechanisms of Life Span Extension by Rapamycin in the Fruit Fly Drosophila melanogaster. *Cell Metab*. 2010;11(1):35-46. doi:10.1016/j.cmet.2009.11.010

51. Harrison DE, Strong R, Sharp ZD, et al. Rapamycin fed late in life extends lifespan in genetically heterogeneous mice. *Nature*. 2009;460(7253):392-395. doi:10.1038/nature08221

52. Powers RW, Kaeberlein M, Caldwell SD, Kennedy BK, Fields S. Extension of chronological life span in yeast by decreased TOR pathway signaling. *Genes Dev*. 2006;20(2):174-184. doi:10.1101/gad.1381406

53. Robida-Stubbs S, Glover-Cutter K, Lamming DW, et al. TOR signaling and rapamycin influence longevity by regulating SKN-1/Nrf and DAF-16/FoxO. *Cell Metab*. 2012;15(5):713-724. doi:10.1016/j.cmet.2012.04.007

54. Wullschleger S, Loewith R, Hall MN. TOR signaling in growth and metabolism. *Cell*. 2006;124(3):471-484. doi:10.1016/j.cell.2006.01.016

55. Sheaffer KL, Updike DL, Mango SE. The Target of Rapamycin Pathway Antagonizes pha-4/FoxA to Control Development and Aging. *Curr Biol*. 2008;18(18):1355-1364. doi:10.1016/j.cub.2008.07.097

56. Saxton RA, Sabatini DM. mTOR Signaling in Growth, Metabolism, and Disease. *Cell*. 2017;168(6):960-976. doi:10.1016/j.cell.2017.02.004

57. Hansen M, Taubert S, Crawford D, Libina N, Lee S-J, Kenyon C. Lifespan extension by conditions that inhibit translation in Caenorhabditis elegans. *Aging Cell*. 2007;6(1):95-110. doi:10.1111/j.1474-9726.2006.00267.x

58. McQuary PR, Liao CY, Chang JT, et al. C. elegans S6K Mutants Require a Creatine-Kinase-like Effector for Lifespan Extension. *Cell Rep*. 2016;14(9):2059-2067. doi:10.1016/j.celrep.2016.02.012

59. Burkewitz K, Zhang Y, Mair WB. AMPK at the nexus of energetics and aging. *Cell Metab*. 2014;20(1):10-25. doi:10.1016/j.cmet.2014.03.002

60. McCay CM, Maynard LA, Sperling G, Barnes LL. Retarded growth, life span, ultimate body size and age changes in the albino rat after feeding diets restricted in calories. *Nutr Rev*. 1975;33(8):241-243. doi:10.1111/j.1753-4887.1975.tb05227.x

61. Kapahi P, Kaeberlein M, Hansen M. Dietary restriction and lifespan: Lessons from invertebrate models. *Ageing Res Rev*. 2017;39:3-14. doi:10.1016/j.arr.2016.12.005

62. Houthoofd K, Braeckman BP, Johnson TE, Vanfleteren JR. Life extension via dietary restriction is independent of the Ins/IGF-1 signalling pathway in Caenorhabditis elegans. *Exp Gerontol*. 2003;38(9):947-954. doi:10.1016/S0531-5565(03)00161-X

63. Lakowski B, Hekimi S. The genetics of caloric restriction in Caenorhabditis

elegans. *Proc Natl Acad Sci U S A*. 1998;95(22):13091-13096. doi:10.1073/pnas.95.22.13091

64. Mair W, Dillin A. Aging and Survival: The Genetics of Life Span Extension by Dietary Restriction. *Annu Rev Biochem*. 2008;77(1):727-754. doi:10.1146/annurev.biochem.77.061206.171059

65. Panowski SH, Wolff S, Aguilaniu H, Durieux J, Dillin A. PHA-4/Foxa mediates diet-restriction-induced longevity of C. elegans. *Nature*. 2007. doi:10.1038/nature05837

66. Riera CE, Dillin A. Can aging be “drugged”? *Nat Med*. 2015;21(12):1400-1405. doi:10.1038/nm.4005

67. Leiser SF, Miller H, Rossner R, et al. Cell nonautonomous activation of flavin-containing monooxygenase promotes longevity and health span. *Science (80-)*. 2015. doi:10.1126/science.aac9257

68. Bennett CF, Kwon JJ, Chen C, et al. Transaldolase inhibition impairs mitochondrial respiration and induces a starvation-like longevity response in Caenorhabditis elegans. *PLoS Genet*. 2017. doi:10.1371/journal.pgen.1006695

69. Wani K, Taubert S, Irazoqui J. NHR-49/PPARα regulates HLH-30/TFEB-mediated innate immune response via a flavincontaining monooxygenase in C. elegans *J Immunol*. 2019;202(1 Supplement):64.6 LP-64.6. http://www.jimmunol.org/content/202/1_Supplement/64.6.abstract.

70. Rossner R, Kaeberlein M, Leiser SF. Flavin-containing monooxygenases in aging and disease: Emerging roles for ancient enzymes. *J Biol Chem*. 2017. doi:10.1074/jbc.R117.779678

71. Robinson R, Badieyan S, Sobrado P. C4a-hydroperoxyflavin formation in N -hydroxylating flavin monooxygenases is mediated by the 2′-OH of the nicotinamide ribose of NADP+. *Biochemistry*. 2013;52(51):9089-9091. doi:10.1021/bi4014903

72. Krueger SK, Williams DE. Mammalian flavin-containing monooxygenases: Structure/function, genetic polymorphisms and role in drug metabolism. *Pharmacol Ther*. 2005. doi:10.1016/j.pharmthera.2005.01.001

73. Rossner R, Kaeberlein M, Leiser SF. Flavin-containing monooxygenases in aging and disease: Emerging roles for ancient enzymes. *J Biol Chem*. 2017. doi:10.1074/jbc.R117.779678

74. Ziegler DM. An overview of the mechanism, substrate specificities, and structure of FMOs. In: *Drug Metabolism Reviews*. ; 2002. doi:10.1081/DMR-120005650

75. Siddens LK, Krueger SK, Henderson MC, Williams DE. Mammalian flavin-

containing monooxygenase (FMO) as a source of hydrogen peroxide. *Biochem Pharmacol*. 2014. doi:10.1016/j.bcp.2014.02.006

76. Rooseboom M, Commandeur JNM, Floor GC, Rettie AE, Vermeiden NPE. Selenoxidation by flavin-containing monooxygenases as a novel pathway for β-elimination of selenocysteine Se-conjugates. *Chem Res Toxicol*. 2001. doi:10.1021/tx0001326

77. Gut I, Conney AH. Trimethylamine N-oxygenation and N-demethylation in rat liver microsomes. *Biochem Pharmacol*. 1993;46(2):239-244. doi:10.1016/0006-2952(93)90409-P

78. Suh JK, Poulsen LL, Ziegler DM, Robertus JD. Yeast flavin-containing monooxygenase generates oxidizing equivalents that control protein folding in the endoplasmic reticulum. *Proc Natl Acad Sci U S A*. 1999;96(6):2687-2691. doi:10.1073/pnas.96.6.2687

79. Krueger SK, Williams DE. Mammalian flavin-containing monooxygenases: Structure/function, genetic polymorphisms and role in drug metabolism. *Pharmacol Ther*. 2005. doi:10.1016/j.pharmthera.2005.01.001

80. Huang S, Howington MB, Dobry CJ, Evans CR, Leiser SF. Flavin-Containing Monooxygenases Are Conserved Regulators of Stress Resistance and Metabolism. *Front Cell Dev Biol*. 2021;9. doi:10.3389/fcell.2021.630188

81. Hernandez D, Janmohamed A, Chandan P, Phillips IR, Shephard EA. Organization and evolution of the flavin-containing monooxygenase genes of human and mouse: Identification of novel gene and pseudogene clusters. *Pharmacogenetics*. 2004;14(2):117-130. doi:10.1097/00008571-200402000-00006

82. Petalcorin MIR, Joshua GW, Agapow P-M, Dolphin CT. The fmo genes of Caenorhabditis elegans and C. briggsae: characterisation, gene expression and comparative genomic analysis. *Gene*. 2005;346:83-96. doi:10.1016/J.GENE.2004.09.021

83. Swindell WR. Genes and gene expression modules associated with caloric restriction and aging in the laboratory mouse. *BMC Genomics*. 2009. doi:10.1186/1471-2164-10-585

84. Steinbaugh MJ, Sun LY, Bartke A, Miller RA. Activation of genes involved in xenobiotic metabolism is a shared signature of mouse models with extended lifespan. *Am J Physiol Metab*. 2012. doi:10.1152/ajpendo.00110.2012

85. Scott F, Gonzalez Malagon SG, O'Brien BA, et al. Identification of flavin-containing monooxygenase 5 (FMO5) as a regulator of glucose homeostasis and a potential sensor of gut bacteria. *Drug Metab Dispos*. 2017. doi:10.1124/dmd.117.076612

86. Veeravalli S, Omar BA, Houseman L, et al. The phenotype of a flavin-containing monooyxgenase knockout mouse implicates the drug-metabolizing enzyme FMO1 as a novel regulator of energy balance. *Biochem Pharmacol*. 2014. doi:10.1016/j.bcp.2014.04.007

87. Miao J, Ling A V., Manthena P V., et al. Flavin-containing monooxygenase 3 as a potential player in diabetes-associated atherosclerosis. *Nat Commun*. 2015;6. doi:10.1038/ncomms7498

88. Dever JT, Elfarra AA. In vivo metabolism of L-methionine in mice: Evidence for stereoselective formation of methionine-d-sulfoxide and quantitation of other major metabolites. *Drug Metab Dispos*. 2006;34(12):2036-2043. doi:10.1124/dmd.106.012104

89. Schugar RC, Shih DM, Warrier M, et al. The TMAO-Producing Enzyme Flavin-Containing Monooxygenase 3 Regulates Obesity and the Beiging of White Adipose Tissue. *Cell Rep*. 2017;19(12):2451-2461. doi:10.1016/j.celrep.2017.05.077

90. Uno M, Honjoh S, Matsuda M, et al. A Fasting-Responsive Signaling Pathway that Extends Life Span in C. elegans. *Cell Rep*. 2013;3(1):79-91. doi:10.1016/j.celrep.2012.12.018

91. Shen C, Nettleton D, Jiang M, Kim SK, Powell-Coffman JA. Roles of the HIF-1 hypoxia-inducible factor during hypoxia response in Caenorhabditis elegans. *J Biol Chem*. 2005;280(21):20580-20588. doi:10.1074/jbc.M501894200

92. Sánchez López de Nava A, Raja A. *Physiology, Metabolism*. StatPearls Publishing; 2020. http://www.ncbi.nlm.nih.gov/pubmed/31536296. Accessed May 22, 2022.

93. Roberts SB, Rosenberg I. Nutrition and aging: Changes in the regulation of energy metabolism with aging. *Physiol Rev*. 2006;86(2):651-667. doi:10.1152/physrev.00019.2005

94. Houtkooper RH, Williams RW, Auwerx J. Metabolic Networks of Longevity. *Cell*. 2010. doi:10.1016/j.cell.2010.06.029

95. Pinu FR, Beale DJ, Paten AM, et al. Systems biology and multi-omics integration: Viewpoints from the metabolomics research community. *Metabolites*. 2019;9(4):76. doi:10.3390/metabo9040076

96. Salzer L, Witting M. Quo vadis caenorhabditis elegans metabolomics-A review of current methods and applications to explore metabolism in the nematode. *Metabolites*. 2021;11(5). doi:10.3390/metabo11050284

97. Beydoun S, Choi HS, Dela-Cruz G, et al. An alternative food source for metabolism and longevity studies in Caenorhabditis elegans. *Commun Biol*.

2021;4(1). doi:10.1038/s42003-021-01764-4

98. Qi B, Kniazeva M, Han M. A vitamin-B2-sensing mechanism that regulates gut protease activity to impact animal's food behavior and growth. *Elife*. 2017. doi:10.7554/elife.26243

99. Virk B, Jia J, Maynard CA, et al. Folate Acts in E. coli to Accelerate C. elegans Aging Independently of Bacterial Biosynthesis. *Cell Rep*. 2016. doi:10.1016/j.celrep.2016.01.051

100. Kim OD, Rocha M, Maia P. A Review of Dynamic Modeling Approaches and Their Application in Computational Strain Optimization for Metabolic Engineering. *Front Microbiol*. 2018;9:1690. doi:10.3389/fmicb.2018.01690

101. Locasale JW. Serine, glycine and one-carbon units: Cancer metabolism in full circle. *Nat Rev Cancer*. 2013. doi:10.1038/nrc3557

102. Cabreiro F, Au C, Leung KY, et al. Metformin retards aging in C. elegans by altering microbial folate and methionine metabolism. *Cell*. 2013. doi:10.1016/j.cell.2013.02.035

103. Kabil H, Kabil O, Banerjee R, Harshman LG, Pletcher SD. Increased transsulfuration mediates longevity and dietary restriction in Drosophila. *Proc Natl Acad Sci*. 2011. doi:10.1073/pnas.1102008108

104. Menendez JA, Joven J. One-carbon metabolism: An aging-cancer crossroad for the gerosuppressant metformin. *Aging (Albany NY)*. 2012.

105. Lionaki E, Ploumi C, Tavernarakis N. One-Carbon Metabolism: Pulling the Strings behind Aging and Neurodegeneration. *Cells*. 2022;11(2). doi:10.3390/cells11020214

106. Varela-Moreiras G, Perez-Olleros L, Garcia-Cuevas M, Ruiz-Roso B. Effects of ageing on folate metabolism in rats fed a long-term folate deficient diet. *Int J Vitam Nutr Res*. 1994;64(4):294-299.

107. Bahous RH, Cosín-Tomás M, Deng L, et al. Early Manifestations of Brain Aging in Mice Due to Low Dietary Folate and Mild MTHFR Deficiency. *Mol Neurobiol*. 2019;56(6):4175-4191. doi:10.1007/s12035-018-1375-3

108. Challet E, Dumont S, Mehdi MKM, et al. Aging-like circadian disturbances in folate-deficient mice. *Neurobiol Aging*. 2013;34(6):1589-1598. doi:10.1016/j.neurobiolaging.2012.11.021

109. Lemon JA, Boreham DR, Rollo CD. A complex dietary supplement extends longevity of mice. *Journals Gerontol - Ser A Biol Sci Med Sci*. 2005;60(3):275-279. doi:10.1093/gerona/60.3.275

110. Virk B, Correia G, Dixon DP, et al. Excessive folate synthesis limits lifespan in the C. elegans: E. coli aging model. *BMC Biol*. 2012;10(1):67. doi:10.1186/1741-7007-10-67

111. Annibal A, George Tharyan R, Fides Schonewolff M, et al. Regulation of the one carbon folate cycle as a shared metabolic signature of longevity. doi:10.1038/s41467-021-23856-9

112. Parkhitko AA, Jouandin P, Mohr SE, Perrimon N. Methionine metabolism and methyltransferases in the regulation of aging and lifespan extension across species. *Aging Cell*. 2019;18(6). doi:10.1111/acel.13034

113. Obata F, Miura M. Enhancing S-adenosyl-methionine catabolism extends Drosophila lifespan. *Nat Commun*. 2015;6(1):1-9. doi:10.1038/ncomms9332

114. Hansen M, Hsu A-L, Dillin A, Kenyon C. New Genes Tied to Endocrine, Metabolic, and Dietary Regulation of Lifespan from a Caenorhabditis elegans Genomic RNAi Screen. Kim S, ed. *PLoS Genet*. 2005;1(1):e17. doi:10.1371/journal.pgen.0010017

115. Chen CC, Lim CY, Lee PJ, Hsu AL, Ching TT. S-adenosyl methionine synthetase SAMS-5 mediates dietary restriction-induced longevity in Caenorhabditis elegans. *PLoS One*. 2020;15(11 November). doi:10.1371/journal.pone.0241455

116. Ostrakhovitch EA, Tabibzadeh S. Homocysteine and age-associated disorders. *Ageing Res Rev*. 2019;49:144-164. doi:10.1016/j.arr.2018.10.010

117. Sbodio JI, Snyder SH, Paul BD. Regulators of the transsulfuration pathway. *Br J Pharmacol*. 2019;176(4):583-593. doi:10.1111/bph.14446

118. Lee HJ, Noormohammadi A, Koyuncu S, et al. Prostaglandin signals from adult germline stem cells delay somatic ageing of Caenorhabditis elegans. *Nat Metab*. 2019;1(8):790-810. doi:10.1038/s42255-019-0097-9

119. Wei Y, Kenyon C. Roles for ROS and hydrogen sulfide in the longevity response to germline loss in Caenorhabditis elegans. *Proc Natl Acad Sci U S A*. 2016;113(20):E2832-E2841. doi:10.1073/pnas.1524727113

120. Wilkie SE, Borland G, Carter RN, Morton NM, Selman C. Hydrogen sulfide in ageing, longevity and disease. *Biochem J*. 2021;478(19):3485-3504. doi:10.1042/BCJ20210517

121. Bazopoulou D, Knoefler D, Zheng Y, et al. Developmental ROS individualizes organismal stress resistance and lifespan. *Nature*. 2019;576(7786):301-305. doi:10.1038/s41586-019-1814-y

122. Okumura M, Saiki M, Yamaguchi H, Hidaka Y. Acceleration of disulfide-coupled protein folding using glutathione derivatives. *FEBS J*. 2011;278(7):1137-1144.

doi:10.1111/j.1742-4658.2011.08039.x

123. Castro-Portuguez R, Sutphin GL. Kynurenine pathway, NAD+ synthesis, and mitochondrial function: Targeting tryptophan metabolism to promote longevity and healthspan. *Exp Gerontol*. 2020;132:110841. doi:10.1016/j.exger.2020.110841

124. Newman AC, Maddocks ODK. One-carbon metabolism in cancer. *Br J Cancer*. 2017;116(12):1499-1504. doi:10.1038/bjc.2017.118

125. Schwarcz R, Bruno JP, Muchowski PJ, Wu HQ. Kynurenines in the mammalian brain: When physiology meets pathology. *Nat Rev Neurosci*. 2012;13(7):465-477. doi:10.1038/nrn3257

126. Sutphin GL, Backer G, Sheehan S, et al. Caenorhabditis elegans orthologs of human genes differentially expressed with age are enriched for determinants of longevity. *Aging Cell*. 2017. doi:10.1111/acel.12595

127. Van Der Goot AT, Zhu W, Vázquez-Manrique RP, et al. Delaying aging and the aging-associated decline in protein homeostasis by inhibition of tryptophan degradation. *Proc Natl Acad Sci U S A*. 2012. doi:10.1073/pnas.1203083109

128. Katsyuba E, Mottis A, Zietak M, et al. De novo NAD+ synthesis enhances mitochondrial function and improves health. *Nature*. 2018;563(7731):354-359. doi:10.1038/s41586-018-0645-6

129. Edwards C, Canfield J, Copes N, et al. Mechanisms of amino acid-mediated lifespan extension in Caenorhabditis elegans. *BMC Genet*. 2015;16(1):8. doi:10.1186/s12863-015-0167-2

130. Lee SK. Endoplasmic Reticulum Homeostasis and Stress Responses in Caenorhabditis elegans. *Prog Mol Subcell Biol*. 2021;59:279-303. doi:10.1007/978-3-030-67696-4_13

131. Kirstein-Miles J, Morimoto RI. Caenorhabditis elegans as a model system to study intercompartmental proteostasis: Interrelation of mitochondrial function, longevity, and neurodegenerative diseases. *Dev Dyn*. 2010;239(5):1529-1538. doi:10.1002/dvdy.22292

132. Nussbaum-Krammer CI, Morimoto RI. Caenorhabditis elegans as a model system for studying non-cellautonomous mechanisms in protein-misfolding diseases. *DMM Dis Model Mech*. 2014;7(1):31-39. doi:10.1242/dmm.013011

133. Shen X, Ellis RE, Sakaki K, Kaisfman RJ. Genetic interactions due to constitutive inducible gene regulation mediated by the unfolded protein in C. *PLoS Genet*. 2005;1(3):355-368. doi:10.1371/journal.pgen.0010037

134. Adams CJ, Kopp MC, Larburu N, Nowak PR, Ali MMU. Structure and molecular mechanism of ER stress signaling by the unfolded protein response signal

activator IRE1. *Front Mol Biosci*. 2019;6(MAR):11. doi:10.3389/fmolb.2019.00011

135. Henis-Korenblit S, Zhang P, Hansen M, et al. Insulin/IGF-1 signaling mutants reprogram ER stress response regulators to promote longevity. *Proc Natl Acad Sci U S A*. 2010;107(21):9730-9735. doi:10.1073/pnas.1002575107

136. Taylor RC, Dillin A. XBP-1 Is a cell-nonautonomous regulator of stress resistance and longevity. *Cell*. 2013;153(7):1435. doi:10.1016/j.cell.2013.05.042

137. Jo H, Shim J, Lee JH, Lee J, Kim JB. IRE-1 and HSP-4 Contribute to Energy Homeostasis via Fasting-Induced Lipases in C. elegans. *Cell Metab*. 2009;9(5):440-448. doi:10.1016/j.cmet.2009.04.004

138. Chen D, Thomas EL, Kapahi P. HIF-1 Modulates Dietary Restriction-Mediated Lifespan Extension via IRE-1 in Caenorhabditis elegans. Mango SE, ed. *PLoS Genet*. 2009;5(5):e1000486. doi:10.1371/journal.pgen.1000486

139. Hou NS, Gutschmidt A, Choi DY, et al. Activation of the endoplasmic reticulum unfolded protein response by lipid disequilibrium without disturbed proteostasis in vivo. *Proc Natl Acad Sci U S A*. 2014;111(22):E2271-80. doi:10.1073/pnas.1318262111

Chapter II

An Alternative Food Source for Metabolism and Longevity Studies in *Caenorhabditis elegans*

Foreword

The work shown in this chapter is from a published manuscript in the peer-reviewed journal, *Communications Biology*. My co-author Dr. Safa Beydoun and I have equally contributed to obtaining and analyzing the experimental data and writing the manuscript under the supervision of my mentor Dr. Leiser. The contributions of other co-authors are listed at the end of the chapter under the Author Contributions section.

Since my thesis focuses on determining the metabolic mechanism by which *fmo-2* promotes longevity and health in *C. elegans*, the first logical step was to figure out a way to stop bacterial metabolism to prevent confounding results. Unfortunately, the existing methods of killing bacteria were not adequate as mentioned in Chapter I. My mentor Dr. Leiser hypothesized that using paraformaldehyde (PFA), a chemical that is commonly used as a crosslinker, could stop bacterial metabolism without damaging the bacterial cellular structure to keep bacteria edible for worms. To test this hypothesis, Dr. Beydoun and I tested various concentrations of PFA to determine the minimal dose to effectively kill bacteria while maintaining them in an edible state. Using the resulting

optimal dose range, we tested lifespan and healthspan phenotypes to ensure that PFA treatment does not cause substantial changes to worm phenotypes. Overall, we find that PFA treatment is a viable way to stop bacterial metabolism and can be used in metabolic studies. The contributions of other co-authors are listed at the end of the chapter under the Authors Contribution section.

Abstract

Caenorhabditis elegans is an instrumental research model used to advance our knowledge in areas including development, metabolism and aging. However, research on metabolism and/or other measures of health/aging are confounded by the nematode's food source in the lab, live *E. coli* bacteria. Commonly used treatments, including ultraviolet irradiation and antibiotics, are successful in preventing bacterial replication, but the bacteria can remain metabolically active. The purpose of this study is to develop a metabolically inactive food source for the worms that will allow us to minimize the confounding effects of bacterial metabolism on worm metabolism and aging. Our strategy is to use a paraformaldehyde (PFA) treated *E. coli* food source and to determine its effects on worm health, metabolism and longevity. We initially determine the lowest possible concentrations of PFA necessary to rapidly and reproducibly kill bacteria. We then measure various aspects of worm behavior, healthspan and longevity, including growth rate, food attraction, brood size, lifespan and metabolic assessments, such as oxygen consumption and metabolomics. Our resulting data show that worms eat and grow well on these bacteria and support the use of 0.5% PFA-killed bacteria as a nematode food source for metabolic, drug and longevity experiments.

Introduction

Caenorhabditis elegans has a rich history as a model organism used in research in genetics, developmental biology and aging. As a model organism, *C. elegans* is a useful tool for studying these aspects of biology, as worms quickly multiply due to their short development cycles and hermaphroditic (self) reproduction[1,2]. Importantly, *C. elegans* share genetic conservation to humans, leading to surprisingly high translational potential for nematode studies[3]. Due to this conservation, multiple studies have used the screening potential of nematodes to understand the implications of drugs and small molecules on various aspects of physiology[4,5].

Recent work has also begun measuring *C. elegans* metabolism through metabolomics, a comprehensive measurement of hundreds of thousands of small molecules and metabolites in biological samples[6,7]. In a typical lab setting, *C. elegans* are fed live *Escherichia coli* OP50. This standard food source can confound metabolic and drug studies since the live bacteria have their own metabolism and can metabolize drugs and other compounds being studied. It is even possible for small compounds to affect the bacteria themselves before affecting the worms, as was observed when studying the effects of metformin on *C. elegans*[8]. Because of the confounding effects of bacterial metabolism, there is great interest in the use of metabolically inactive (dead) bacteria in these types of studies.

Multiple procedures for killing bacteria have been previously reported[9–12]. Ultraviolet (UV) irradiation is one of the most widely used methods for killing OP50 in *C. elegans* studies.

UV-killing generally involves exposing plates seeded with live OP50 to UV using a Crosslinker[13]. While UV-killing is relatively simple and an easy procedure, it is low throughput and inconsistent. The number of plates that can be exposed at a time is limited by the size of the UV Crosslinker, hampering the rate at which these plates can be treated. After OP50 is UV-treated, a representative plate from each batch can be used to test for growth by streaking out a sample of the UV-treated bacteria on LB agar plates and incubating overnight at 37ºC. In practice, some plates show growth even after the treatment, and these could be missed when sampling a small portion of the lawn or plates in different parts of the crosslinker. For small studies, testing each plate is possible and likely successful, but for larger reproducible studies the procedure is laborious and impractical. Furthermore, while the reproductive death of OP50 is confirmed in many studies, the metabolic activity of these treated bacteria is not verified using available tools, such as Seahorse® respirometers[14]. Thus, it is unclear whether UV-treated bacteria still have intrinsic metabolic activity that can confound the types of experiments mentioned above. Another method of killing OP50 uses heat, where the bacterial culture is exposed to high heat (>60°C) before being seeded on agar plates[9]. Growing worms on heat-killed OP50 is reportedly challenging, as heat destroys some of the necessary nutrients for the worms to develop and renders the bacteria less edible, causing the worms to arrest at early development[9]. Antibiotic treatment has also been used to kill OP50[10], but these methods are potentially confounding for experiments, as the antibiotics can have effects on worm growth and metabolism[15].

To overcome the challenges of bacterial metabolism in *C. elegans* studies, here we optimize a new method to kill the bacteria using paraformaldehyde. Paraformaldehyde (PFA), a polymer of formaldehyde, has been used in the literature as a tool to crosslink proteins and create a mesh-like structure inside the cell[16]. PFA is an organic solution that permeabilizes the cells, making them no longer viable, without lysing or destroying the inner structure, specifically the plasma membrane[17]. Maintaining an intact cell structure when killing the bacteria is crucial in keeping the bacteria edible for the worms. We find that treating bacteria with 0.5% PFA for 1 hour prevents growth and respiration, and thus allows for more reproducible metabolic studies in the nematode *C. elegans.*

Results

Developing a high-throughput method to consistently kill bacteria has become necessary for the growing field of metabolic and drug studies in *C. elegans* research. We hypothesized that paraformaldehyde could be a potent tool to neutralize bacterial growth and metabolism, while keeping the overall structure of the bacteria intact and thus easy for worms to eat. To test this, we optimized a protocol using bacterial exposure to paraformaldehyde as a method to prevent bacterial growth and metabolism by determining the lowest concentration of PFA and shortest amount of time necessary to consistently kill the bacteria (**Table 2.1**). Details of the methodology are illustrated in **Figure 2.1**.

We treated *E. coli* OP50 bacteria with PFA at multiple concentrations over multiple exposure durations. In each of the PFA treatment conditions tested, we assessed for

ability of the treated bacteria to replicate by streaking the bacteria on a lysogeny broth plate and for their metabolic activity by measuring oxygen consumption rate and extracellular acidification rate. We determined that treating the bacteria with 0.5% PFA for a 1-hour period was optimal for killing the bacteria.

To test if PFA-treated OP50 is replicatively dead, we struck out the concentrated bacteria aliquots on an LB plate and incubated at 37ºC overnight. As shown in **Figure S2.1,** we did not observe any growth of PFA-treated OP50.

Paraformaldehyde treatment of bacteria prevents replication and metabolic activity

Having established our protocol, we next sought to determine if treating *E. coli* OP50 with paraformaldehyde (PFA) would prevent replication. While ultraviolet (UV) treatment of *E. coli* bacteria is reported to inhibit bacterial replication, the protocols for replicative killing of bacteria under UV-irradiation are inconsistent, making it necessary to assess multiple UV treatments for bacterial growth[13]. We used viable plate count assays to compare the reproductive capacity of PFA-treated bacteria and UV-treated bacteria with their untreated control bacteria. We found that UV-treated bacteria have variability in the efficacy of replicative arrest (**Figure 2.2a, Figure S2.2a**), where two replicates under identical conditions resulted in different viable plate count results, consistent with previous observations that UV treatment does not prevent replication consistently[13]. In contrast, we consistently found no replication in *E. coli* treated with PFA at both 0.25% and 0.5% concentrations (**Figure 2.2a**). When comparing live and mock-treated OP50

conditions, we did not see any difference in CFU (**Figure 2.2a**). The comparison between the live and mock-treated conditions controls for any phenotypic changes that may occur due to the additional washing steps that were carried out for the PFA conditions to remove residual PFA from the culture.

We next sought to determine if treating *E. coli* OP50 with PFA would kill the bacteria metabolically. We used the Seahorse® XF96 respirometer to run real-time measurements of the oxygen consumption (OCR) and extracellular acidification rates (ECAR)[18] of our bacteria conditions. OCR is an indicator of bacterial respiration, and ECAR is an indicator for glycolytic activity. Control and treated bacteria were plated onto a 96-well plate and their basal oxygen consumption was measured at 37^{o}C with a sensor cartridge that included individual sensor probes to obtain OCR. After obtaining basal OCR measurements, additional steps were followed to obtain ECAR measurements, which included the addition of glucose (to induce glycolysis), oligomycin (to inhibit ATP synthase activity) and 2-deoxy-glucose (2-DG) (to inhibit glycolysis). We found that both the UV-treated and the PFA-treated conditions showed minimal OCR, suggesting that these bacteria do not have functional metabolic activity to undergo respiration (**Figure 2.2b**). Similarly, we detected minimal ECAR for the killed conditions compared to the live and mock-treated OP50 control groups (**Figure 2.2c**). Consistent with what we observed with the viable plate count experiment, we found that different replicates yield inconsistent basal OCR level for the UV-treated conditions, further supporting the inconsistency of the UV-killing method (**Figure S2.2b**). We also treated the HB101 strain of *E. coli* and the

pathogenic bacteria *Enterococcus faecalis* with PFA and found that it is effective in killing both types of bacteria consistently (**Figure 2.2d-e, Figure S2.3**).

PFA-treated bacteria are metabolically different than live and mock-treated bacteria

Separating bacterial metabolism from worm metabolism is essential for removing the confounding effects of bacterial metabolism in metabolomics experiments[19]. We next sought to determine if feeding either of the killed conditions would differentiate the worm metabolome from worms grown on live and mock-treated bacteria. Principal component analysis (PCA) using untargeted metabolomics data (**Data S2.1**) suggests that the metabolome of worms grown on bacteria treated with PFA is different from that of worms grown on live and mock-treated OP50 conditions (**Figure 2.3a**). We also performed partial least squares discriminant analysis (PLS-DA) to determine which metabolites are being altered by PFA treatment (**Figure 2.3b**). Of the 3,284 metabolic features that were captured in our metabolomics analysis, more than one third of them (1,349) had Variable Importance in Projection (VIP) score of greater than 1 in component 1 (**Figures 2.3c, Data S2.2**), suggesting that there may be systemic alterations in the metabolome when eating PFA-treated bacteria. In order to determine if these effects were solely due to changes resulting from the PFA treatment, we performed PLS-DA to compare worms grown on live OP50 to mock-treated OP50, live OP50 to UV-treated OP50, and mock-treated OP50 to PFA-treated OP50. There were 1,211 metabolic features with VIP score of greater than 1 when comparing worms on live OP50 to those on mock-treated OP50, 1,426 modified metabolic features when comparing mock-treated OP50 to those on PFA-

treated OP50, and 1,172 modified metabolic features when comparing worms on live OP50 to those on UV-treated OP50 (**Data S2.2**). These results suggest that the worm metabolome is highly sensitive to any changes in bacterial conditions. We then used a targeted metabolomics approach to identify metabolites whose abundance level is directly affected by the PFA treatment. Using a panel of 95 known metabolites, our targeted metabolomics analysis (**Data S2.3**) shows that there are significant differences in the abundance level of 25 metabolites in the worms grown on 0.25% PFA-treated bacteria and of 27 metabolites in the worms grown on 0.5% PFA-treated bacteria compared to the worms grown on mock-treated bacteria (**Figure 2.3d, Data S2.4**). Pathway analyses on MetaboAnalyst using these significantly different metabolites reveal that phenylalanine, tyrosine and tryptophan biosynthesis, phenylalanine metabolism, aminoacyl-tRNA biosynthesis, and arginine and proline metabolism are all enriched in the worms grown on 0.25% and 0.5% PFA-treated bacteria (**Figures 2.3e and 2.3f, Data S2.5**). Previous studies show that formaldehyde can react with multiple nucleophiles to form a Schiff-base, which can then react with another nucleophile to produce a crosslinked product[20]. *In vivo*, formaldehyde reactions are studied mainly in the context of protein and DNA bases[20]. The amino acid that most commonly reacts with formaldehyde is lysine, which can then crosslink with other amino acids, DNA bases, or small molecules[20]. Indeed, lysine abundance was significantly reduced in the worms grown on 0.25% and 0.5% PFA-treated OP50 **(Data S2.3)**. These findings support our data suggesting that paraformaldehyde treatment, like other treatments including just washing bacteria, can have a systemic effect on the metabolome.

We hypothesized that while PFA treatment may effectively kill bacteria, there could be a downside in that worms could sense the differences in metabolites, leading to a reduced food preference for PFA-treated bacteria compared to live and mock-treated bacteria. Therefore, we were interested in determining if worms were still attracted to bacteria after they were treated with PFA. Our data suggest that worms are still attracted to PFA-treated OP50, as most of the worms remained on the bacterial lawn rather than off of the food (**Figure S2.4**).

After we determined that the worms were attracted to the PFA-treated OP50, we asked whether *C. elegans* show food preference between PFA-treated and live food. We tested for preference between the different groups of treated OP50 using a sensitive pairwise assay[21] as shown in **Figure 2.4a**. *C. elegans* exhibited a preference for live and mock-treated bacterial conditions over PFA-treated bacteria (**Figure 2.4b-e**). This may be due to either the chemo-attractants synthesized by the live and mock-treated bacteria being no longer made in PFA-treated food[22], or the worms may be repulsed by PFA. We found that the worms are not repulsed by any possible residual PFA (**Figure S2.5**), and consistent with the hypothesis that PFA-treated food lacks chemo-attractants, the worms exhibited preference for the live conditions compared to any of the treated-bacterial conditions (**Figure S2.6**).

PFA treatment does not affect lifespan and fecundity but slightly delays development compared to live conditions

Previous studies show that different food conditions physiologically affect worms[9,23]. We next sought to determine the physiological effects of PFA-treated bacteria on *C. elegans*. We first measured brood size to compare the egg-laying capacity of the worms fed PFA-treated OP50 to those fed untreated OP50. We observed no significant difference in the brood size between worms grown on the live and PFA-treated OP50 bacteria (**Figure 2.5a**). However, we did observe a small, but significant decrease in the brood size between the mock-treated OP50 and the PFA-treated conditions (**Figure 2.5a**).

We next asked if PFA-treated bacteria affect the developmental rate of worms. We performed time-of-flight (TOF) analysis using the COPAS Biosorter on synchronized worms. The Biosorter is a flow cytometer that can sort worms based on their length and optical density[24]. We found that L4 worms grown on the PFA-treated OP50 bacteria showed reduced TOF, suggesting that their population is smaller in size (**Figure 2.5b and Figure S2.7**). Development time quantification (**Figure 2.5c**) also showed that PFA-treated bacteria delayed development of worms by approximately 4-5 hours. However, we found that the worms grown on the PFA-treated bacteria catch up in size to the worms grown on the live OP50 condition in young adulthood (**Figures 2.5d and 2.5e**).

Since we observed a slight delay in development, we were interested to see whether PFA treatment has an effect on longevity in worms. To address this, we measured worm lifespan on control and PFA-treated bacteria. We found that the lifespan of worms grown on the PFA-treated bacteria were not significantly different compared to their counterparts

grown on live or mock-treated bacteria, suggesting that PFA-treated bacteria do not substantially affect the lifespan of the worms (**Figure 2.5f, Table 2.2**).

Discussion

The use of killed bacteria is important in nematode studies that deal with metabolism and drugs. The metabolome of live bacteria is a potential confounder in these studies[8,9,19]. Multiple methods have been used in such studies, including UV irradiation and exposing the bacteria to heat or to antibiotics[9,10,13], but these techniques have various limitations. The UV method is low-throughput and inconsistent[13]. To appropriately use the UV-treatment that we have referred to in this manuscript, one would have to test each individual NGM plate after treating it with UV light. While this may be feasible for some types of experiments, it is impractical to do so in experiments where there is a need to prepare hundreds of plates (e.g. lifespans). Heat-killed bacteria lose their structure and become less palatable to the worm. Antibiotics prevent the bacteria from replicating but leave them metabolically active while also affecting the worms[14].

We have optimized a new method to kill bacteria for metabolic studies using PFA. Unlike the inconsistency seen with the UV-treated bacteria, PFA consistently kills the bacteria. PFA-treated OP50 is prepared in large quantities, allowing for use over long or multiple experiments. While we find substantial metabolic changes in worms consuming PFA-treated bacteria, the changes are similar in scope and number to changes observed when UV-treating or washing bacteria, suggesting that any alteration to the food source greatly

affects the worm metabolome. The worms consume the PFA-treated bacteria well, leading to only a slight developmental delay, contrary to heat-killed bacteria[9]. However, worms have a significant preference to live bacteria compared with PFA-treated bacteria, plausibly due to sensing the metabolic activity and related chemo-attractants in live OP50. While treating the bacteria with PFA slightly delays worm development as compared to live conditions, it does not have a significant effect on brood size or lifespan, suggesting the worms are generally healthy. Considering the lack of metabolic activity associated with PFA-killed bacteria, it is anticipated that this bacterial condition will also be useful in conducting drug and toxicity assays in *C. elegans,* and we are currently deploying this technique for studies of this nature in our own laboratory.

Materials and Methods

Strain and Growth Conditions

Standard *Caenorhabditis elegans* cultivation procedures were followed as previously described[11,12]. N2 wild type worms were maintained on nematode growth media (NGM) and housed in a 20°C Percival incubator.

Food Source

Animals were fed live and treated OP50 *E. coli,* HB101 *E. coli*, or *Enterococcus faecalis.* A single colony of bacteria was inoculated in 400 mL lysogeny broth (LB) and cultured overnight (18 hours) in a 37^{o}C shaking incubator. The bacteria were transferred to 50 mL conical tubes and centrifuged at 3000 x g for 20 min, then concentrated 5X or 10X and seeded as live bacteria. We refer to this standard plated and untreated condition as “live”

condition. For OP50, some of these plates were used to make the UV conditions 24 hours after seeding by exposing the plates to UV (9999* 100 μJ/cm^2) for 5 or 10 minutes using a UV Crosslinker (CL-600 Ultraviolet Crosslinker, UVP, USA). For the paraformaldehyde (Electron Microscopy Sciences, cat # 15714-S) treated bacteria, reference the "Paraformaldehyde Treatment of Bacteria" section of the Materials and Methods for details. The same method without paraformaldehyde treatment is followed for the mock-treated condition as a control group for the PFA treatment.

Paraformaldehyde Treatment of Bacteria

After culturing, 50 mL of the bacteria were aliquoted into 250 mL Erlenmeyer flasks. 32% PFA was added to the flasks to get the desired final PFA concentration (e.g., 390 μL of PFA was added to get the final concentration of 0.25% PFA). PFA-treated bacteria were shaken at 37^{o}C in a shaking incubator at 200 rpm for 1 hour to allow for even mixing and sufficient exposure to PFA. The treated bacteria were transferred to 50 mL conical tubes using sterile 50 mL serological pipettes and centrifuged at RCF of 3000 x g for 20 minutes. Supernatant was removed and 25 mL of LB was added to the pellet to wash off the PFA. The washing was repeated for a total of five times with centrifugation and removal of the supernatant between each washing step. After the final wash, the treated bacteria were resuspended in either 10 mL (5-fold concentrated, 5X) or 5 mL (10-fold concentrated, 10X) to concentrate the aliquots for lifespan assays (10X) or other downstream applications (5X). The bacteria were seeded on NGM plates and were left to dry for 48 hours before the experiments.

Viable Plate Count Assay

E. coli OP50 bacteria were grown and treated as described above. Each condition of bacteria that was seeded as 10X concentration on NGM plates was transferred to 15 mL conical tubes using M9 and pelleted using a clinical centrifuge. The supernatant was removed via aspiration and the pellet was re-suspended in 250 µL M9 to dilute the concentration back to 10X. 10 µL of the bacteria was serially diluted in 90 µL of LB ten times. 50 µL of the bacterial dilutions were then spread onto solid LB agar plates with a sterile glass rod and incubated in a 37^{o}C incubator overnight. The number of colony-forming units (CFUs) on the plates was determined by counting each colony and multiplying by the total dilution of the solution. Since the same volume of bacteria and wash were used for each condition, it was not necessary to do further normalization. For the UV-treated condition, plates were left to dry for 24 hours before they were treated with UV light. Following the UV treatment, the plates were prepared for the viable plate count assay in the same manner as other conditions.

Seahorse Assay

The Seahorse cartridge was hydrated and calibrated as previously published[18]. *E. coli* OP50 bacteria were grown and treated as described above. Each condition of bacteria seeded as 10X concentration on NGM plates was transferred to 15 mL conical tubes using M9 and pelleted using a clinical centrifuge. The supernatant was removed via aspiration and the pellet was re-suspended in 250 µL M9 to dilute the concentration back to 10X.

Basal Oxygen Consumption 20 µL of the re-suspended bacteria was added to the assay plate containing 180 µL of M9 to bring the concentration down to 1X. After the cartridge calibration completed, the assay plate was inserted in the machine for analysis (Mix, Wait, Measure, and Loop). The results are shown as oxygen consumption rate (OCR).

Glycolytic stress test 20 µL of the re-suspended bacteria was added to the assay plate containing 112 µL of M9. 20 µL of 100mM glucose was added in Port A, 22 µL of 20uM oligomycin was added in Port B and 25 µL of 500 mM 2-DG was added in port C. *Each compound was added in its respective port before calibrating the cartridge*. After the cartridge calibration completed, the assay plate was inserted in the machine for analysis (Equilibrate, Mix, Wait, Measure, Inject (Ports A, B then C), and Loop). The results are shown as OCR and ECAR (Extracellular acidification rate).

Attraction Assays

Food preference assays (four pairs of two bacterial conditions) Food preference assays were conducted as previously described[21] with minor modifications. *E. coli* strain OP50 was cultured overnight at 37°C and treated as described above. 50 µL of two bacterial conditions were seeded side-by-side on standard 60mm NGM plates (total of four pairs). Lawns were placed evenly 1 cm apart from each other and 2 cm from the center of the plate using a template. Nematode cultures were synchronized by washing mixed staged populations from two to three 100 mm NGM plates with M9. They were then treated with 0.3 mL 5 M NaOH and 0.8 mL of 5% sodium hypochlorite solution in 5 mL M9 buffer and vortexed for three minutes to isolate the eggs. Eggs were suspended in approximately 5

mL of M9 buffer in a vented Petri plate and allowed to hatch overnight in the absence of food. Hatched L1 larvae were pelleted in a clinical centrifuge and M9 was aspirated to 2 mL. 50 µL of synchronized L1 culture were seeded in the center of each attraction plate at an equal distance from all bacterial lawns. After 24 hours at 20°C the number of worms in each lawn was counted under a dissecting microscope.

Chemoattraction assays (1, 2, 4 or 8 lawns per plate) *E. coli* strain OP50 was cultured overnight at 37°C, treated as described previously, and 1, 2, 4, or 8 20 µL lawns were seeded on standard 60 mm NGM plates. Lawns were placed 2 cm from the center of the plate using a template. Synchronized nematode cultures were generated as described for food preference assays, and 50 µL were seeded at the center of each plate at an equal distance from all bacterial lawns. After 24 hours at 20°C, the number of worms in each lawn was counted under a dissecting microscope.

Chemotaxis Assay

N2 worms were synchronized by timed egg lay and grown on OP50 seeded plates. Young adult worms were then transferred to empty NGM plates 30 min before the experiment (to allow the worms to crawl out of the food) and then transferred to 35 mm plates seeded with 4 µL of equidistant 1) LB and PFA-containing LB or 2) Live and PFA-treated OP50. Worms were counted and imaged at 30 min and 1 hour to calculate chemotaxis index (# of worms on test condition - # of worms on control condition)/ (total number of worms). An index of -1.0 is an indication of maximum repulsion[25].

Fecundity Assay

Six-hour timed egg lays were conducted on NGM plates seeded with live or treated OP50 and worms were reared to L4 at 20°C. Ten worms per condition were singled onto 35 mm plates with the corresponding food source prior to onset of egg laying. Animals were transferred to fresh plates daily for the first seven days of adulthood to prevent starvation or formation of mixed generation cultures. F1 progeny were counted prior to onset of fertility. Animals that fled the plate before loss of fertility were censored.

Development Assay

Worm sorting

N2 worms were grown on live OP50 until gravid adults and then bleach prepped. 1000 bleach prepped eggs were added to 100 mm plates seeded with control and treated OP50 and were left to grow for ~2.5 days. Worms were then transferred to 15 mL conical tubes and washed with M9 and spun down at 150 x g three times to remove bacteria. After the final wash, the supernatant was aspirated out and the worms were resuspended in 5 mL M9 and transferred to 50 mL conical tubes for sorting. The Biosorter was run according to manufacturer recommendation and was used to determine differences in development between the groups. The extinction signal from the 488 nm laser was used to gate worms at the L4 stage by including ~95% of the control (N2 on live OP50) population. Analysis was based on the relative axial length (TOF, Time of Flight).

Metabolomics

OP50 bacteria were treated as mentioned above and seeded onto 60 mm NGM plates. Approximately 1000 eggs derived from bleaching gravid adults were plated onto each of

these plates and grown until they reached late L4 growth stage. The synchronous population of worms was washed off the plates with 10 mL M9 buffer and transferred to 15 mL conical tubes. The worms were pelleted using a clinical centrifuge for 1 minute at 150 x g and the supernatant was aspirated. The worms were washed twice, once with 10 mL M9 buffer and then with 10 mL 150 mM ammonium acetate to remove phosphates from M9, each time being centrifuged and the supernatant was vacuum aspirated after washing. Subsequently, the pellets were flash frozen in liquid nitrogen.

Metabolites were extracted from pellets by addition of 500 µL of ice-cold 9:1 methanol: chloroform, followed immediately by probe sonication for 30 seconds with a Branson 450 Sonicator. The resulting homogenates were kept on ice for 5 minutes and were then centrifuged for 10 min at 4000 x g at 4°C. Supernatant was then transferred to autosampler vials for analysis. Hydrophilic interaction liquid chromatography-electrospray ionization mass spectrometry (HILIC-LC-ESI -MS) analysis was performed in negative ion mode using an Agilent 1200 LC system coupled to an Agilent 6220 time-of-flight mass spectrometer. Chromatography was performed as previously described[26,27], with the exception that the Phenomenex Luna NH2 column used had dimensions of 150 mm x 1.0 mm ID, the flow rate was 0.07 mL/min, and the injection volume was 10 µL. Untargeted peak detection and alignment was performed using XCMS[28]. The resulting metabolomics data were analyzed using Metaboanalyst 4.0 (http://metaboanalyst.ca). Within Metaboanalyst, the data were median normalized, adjusted using auto scaling, and were then subjected to principal component analysis and partial least squares discriminant analysis using default parameters. Targeted metabolomics analysis used the same LC-MS parameters as untargeted, but data

analysis was performed using Agilent MassHunter Quantitative Analysis software. Metabolites were identified by matching accurate mass and retention time with authentic standards analyzed by the same method. Average peak area values of the blank sample were subtracted from each sample. Statistical analysis for targeted metabolomics data was performed using Metaboanalyst. Within Metaboanalyst, metabolite abundance values were normalized using the “Normalization by a pooled sample from group” option. They were then adjusted using log transformation and range scaling and then subjected to one-way ANOVA and Tukey’s HSD post-hoc test. The heatmap was generated using default parameters. Significant metabolites identified from the statistical analysis were used for pathway analysis using default parameters and nematode pathway library. Metabolites without KEGG ID were removed from the analysis.

Microscopy

N2 worms were synchronized by a timed egg lay on condition plates seeded with live and treated OP50 bacteria. The animals (n=20-25) were allowed to develop and were imaged at L4, day 2 and day 4 of adulthood. Microscope slides were prepared 1 h prior to microscopy with a 3% agar mount. The worms were immobilized in 10 µL of 30 mM sodium azide placed on the agar pad for 2 min. Pictures were taken immediately after slide preparation using a Leica M165FC dissecting microscope. The outline of each worm was traced using ImageJ analysis[29] to obtain area measurements in pixels^2. The pixel calibration formula (camera pixel size in microns/product of all magnifications) was used to calculate the area in µm^2.

Lifespan measurements

Synchronization and preparation of animals for lifespan experiments followed previously published techniques. Briefly, ~ 30 gravid adults were placed on new NGM plates. After 4 hours the gravid adults were removed and the plates with synchronized eggs were placed back in the 20°C incubator until they reached late L4/young adult (~ 2.5 days). From here approximately 75 worms were placed on each NGM plate and transferred to fresh NGM plates once a day for 7 days. A minimum of two plates per strain per condition were used per replicate experiment. Experimental animals were scored every 2-3 days and considered dead when they did not move in response to prodding under a dissection microscope. Worms that crawled off the plate were not considered.

Statistical analyses

One-way ANOVA with Tukey Post-Hoc analysis was used to derive p-values for comparisons such as fecundity and attraction assays. Log-rank test was used to derive p-value for lifespan comparisons. All error bars shown in figures represent the standard error of the mean (SEM) except in figure S6 where standard deviation (SD) was shown.

Author Contributions

S.B., H.S.C. and S.F.L. developed the conceptual framework and wrote the manuscript. S.B., H.S.C., G.D.C., J.K., S.H., D.B., H.A.M., M.L.S., C.R.E. and S.F.L. contributed to data collection and analysis. S.B. and H.S.C. prepared the figures and tables. All authors reviewed and approved the manuscript.

Table 2.1: Growth and metabolism of PFA-Treated bacteria.

PFA (%)	Time	Growth	OCR
0	24 hours	10^7	High
0.25	30 min	10^5	High
0.25	1 hour	10^2	Low
0.25	2 hours	0	None
0.5	30 min	10^2	Low
0.5	1 hour	0	None
0.5	2 hours	0	None
0.75	30 min	0	Low
0.75	1 hour	0	None
0.75	2 hours	0	None

Growth= colony forming units
OCR= Oxygen Consumption
High = >75% of control, Medium = 25-75% of control, Low = <25% of control, None = no difference from blank.
OCR is compared to Mock-Treated OP50

Table 2.2: Summary of Lifespan Data.

		Lifespan (days)			p-value (vs.	p-value (vs. Mock-
Condition	Experiment	Median	Max	n	Live OP50)	Treated OP50)
Live OP50	1	22	35	84	--	--
Mock-Treated OP50	1	22	35	67	0.554	--
0.25% PFA-Treated	1	22	35	88	0.335	0.673
0.5% PFA-Treated	1	22	35	128	0.149	0.447
Live OP50	2	21	36	152	--	--
Mock-Treated OP50	2	21	36	158	0.640	--
0.25% PFA-Treated	2	21	36	162	0.271	0.528
0.5% PFA-Treated	2	23	38	152	0.005	0.020
Live OP50	3	20	35	115	--	--
Mock-Treated OP50	3	22	35	114	0.493	--
0.25% PFA-Treated	3	22	35	99	0.134	0.551
0.5% PFA-Treated	3	22	35	106	0.103	0.378

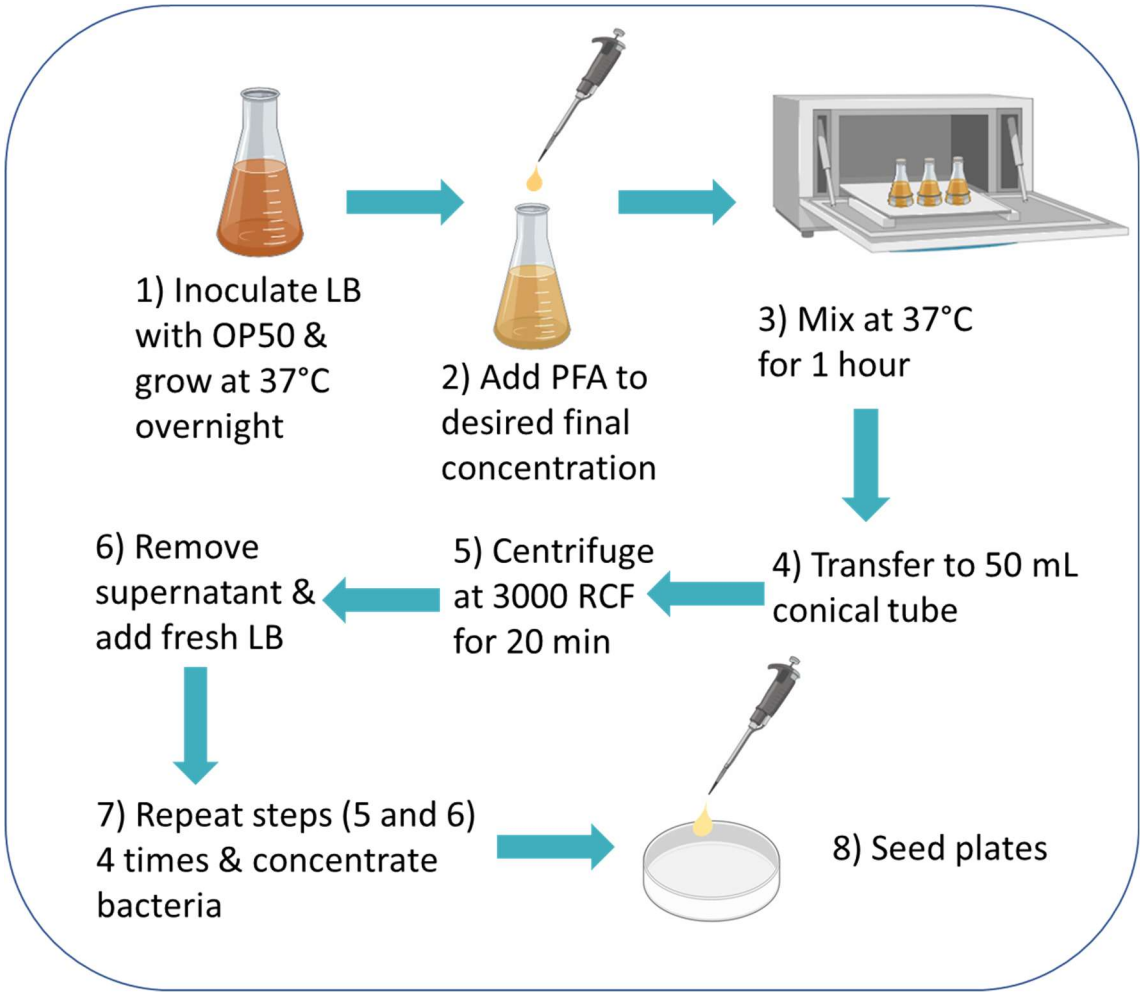

Figure 2.1. Workflow of paraformaldehyde treated OP50. A single colony of *E. coli* OP50 bacteria is inoculated in lysogenic buffer (LB) and cultured overnight (18 hours) in a 37°C shaking incubator. The bacterial culture is then aliquoted into Erlenmeyer flasks and 32% paraformaldehyde (PFA) is added to the aliquots to bring the final PFA concentration down to 0.5%. The PFA-treated bacterial aliquots are then mixed in the 37°C shaking incubator for 1 hour to allow for even mixing and sufficient exposure to PFA. The aliquots are transferred to 50 mL conical tubes and centrifuged at RCF (relative centrifugal force) of approximately 3000 x g (relative centrifugal force) for 20 minutes and washed with 25 mL of LB five times. The aliquots are concentrated 10-fold for lifespan assays and 5-fold for other downstream applications and seeded on the NGM plates.

a

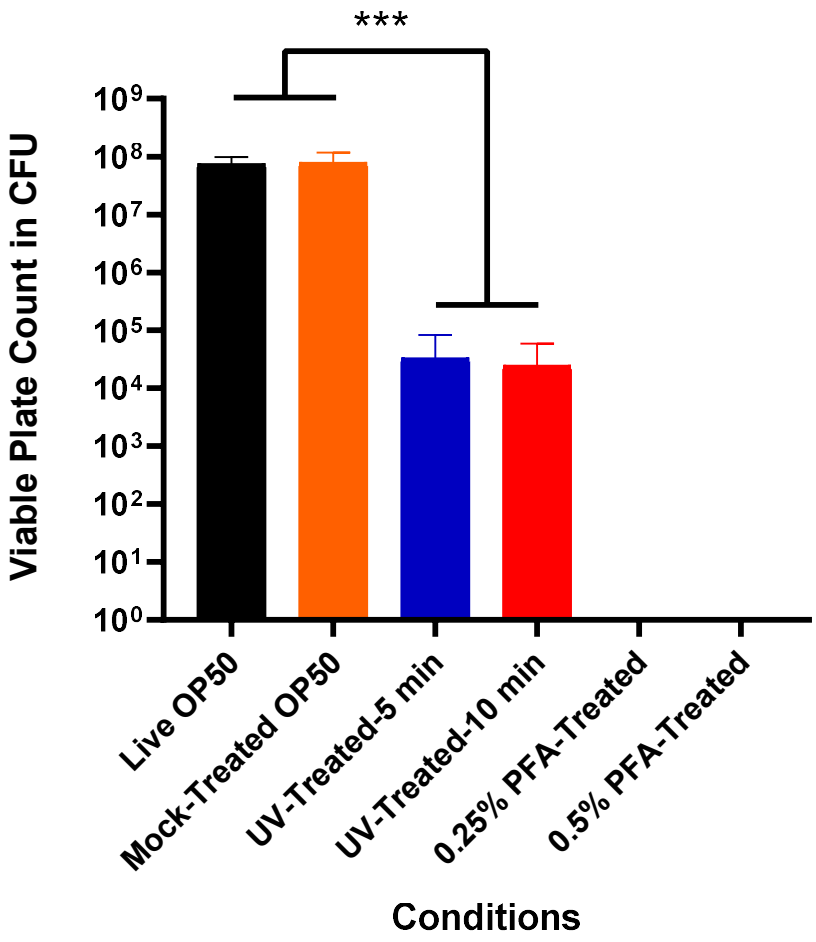
***
Viable Plate Count in CFU
10^9
10^8
10^7
10^6
10^5
10^4
10^3
10^2
10^1
10^0
Live OP50
Mock-Treated OP50
UV-Treated-5 min
UV-Treated-10 min
0.25% PFA-Treated
0.5% PFA-Treated
Conditions

b

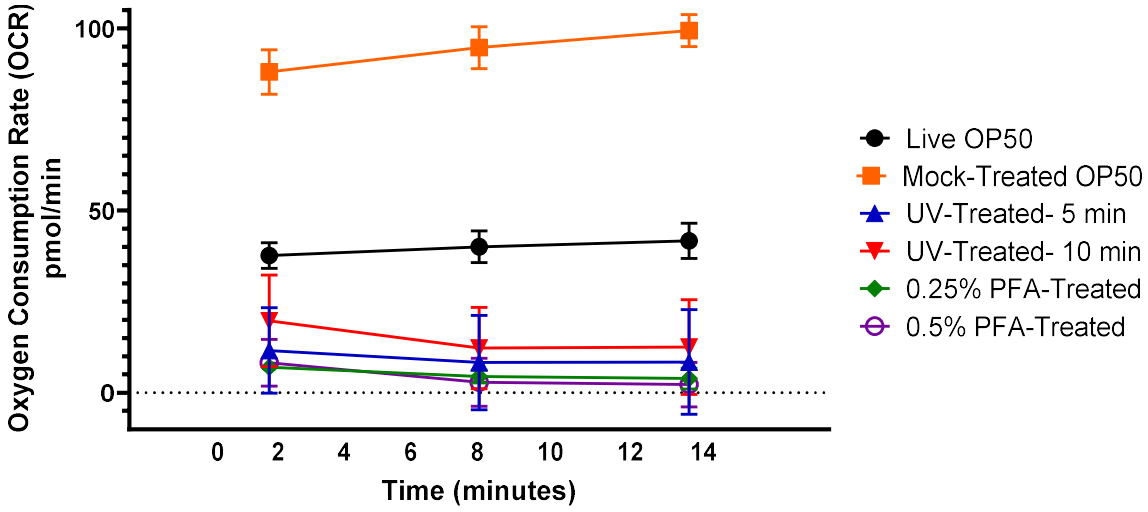
Oxygen Consumption Rate (OCR)
pmol/min
100
50
0
0
2
4
6
8
10
12
14
Time (minutes)
Live OP50
Mock-Treated OP50
UV-Treated- 5 min
UV-Treated- 10 min
0.25% PFA-Treated
0.5% PFA-Treated

c

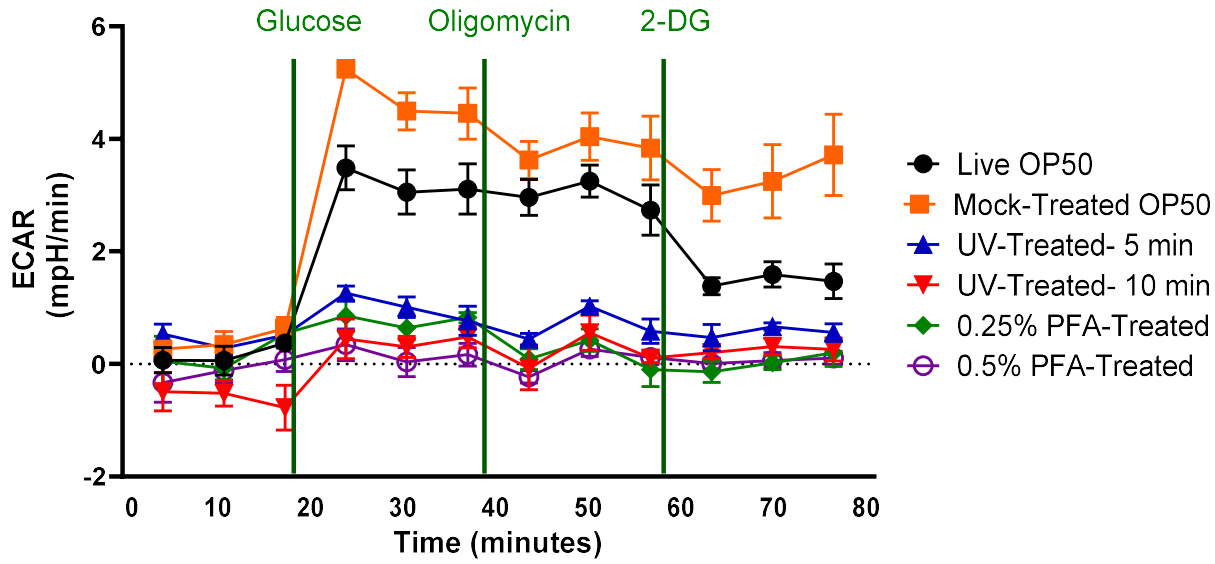
Glucose
Oligomycin
2-DG
ECAR (mpH/min)
6
4
2
0
-2
0
10
20
30
40
50
60
70
80
Time (minutes)
Live OP50
Mock-Treated OP50
UV-Treated- 5 min
UV-Treated- 10 min
0.25% PFA-Treated
0.5% PFA-Treated

d

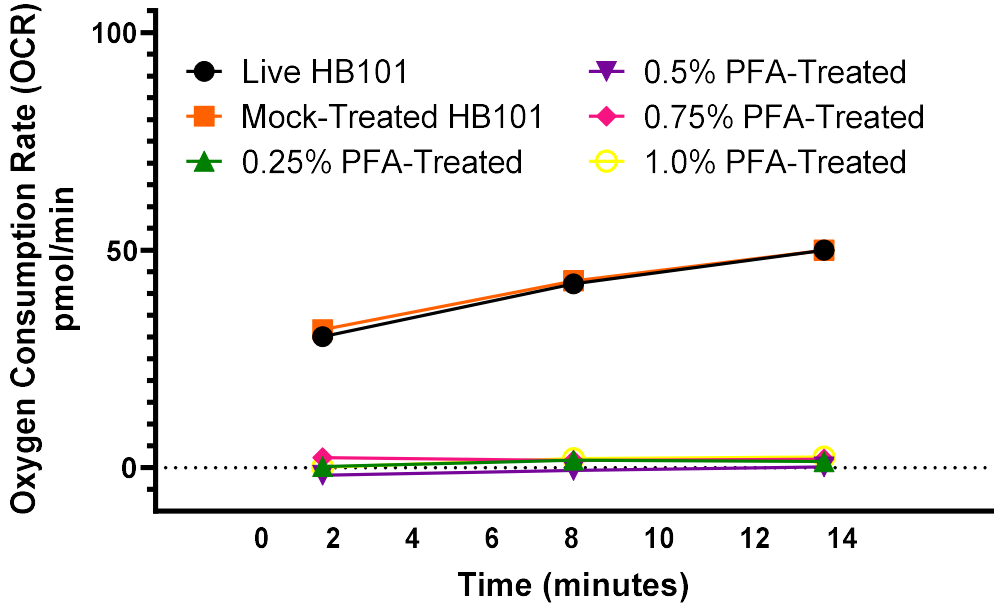
Oxygen Consumption Rate (OCR) pmol/min
100
50
0
0
2
4
6
8
10
12
14
Time (minutes)
Live HB101
Mock-Treated HB101
0.25% PFA-Treated
0.5% PFA-Treated
0.75% PFA-Treated
1.0% PFA-Treated

e

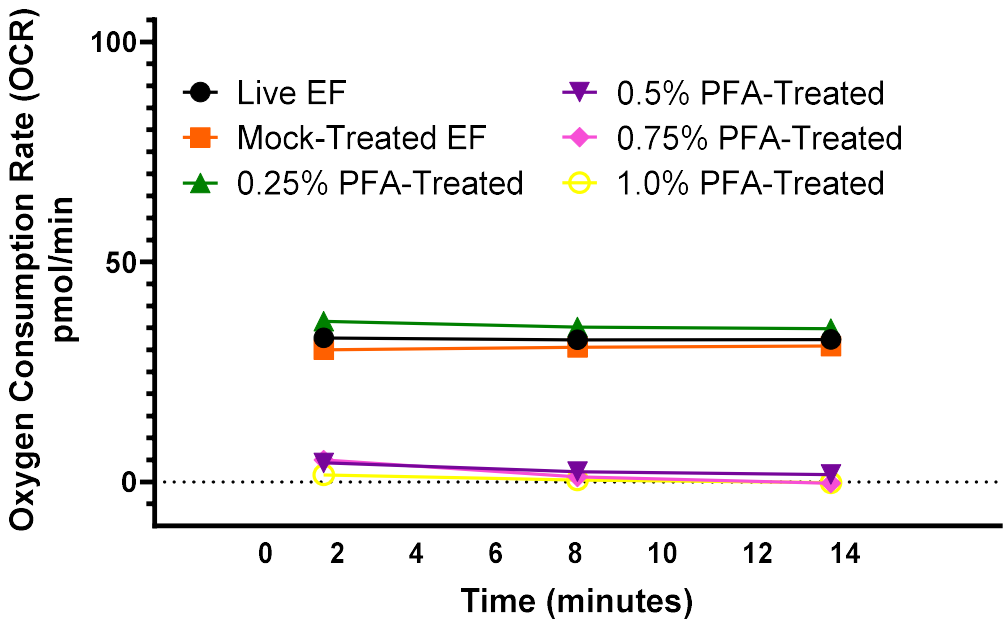

Figure 2.2- Paraformaldehyde treated nonpathogenic and pathogenic bacteria are replicatively and metabolically dead. (a) Bacteria growth in colony forming units (CFU) of various OP50 conditions. Respiration determined using (b) Oxygen consumption rate (OCR) of live and treated bacteria in pmol/min (c) Extracellular acidification rate (ECAR) in mpH/min of all OP50 conditions and OCR of live and treated conditions of (d) HB101 and (e) *E. faecalis* in pmol/min. ** denotes p-value < 0.01.

a

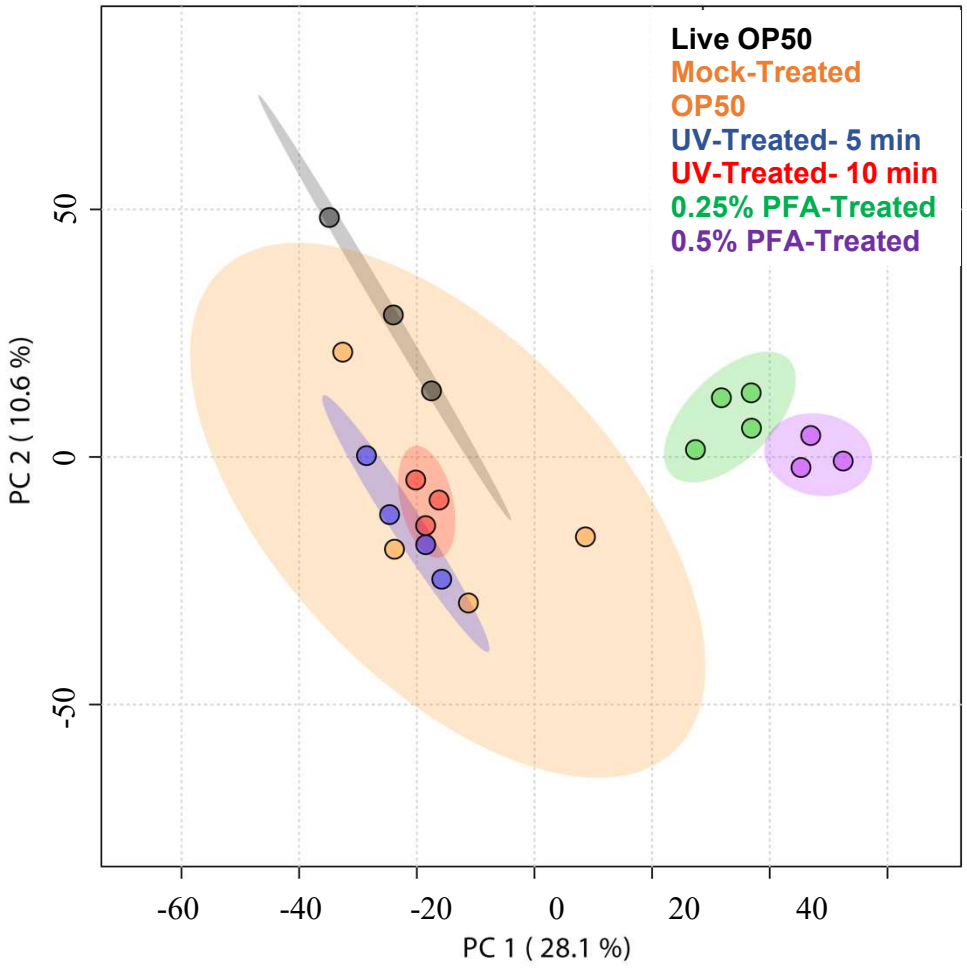
Live OP50
Mock-Treated
OP50
UV-Treated- 5 min
UV-Treated- 10 min
0.25% PFA-Treated
0.5% PFA-Treated
PC 2 (10.6 %)
50
0
-50
-60
-40
-20
0
20
40
PC 1 (28.1 %)

b

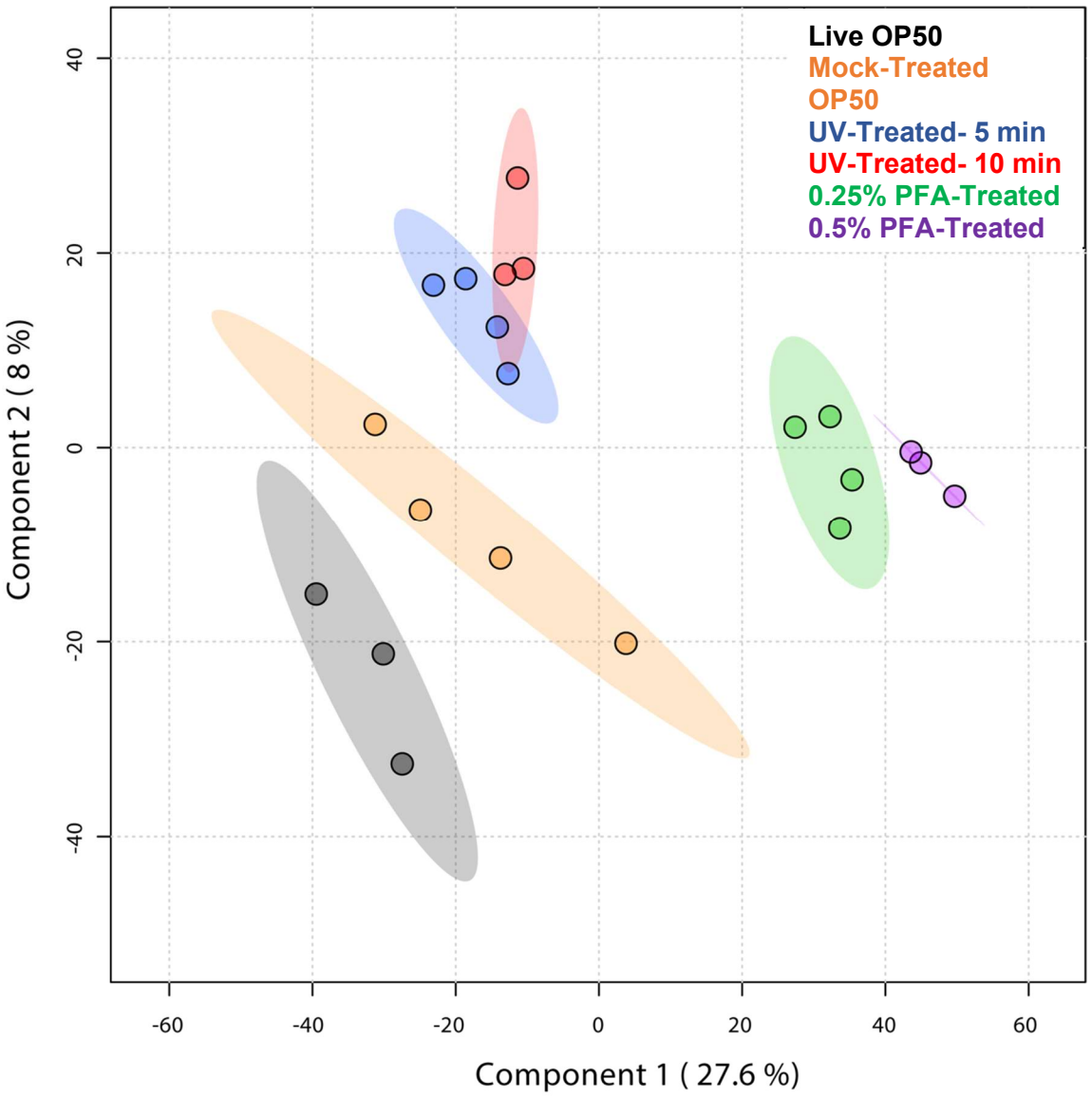
Live OP50
Mock-Treated
OP50
UV-Treated- 5 min
UV-Treated- 10 min
0.25% PFA-Treated
0.5% PFA-Treated
Component 2 (8 %)
Component 1 (27.6 %)
40
20
0
-20
-40
-60
-40
-20
0
20
40
60

c

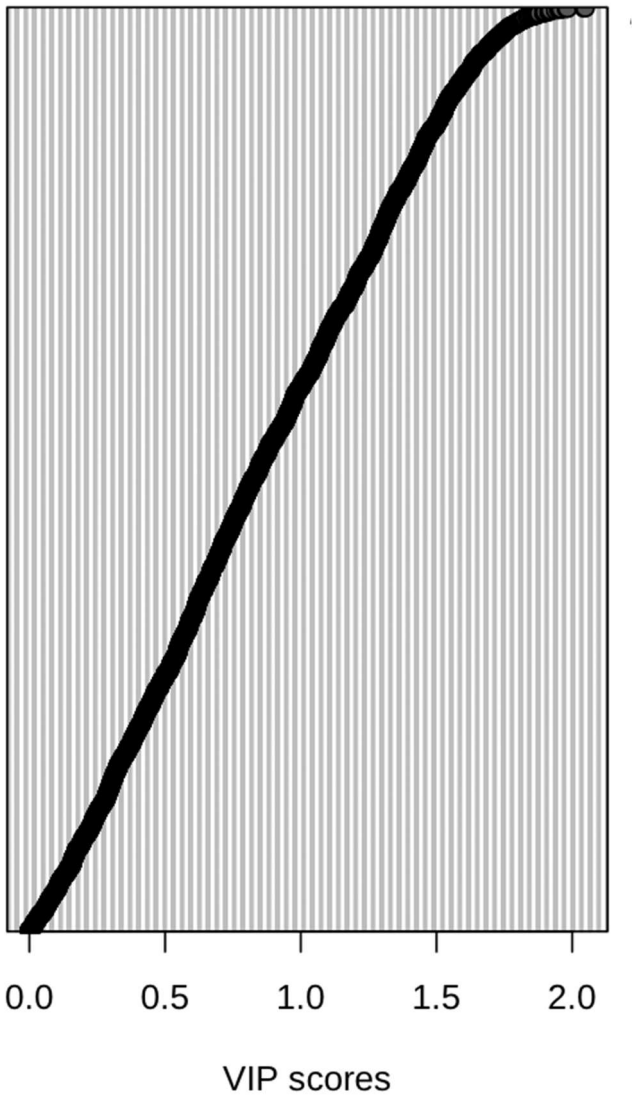

d

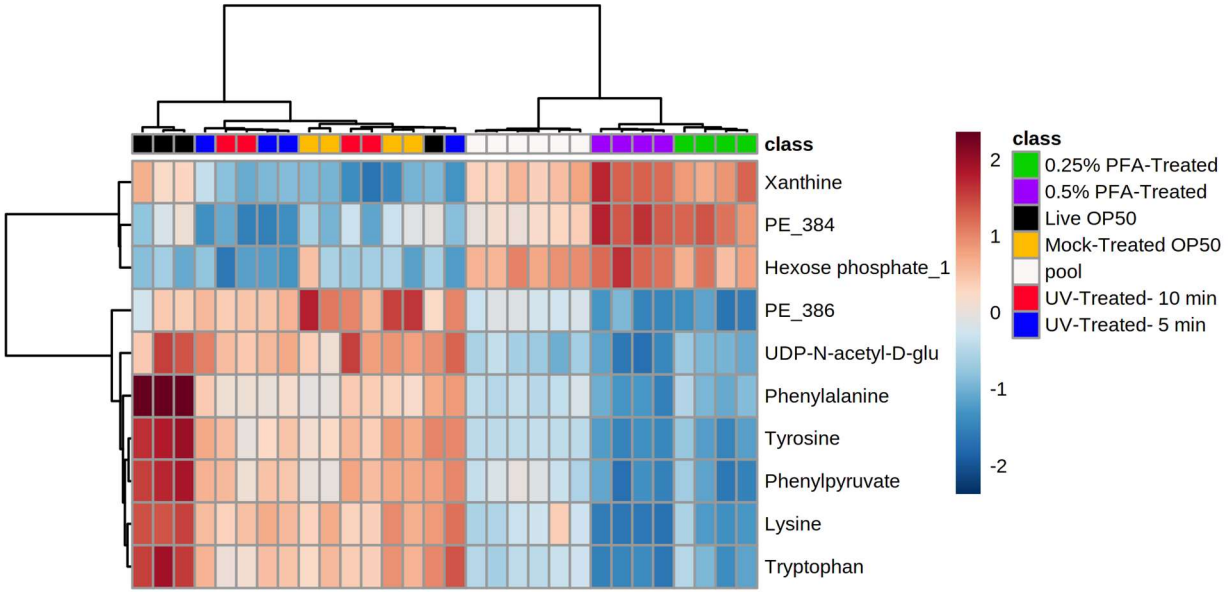
class
Xanthine
PE_384
Hexose phosphate_1
PE_386
UDP-N-acetyl-D-glu
Phenylalanine
Tyrosine
Phenylpyruvate
Lysine
Tryptophan
class
0.25% PFA-Treated
0.5% PFA-Treated
Live OP50
Mock-Treated OP50
pool
UV-Treated- 10 min
UV-Treated- 5 min
2
1
0
-1
-2

e

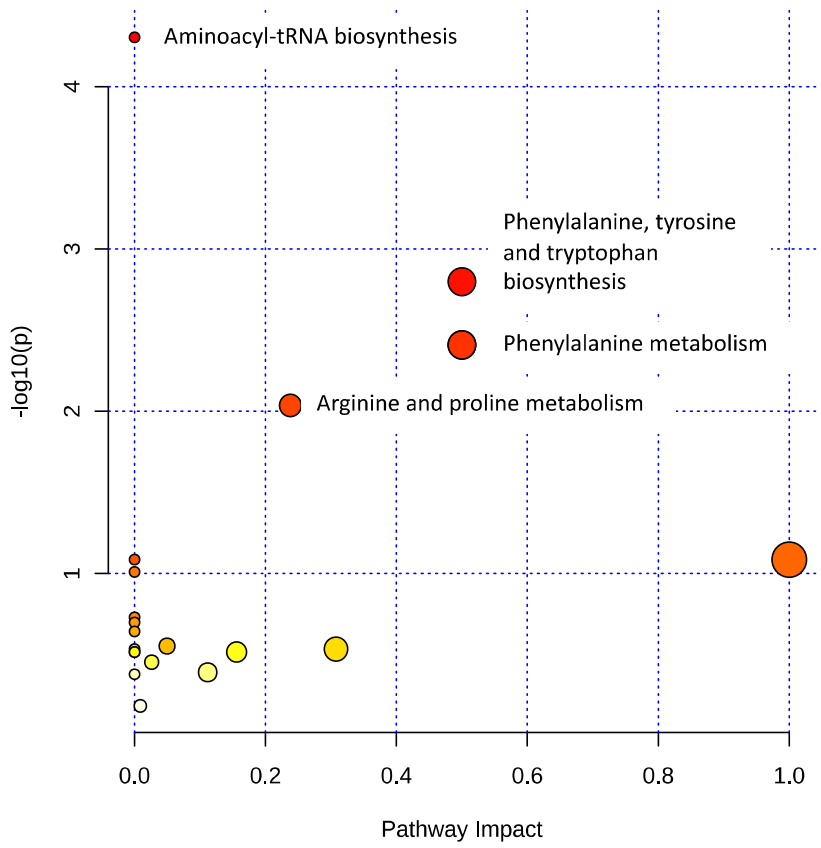
Aminoacyl-tRNA biosynthesis
Phenylalanine, tyrosine and tryptophan biosynthesis
Phenylalanine metabolism
Arginine and proline metabolism
-log10(p)
4
3
2
1
0.0
0.2
0.4
0.6
0.8
1.0
Pathway Impact

f

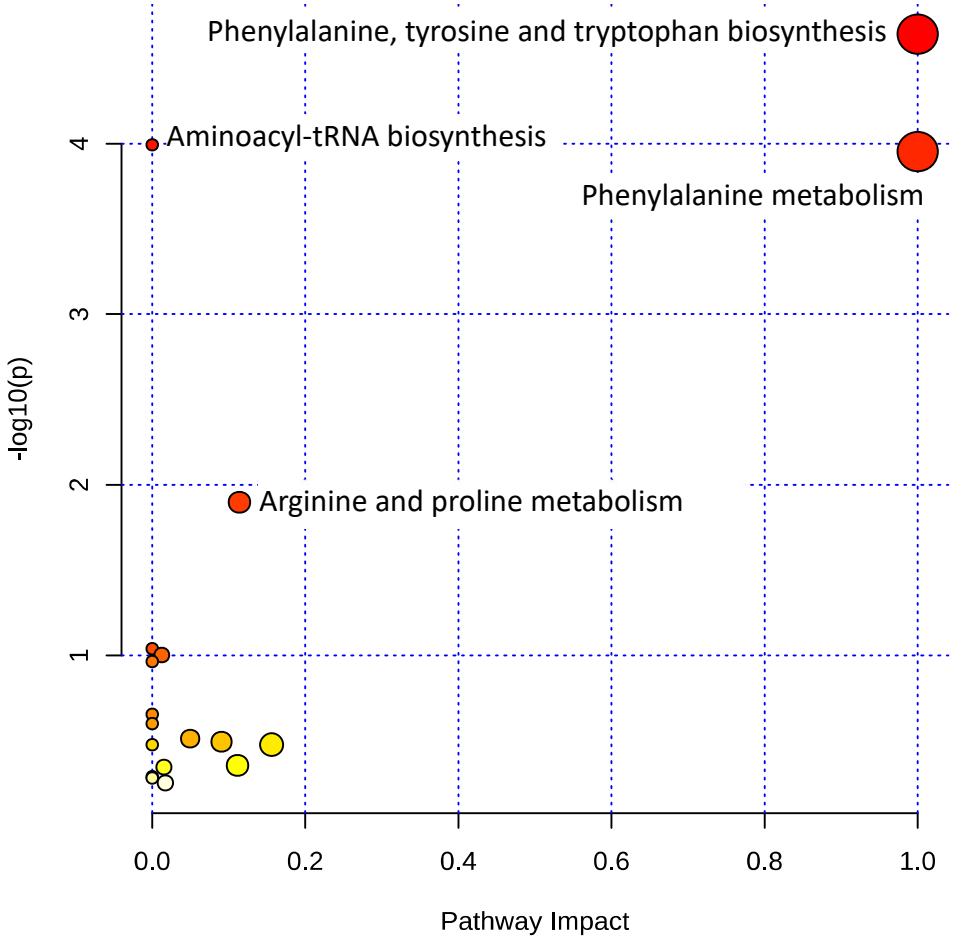

Figure 2.3: The metabolome of worms fed PFA-treated OP50 differs from the metabolome of the worms fed live and UV-treated OP50. (a) Principal component analysis and (b) PLS-DA analysis of untargeted LC-MS metabolomics data of *C. elegans* fed with control, UV-treated and PFA-treated OP50. (c) VIP analysis of component 1 of LC-MS metabolomics data of *C. elegans* fed with control, UV-treated and PFA-treated OP50. (d) Heatmap of targeted LC-MS metabolomics data of *C. elegans* fed with control, UV-treated and PFA-treated OP50. (e) Pathway analysis of metabolites with significant abundance change between worms grown on mock-treated and 0.25% PFA-treated OP50 and (f) between worms grown on mock-treated and 0.5% PFA-treated OP50. PE_384 = Phosphatidylethanolamine (PE) (38:4) and PE_386 = PE(38:6).

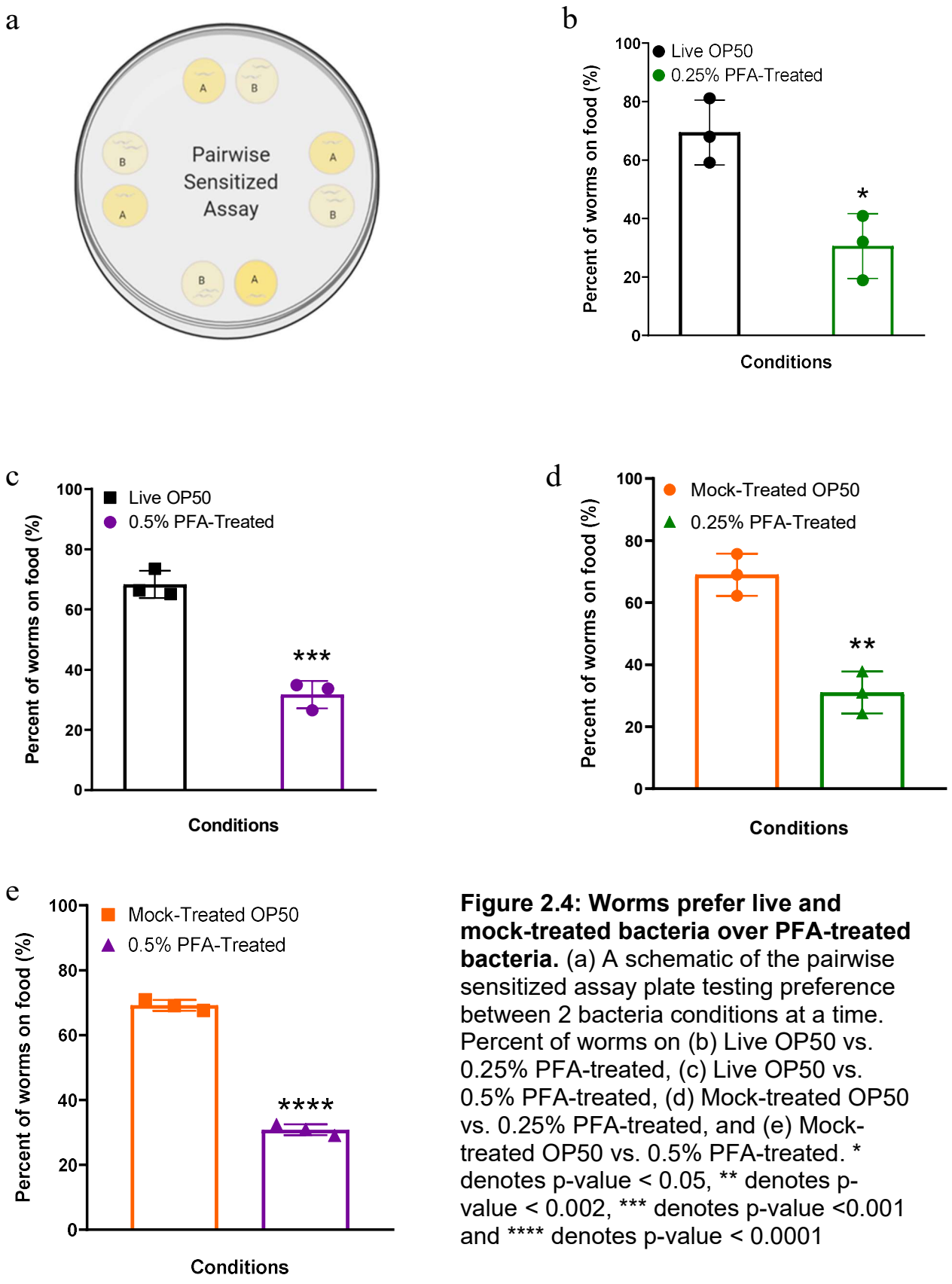

Figure 2.4: Worms prefer live and mock-treated bacteria over PFA-treated bacteria. (a) A schematic of the pairwise sensitized assay plate testing preference between 2 bacteria conditions at a time. Percent of worms on (b) Live OP50 vs. 0.25% PFA-treated, (c) Live OP50 vs. 0.5% PFA-treated, (d) Mock-treated OP50 vs. 0.25% PFA-treated, and (e) Mock-treated OP50 vs. 0.5% PFA-treated. * denotes p-value < 0.05, ** denotes p-value < 0.002, *** denotes p-value <0.001 and **** denotes p-value < 0.0001

a

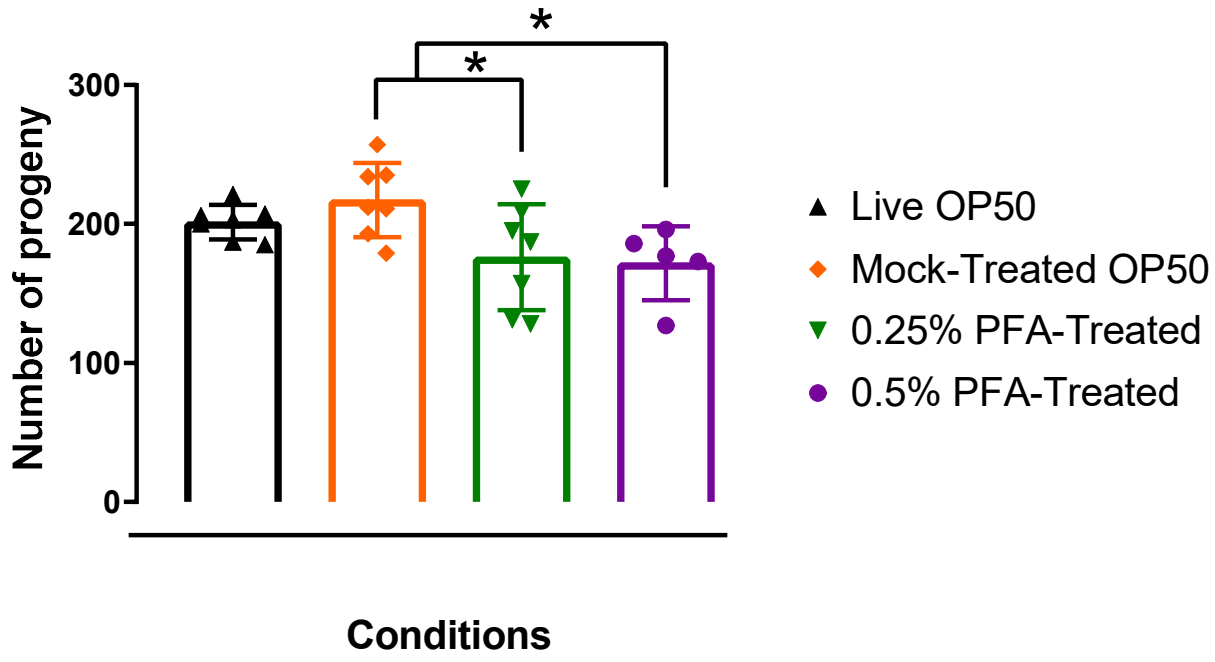
*
*
300
200
100
0
Number of progeny
Conditions
Live OP50
Mock-Treated OP50
0.25% PFA-Treated
0.5% PFA-Treated

b

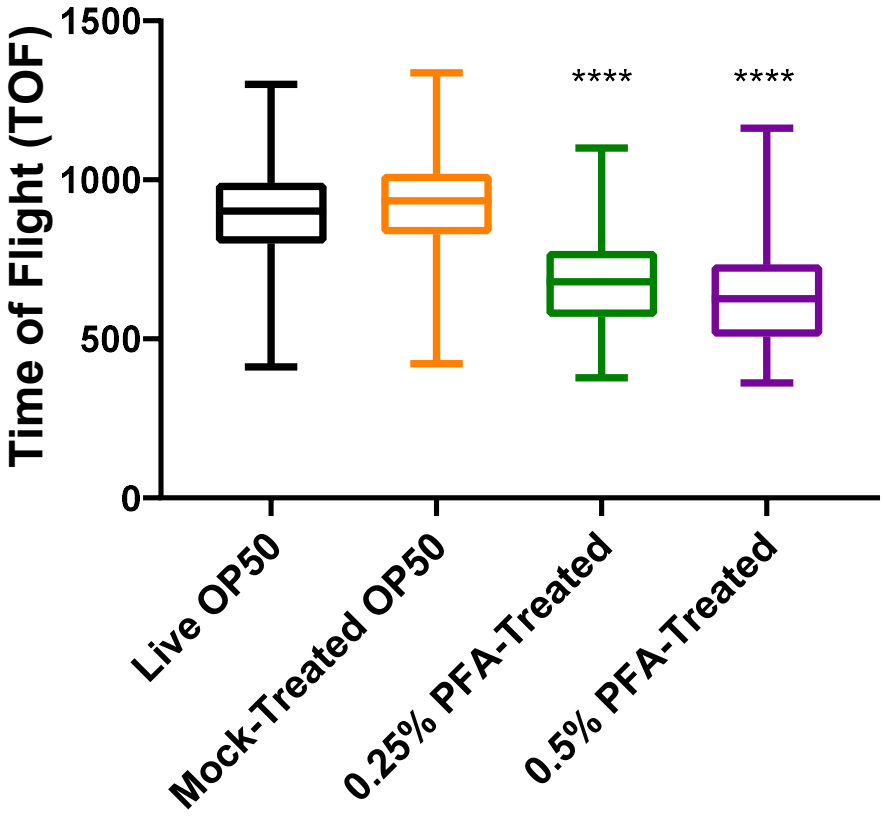
1500
1000
500
0
Time of Flight (TOF)
****
****
Live OP50
Mock-Treated OP50
0.25% PFA-Treated
0.5% PFA-Treated

c

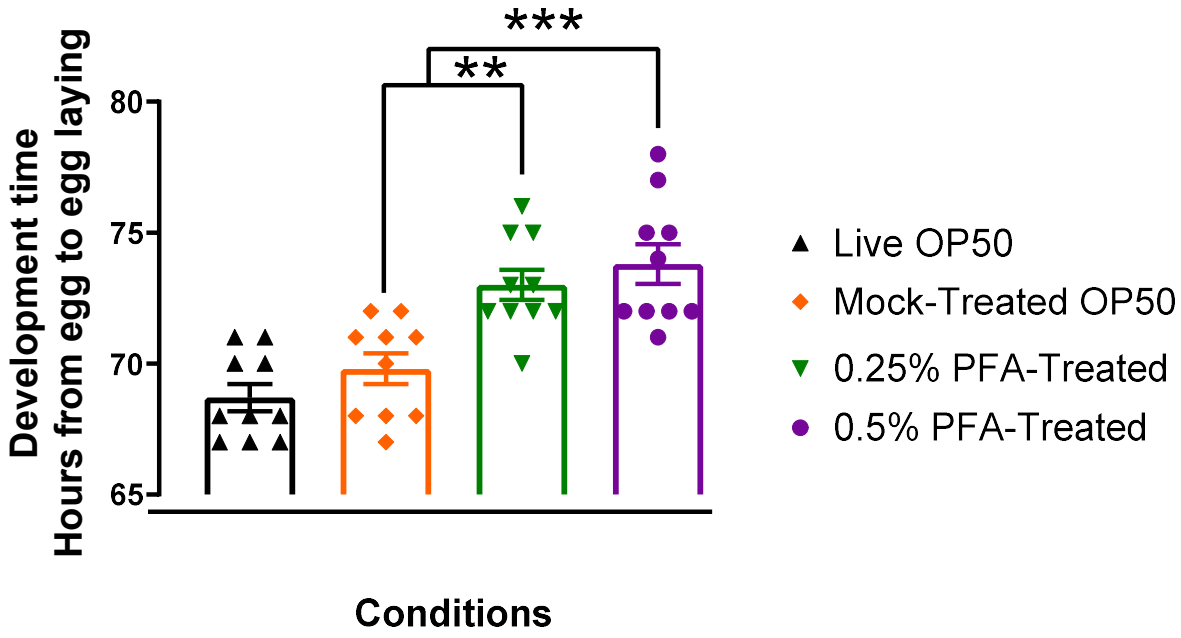
***
**
80
75
70
65
Development time
Hours from egg to egg laying
Conditions
Live OP50
Mock-Treated OP50
0.25% PFA-Treated
0.5% PFA-Treated

d

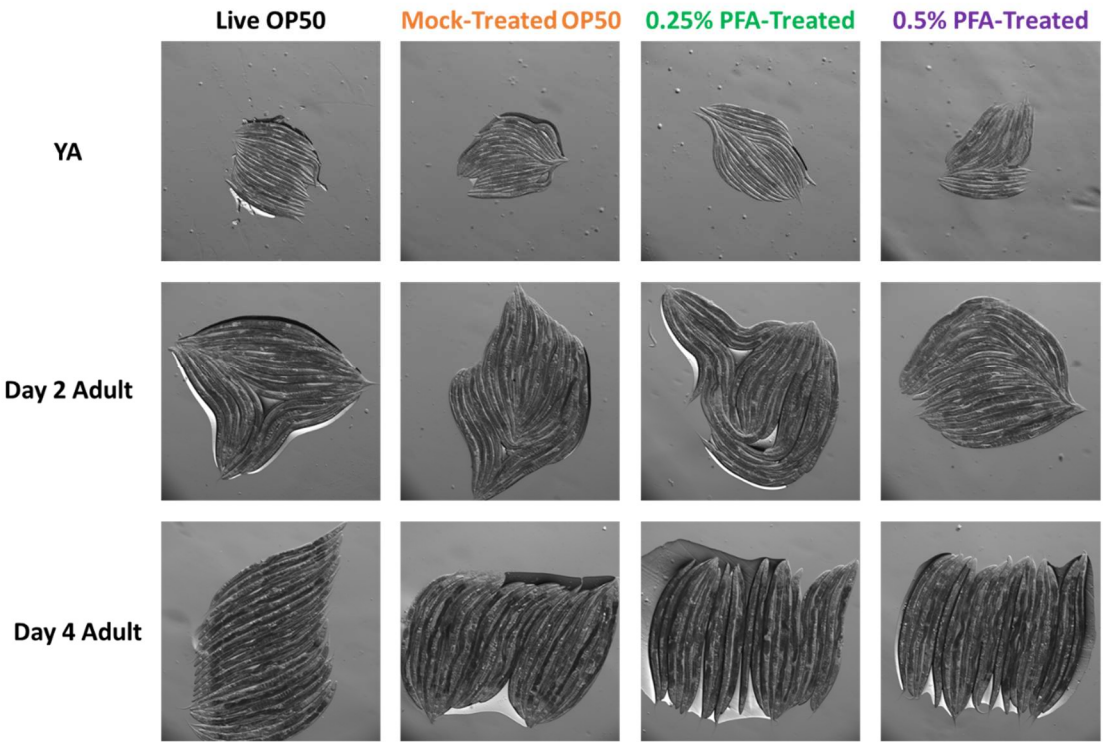
Live OP50
Mock-Treated OP50
0.25% PFA-Treated
0.5% PFA-Treated
YA
Day 2 Adult
Day 4 Adult

e

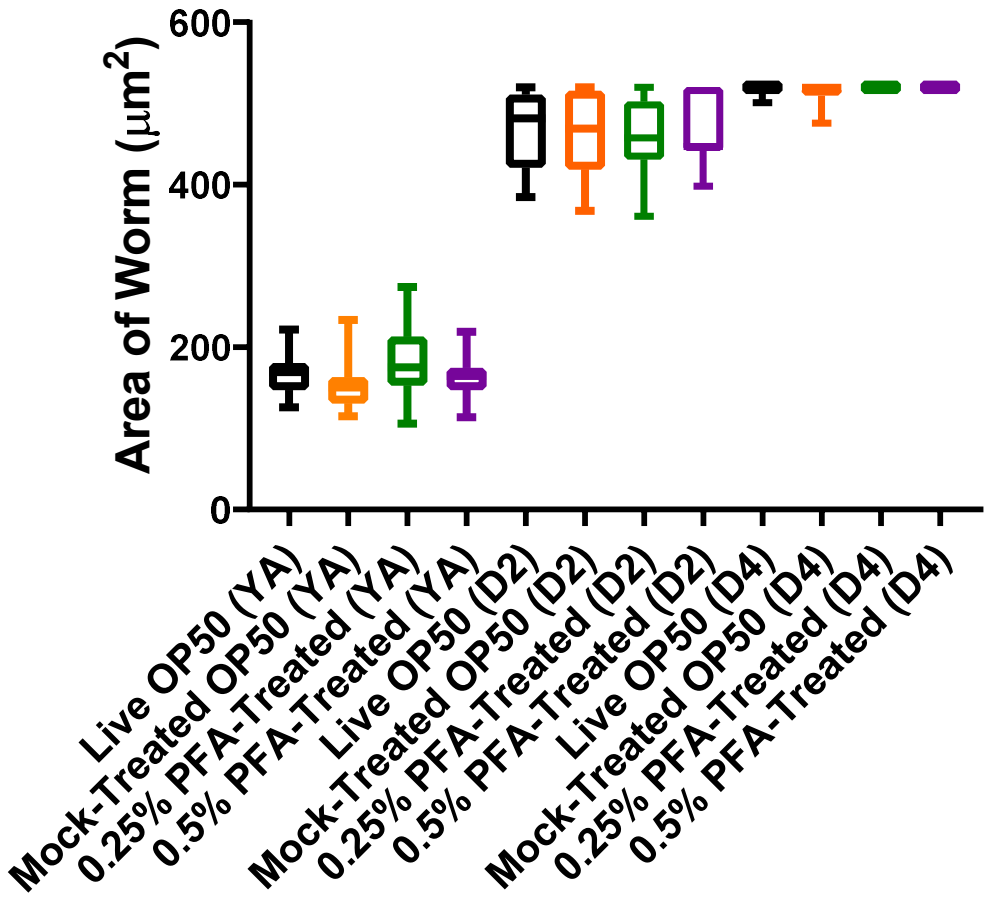
Area of Worm (μm²)
600
400
200
0
Live OP50 (YA)
Mock-Treated OP50 (YA)
0.25% PFA-Treated (YA)
0.5% PFA-Treated (YA)
Live OP50 (D2)
Mock-Treated OP50 (D2)
0.25% PFA-Treated (D2)
0.5% PFA-Treated (D2)
Live OP50 (D4)
Mock-Treated OP50 (D4)
0.25% PFA-Treated (D4)
0.5% PFA-Treated (D4)

f

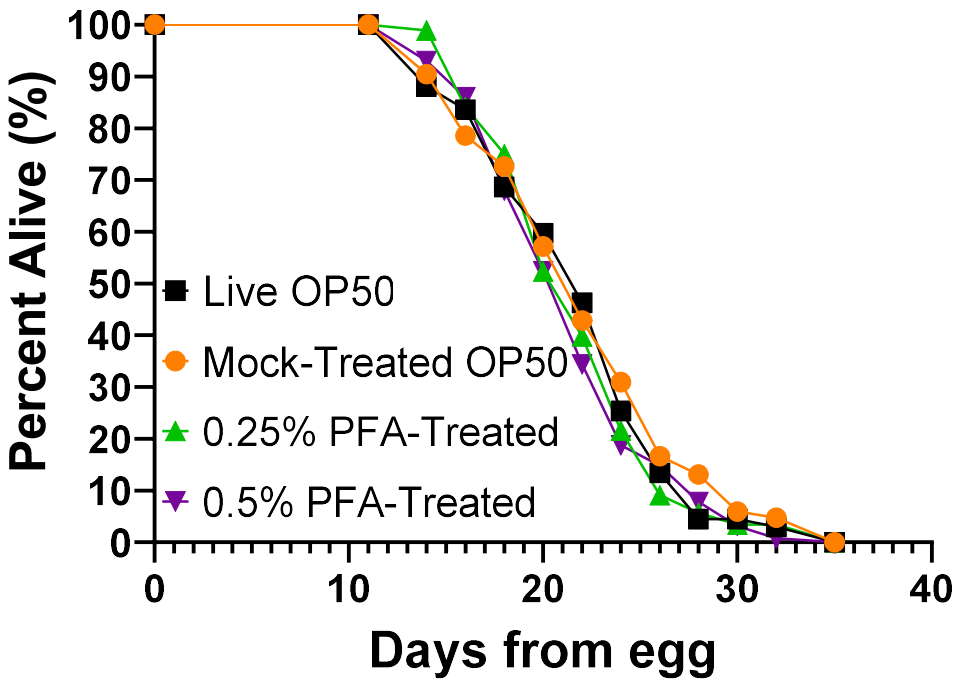
Percent Alive (%)
100
90
80
70
60
50
40
30
20
10
0
Live OP50
Mock-Treated OP50
0.25% PFA-Treated
0.5% PFA-Treated
0
10
20
30
40
Days from egg

Figure 2.5: The effects of paraformaldehyde killed OP50 on fecundity, development and lifespan. (a) Average progeny number of worms fed with different bacteria conditions. (b) Development of worms sorted based on relative axial length (Time of flight, TOF) at L4. (c) Development time (hours) of worms from egg to egg laying on different conditions of OP50. (d) Images of worms on various food sources at young adult (YA), day 2, and day 4 adult. (e) Area of the worms (μm^2) quantified from images in figure 5d. (f) Percent alive of worms fed with treated and control OP50. * denotes p-value < 0.05, ** denotes p-value < 0.005, *** denotes p-value < 0.0005, and **** denotes p-value < 0.0001.

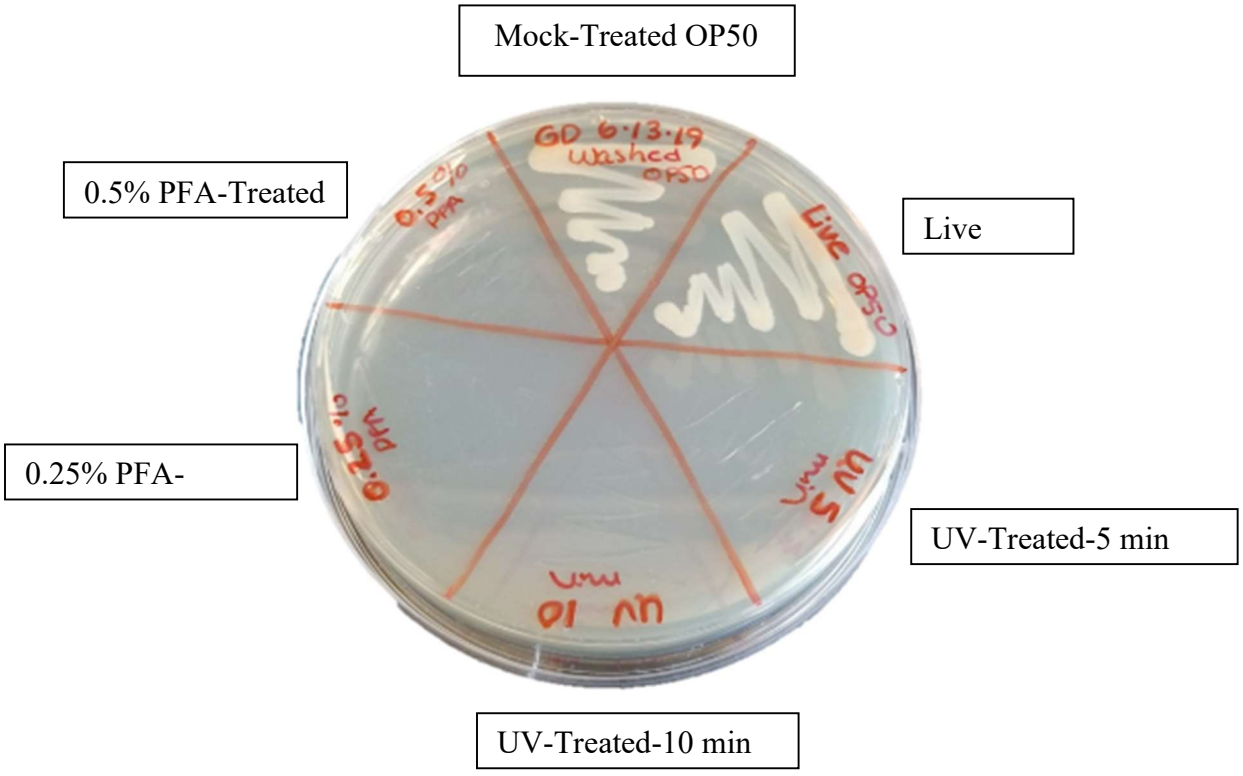

Figure S2.1: Bacterial streaks testing the growth of live controls, UV-treated and PFA-treated bacteria on an LB agar plate.

a

Replicate 1

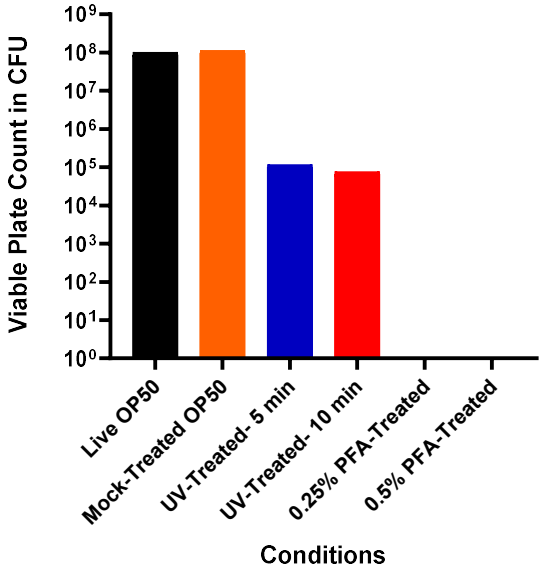

Replicate 2

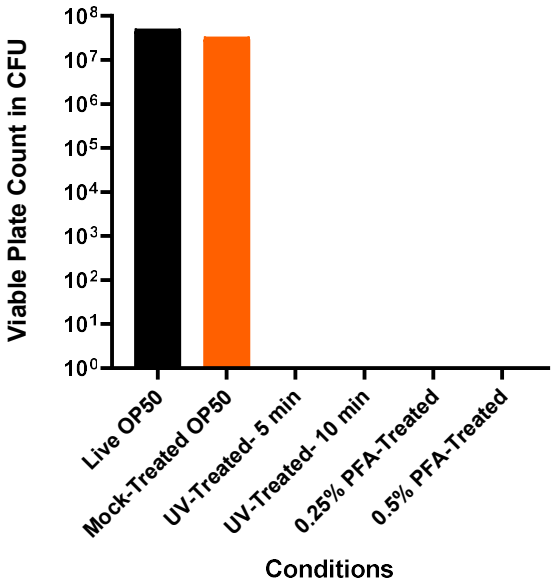

Replicate 3

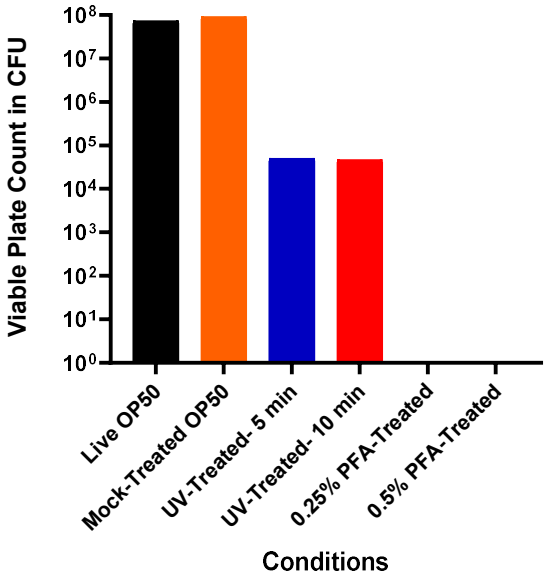

b

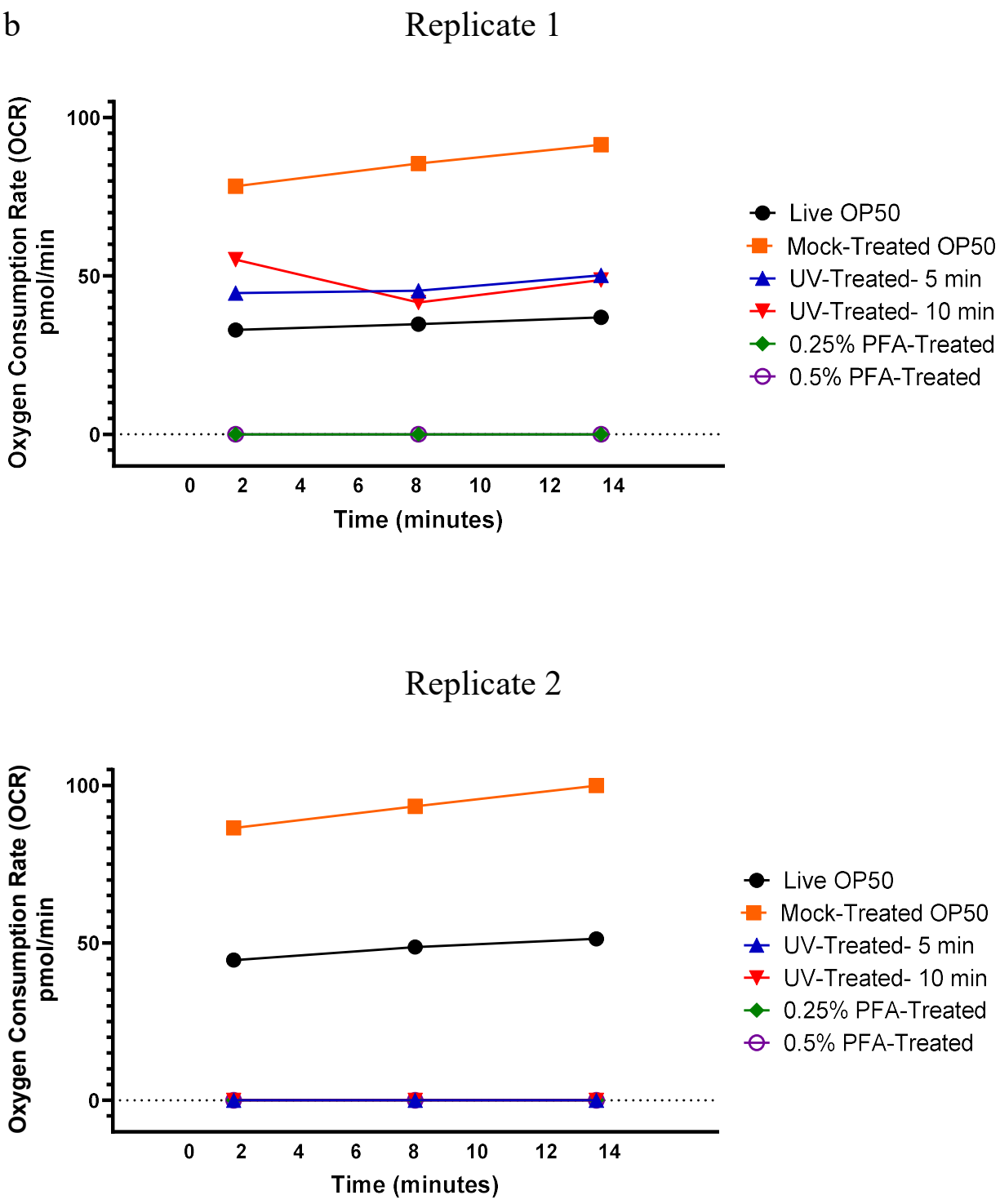

Figure S2.2: UV as a method of killing bacteria is not consistent. Individual replicates of (a) viable plate count in colony forming units (CFU) and (b) oxygen consumption rate (OCR) in pmol/min of different conditions of OP50.

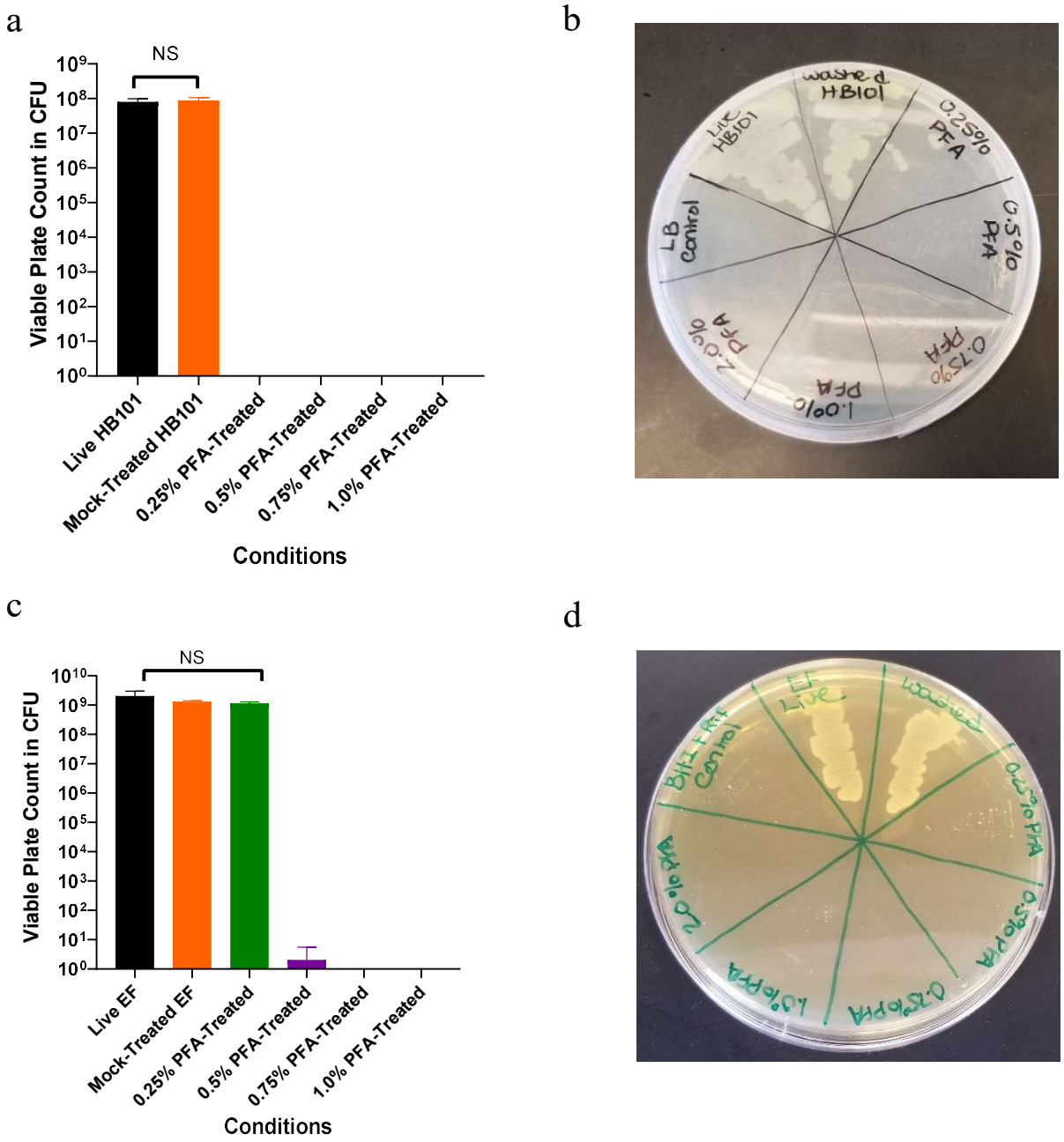

Figure S2.3: PFA killing works in multiple bacterial strains. (a) Viable plate count in colony forming unit (CFU), (b) bacterial streaks testing the growth of live controls and PFA-treated bacteria on an LB agar plate of different conditions of HB101 and (c) Viable plate count in CFU, (d) bacterial streaks testing the growth of live controls and PFA-treated bacteria on an LB agar plate of different conditions of *E. faecalis*. Washed= Mock-Treated

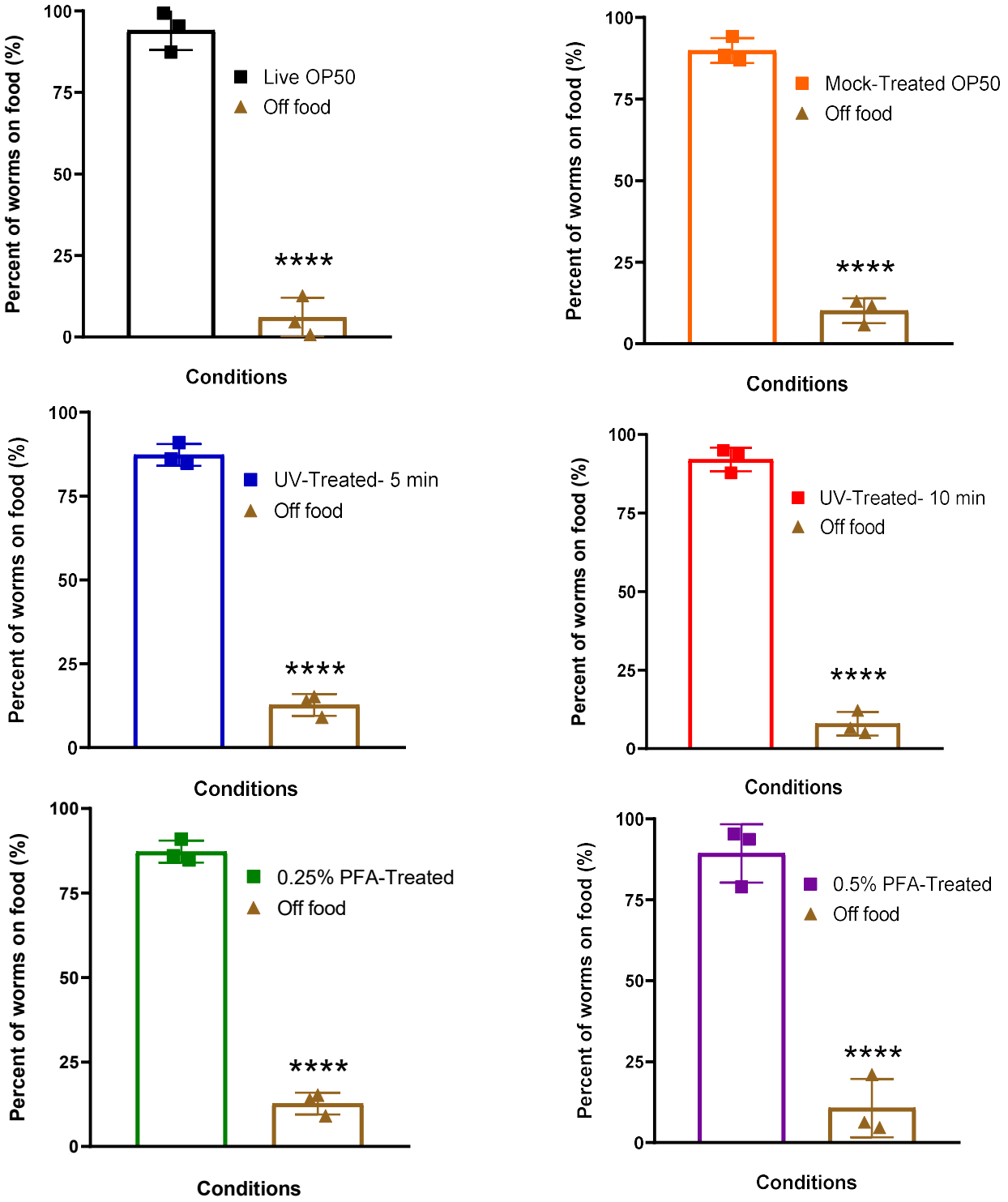

Figure S2.4: Single lawn attraction assay showing preference to food source over no food. Percent of worms on each of the control or treated OP50 conditions compared to percent of worms off the food. **** denotes p-value < 0.0001.

a

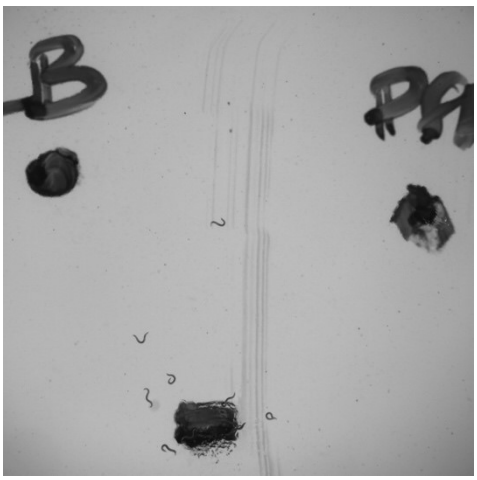

b

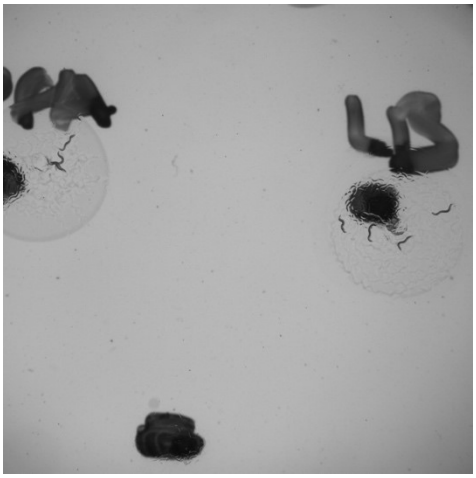

c

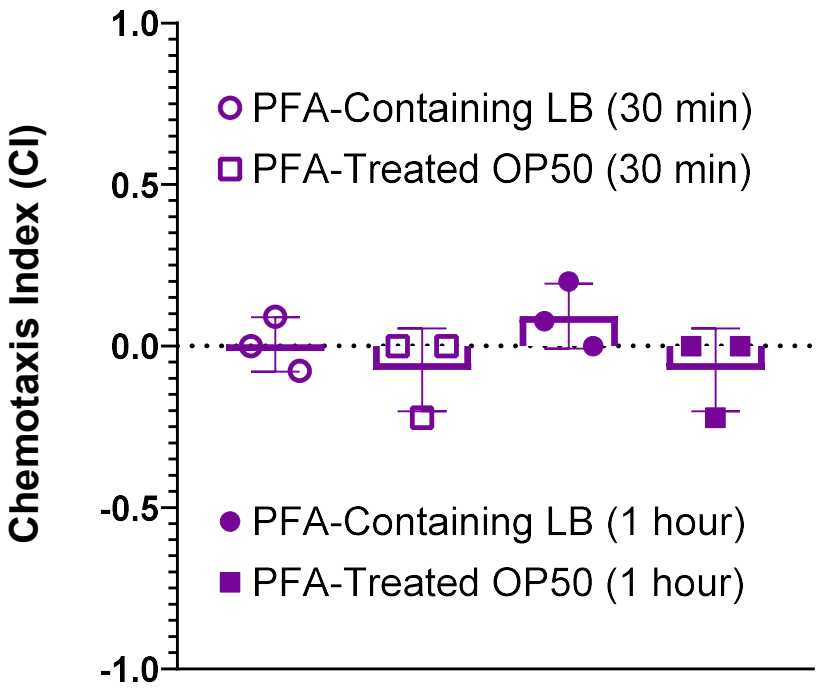

Figure S2.5: Worms are not repulsed by PFA. (a) Young adult worms grown on OP50 transferred to 35 mm plate seeded with 4 µl of LB or PFA-containing LB. Image of worms after 1 hour showing no preference to LB or PFA-containing LB. (b) Young adult worms grown on OP50 transferred to 35 mm plate seeded with 4 µl of live OP50 or PFA-treated OP50. Image of worms after 1 hour showing no repulsion to any possible residual PFA in the bacteria prep. (c) Quantification of chemotaxis index after exposure to either PFA-containing LB or PFA-treated OP50 for 30 min or 1 hour.

a

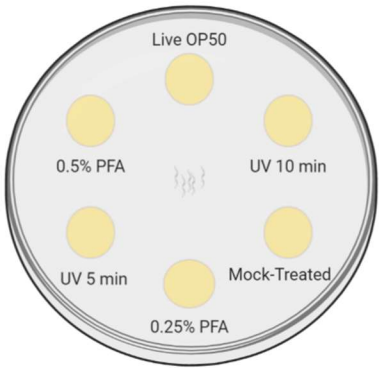

b

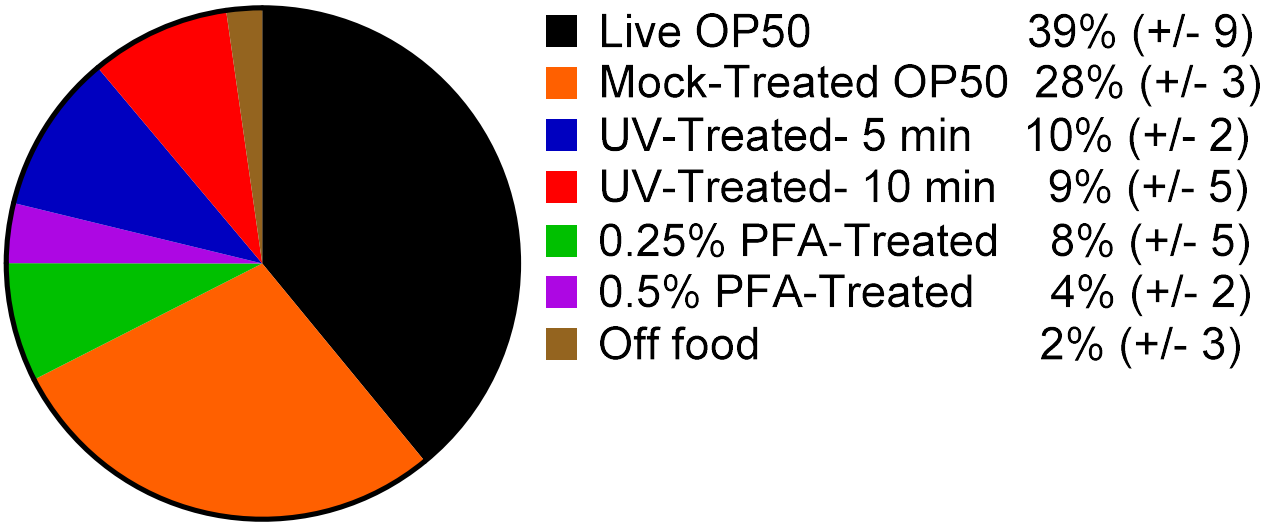

c

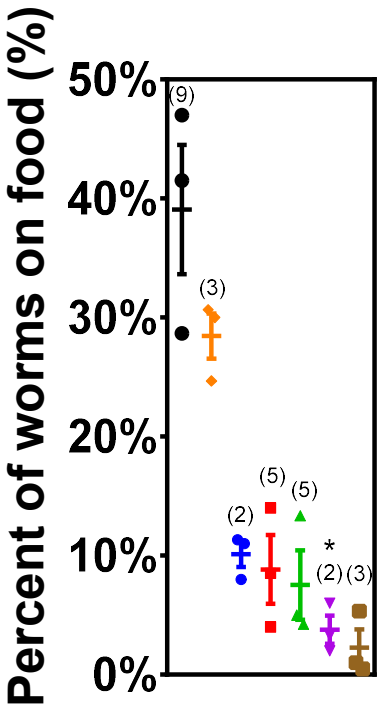

Figure S2.6: Food attraction showing preference to live OP50 over all treated conditions (a) A schematic of the attraction assay plate testing worm food preference among all groups of bacteria conditions. (b) Percent average of worms on each of the bacteria conditions (+/- SD). (c) Individual replicates with standard deviation. * denotes p-value < 0.05 compared to mock-treated OP50.

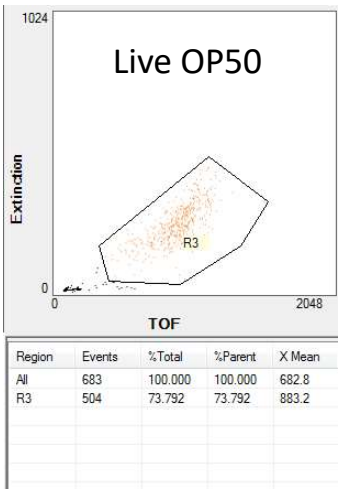

Region	Events	%Total	%Parent	X Mean
All	683	100.000	100.000	682.8
R3	504	73.792	73.792	883.2

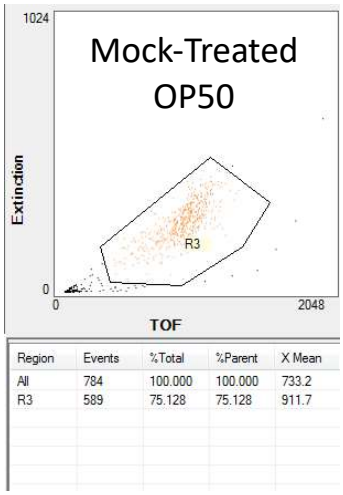

Region	Events	%Total	%Parent	X Mean
All	784	100.000	100.000	733.2
R3	589	75.128	75.128	911.7

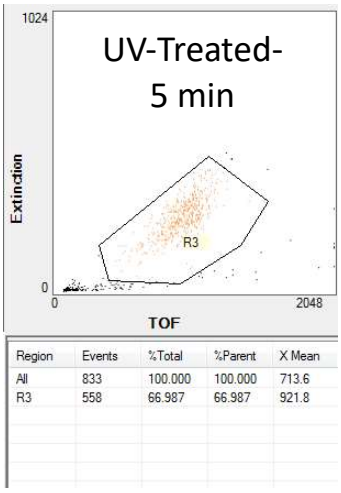

Region	Events	%Total	%Parent	X Mean
All	833	100.000	100.000	713.6
R3	558	66.987	66.987	921.8

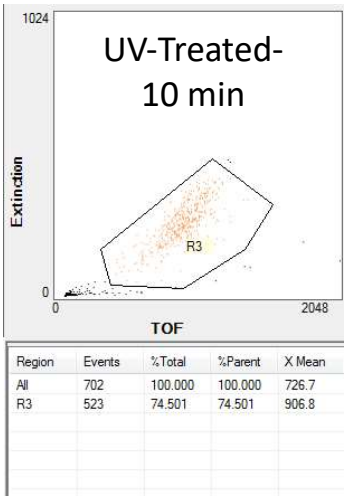

Region	Events	%Total	%Parent	X Mean
All	702	100.000	100.000	726.7
R3	523	74.501	74.501	906.8

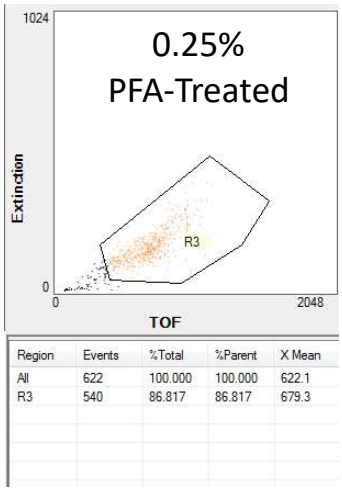

Region	Events	%Total	%Parent	X Mean
All	622	100.000	100.000	622.1
R3	540	86.817	86.817	679.3

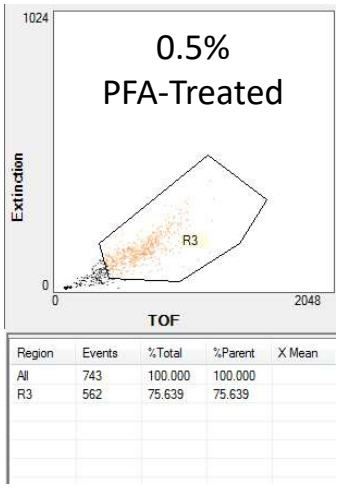

Region	Events	%Total	%Parent	X Mean
All	743	100.000	100.000	
R3	562	75.639	75.639	

Figure S2.7: Extinction signal from the 488 nm laser was used to gate worms at L4 to determine differences in rate of development. Analysis is based on the Relative axial length (TOF, Time of Flight).

* Data S2.1-2.5 were too large to be included in the thesis, but are available online at https://pubmed.ncbi.nlm.nih.gov/33637830/ as supplementary data files.

References

1. Corsi AK, Wightman B, Chalfie M. A Transparent window into biology: A primer on Caenorhabditis elegans (June 18, 2015), WormBook, ed. The C. elegans Research Community. WormBook. Published online 2015. doi:doi/10.1895/wormbook.1.177.1

2. Soediono B. Alberts - Molecular Biology Of The Cell 4th Ed. J Chem Inf Model. Published online 1989. doi:10.1017/CBO9781107415324.004

3. Lai CH, Chou CY, Ch'ang LY, Liu CS, Lin WC. Identification of novel human genes evolutionarily conserved in Caenorhabditis elegans by comparative proteomics. Genome Res. Published online 2000. doi:10.1101/gr.10.5.703

4. Artal-Sanz M, de Jong L, Tavernarakis N. Caenorhabditis elegans: A versatile platform for drug discovery. Biotechnol J. Published online 2006. doi:10.1002/biot.200600176

5. O'Reilly LP, Luke CJ, Perlmutter DH, Silverman GA, Pak SC. C. elegans in high-throughput drug discovery. Adv Drug Deliv Rev. Published online 2014. doi:10.1016/j.addr.2013.12.001

6. Atherton HJ, Jones OAH, Malik S, Miska EA, Griffin JL. A comparative metabolomic study of NHR-49 in Caenorhabditis elegans and PPAR-α in the mouse. FEBS Lett. Published online 2008. doi:10.1016/j.febslet.2008.04.020

7. Castro C, Sar F, Shaw WR, Mishima M, Miska EA, Griffin JL. A metabolomic strategy defines the regulation of lipid content and global metabolism by Δ9 desaturases in Caenorhabditis elegans. BMC Genomics. Published online 2012. doi:10.1186/1471-2164-13-36

8. Cabreiro F, Au C, Leung KY, et al. Metformin retards aging in C. elegans by altering microbial folate and methionine metabolism. Cell. Published online 2013. doi:10.1016/j.cell.2013.02.035

9. Qi B, Kniazeva M, Han M. A vitamin-B2-sensing mechanism that regulates gut protease activity to impact animal's food behavior and growth. Elife. Published online 2017. doi:10.7554/eLife.26243

10. Garigan D, Hsu AL, Fraser AG, Kamath RS, Abringet J, Kenyon C. Genetic analysis of tissue aging in Caenorhabditis elegans: A role for heat-shock factor and bacterial proliferation. Genetics. Published online 2002.

11. Smith ED, Kaeberlein TL, Lydum BT, et al. Age- and calorie-independent life span extension from dietary restriction by bacterial deprivation in Caenorhabditis elegans. BMC Dev Biol. Published online 2008. doi:10.1186/1471-213X-8-49

12. Kaeberlein TL, Smith ED, Tsuchiya M, et al. Lifespan extension in Caenorhabditis elegans by complete removal of food. Aging Cell. Published online 2006. doi:10.1111/j.1474-9726.2006.00238.x

13. Gems D, Riddle DL. Genetic, behavioral and environmental determinants of male longevity in Caenorhabditis elegans. Genetics. Published online 2000.

14. Lobritz MA, Belenky P, Porter CBM, et al. Antibiotic efficacy is linked to bacterial cellular respiration. Proc Natl Acad Sci U S A. 2015;112(27):8173-8180. doi:10.1073/pnas.1509743112

15. Virk B, Jia J, Maynard CA, et al. Folate Acts in E. coli to Accelerate C. elegans Aging Independently of Bacterial Biosynthesis. Cell Rep. Published online 2016. doi:10.1016/j.celrep.2016.01.051

16. Thavarajah R, Mudimbaimannar V, Rao U, Ranganathan K, Elizabeth J. Chemical and physical basics of routine formaldehyde fixation. J Oral Maxillofac Pathol. Published online 2012. doi:10.4103/0973-029X.102496

17. Felix H. Permeabilized and Immobilized Cells. Methods Enzymol. Published online 1988. doi:10.1016/0076-6879(88)37060-6

18. Nadanaciva S, Rana P, Beeson GC, et al. Assessment of drug-induced mitochondrial dysfunction via altered cellular respiration and acidification measured in a 96-well platform. J Bioenerg Biomembr. Published online 2012. doi:10.1007/s10863-012-9446-z

19. Hastings J, Mains A, Artal-Sanz M, et al. WormJam: A consensus C. elegans Metabolic Reconstruction and Metabolomics Community and Workshop Series . Worm. Published online 2017. doi:10.1080/21624054.2017.1373939

20. Hoffman EA, Frey BL, Smith LM, Auble DT. Formaldehyde crosslinking: A tool for the study of chromatin complexes. J Biol Chem. Published online 2015. doi:10.1074/jbc.R115.651679

21. Shtonda BB, Avery L. Dietary choice behavior in Caenorhabditis elegans. J Exp Biol. Published online 2006. doi:10.1242/jeb.01955

22. Yu L, Yan X, Ye C, et al. Bacterial respiration and growth rates affect the feeding preferences, brood size and lifespan of Caenorhabditis elegans. PLoS One. Published online 2015. doi:10.1371/journal.pone.0134401

23. MacNeil LT, Watson E, Arda HE, Zhu LJ, Walhout AJM. Diet-induced developmental acceleration independent of TOR and insulin in C. elegans. Cell. Published online 2013. doi:10.1016/j.cell.2013.02.049

24. Pulak R. Techniques for analysis, sorting, and dispensing of C. elegans on the COPAS flow-sorting system. Methods Mol Biol. Published online 2006.

25. Margie O, Palmer C, Chin-Sang I. C. elegans chemotaxis assay. J Vis Exp. Published online 2013. doi:10.3791/50069

26. Overmyer KA, Thonusin C, Qi NR, Burant CF, Evans CR. Impact of anesthesia and euthanasia on metabolomics of mammalian tissues: Studies in a C57BL/6J mouse model. PLoS One. Published online 2015. doi:10.1371/journal.pone.0117232

27. Overmyer KA, Thonusin C, Qi NR, et al. Maximal oxidative capacity during exercise is associated with skeletal muscle fuel selection and dynamic changes in mitochondrial protein acetylation. PLoS One. Published online 2015. doi:10.1016/j.cmet.2015.02.007

28. Smith CA, Want EJ, O'Maille G, Abagyan R, Siuzdak G. XCMS: Processing mass spectrometry data for metabolite profiling using nonlinear peak alignment, matching, and identification. Anal Chem. Published online 2006. doi:10.1021/ac051437y

29. Schneider CA, Rasband WS, Eliceiri KW. NIH Image to ImageJ: 25 years of image analysis. Nat Methods. Published online 2012. doi:10.1038/nmeth.2089

Chapter III

FMO Rewires Metabolism to Promote Longevity Through Tryptophan and One Carbon Metabolism

Foreword

The work presented in this chapter follows up on my mentor Dr. Leiser's postdoctoral work in identifying *C. elegans* FMO-2 as a regulator of longevity. Given the recent evidence that FMOs regulate the endogenous metabolism, as mentioned in Chapter I, my initial hypothesis was that FMO-2 modifies endogenous metabolic processes to regulate longevity. Using metabolomics and follow-up RNAi gene knockdown approach, I was able to determine that FMO-2 affects the one-carbon metabolism (OCM) network and that it interacts with enzymes involved in OCM to regulate lifespan and stress resistance. In order to interpret these findings, I generated a computational model under the guidance of my co-mentor Dr. Beard that predicts the OCM metabolic flux outputs. The resulting model predicts that the flux through methylation processes are reduced in *fmo-2* overexpression animals compared to their wildtype counterparts, suggesting methylation as a key regulator of longevity downstream of FMO-2. While this project was initiated by me, my co-author Dr. Ajay Bhat contributed equally to completing the metabolomics, lifespan and stress resistance experiments. In addition, another co-author, a fellow graduate student Marshall Howington, identified tryptophan as a major

endogenous substrate of FMO-2 using biochemical approaches, which further allowed us to determine that the kynurenine pathway interacts with FMO-2 to regulate longevity and that formate, a byproduct of the kynurenine pathway, might be a link between the kynurenine pathway and OCM downstream of FMO-2 longevity regulation. A revised version of this work is currently under peer-review at *Nature Communications*. My co-authors Dr. Bhat, Marshall, and I have contributed equally to the writing of the manuscript under the supervision of Dr. Leiser. The contributions of other co-authors are listed at the end of the chapter under the Authors Contribution section.

Abstract

Flavin containing monooxygenases (FMOs) are promiscuous enzymes known for metabolizing a wide range of exogenous compounds. In *C. elegans*, *fmo-2* expression increases lifespan and healthspan downstream of multiple longevity-promoting pathways through an unknown mechanism. Here, we report that, beyond its classification as a xenobiotic enzyme, *fmo-2* expression leads to rewiring of endogenous metabolism principally through changes in one carbon metabolism (OCM). These changes are likely relevant, as we find that genetically modifying OCM enzyme expression leads to alterations in longevity that interact with *fmo-2* expression. Using computer modeling, we identify decreased methylation as the major OCM flux modified by FMO-2 that is sufficient to recapitulate its longevity benefits. We further find that tryptophan is decreased in multiple mammalian FMO overexpression models and is a validated substrate for FMO-2. Our resulting model connects a single enzyme to two previously unconnected key metabolic pathways and provides a framework for the

metabolic interconnectivity of longevity-promoting pathways such as dietary restriction. FMOs are well-conserved enzymes that are also induced by lifespan-extending interventions in mice, supporting a conserved and critical role in promoting health and longevity through metabolic remodeling.

Introduction

Flavin-containing monooxygenases (FMOs) are a family of enzymes that oxygenate substrates with nucleophilic centers, such as nitrogen and sulfur[1]. They were first discovered 50 years ago and have been studied extensively under the context of xenobiotic and drug metabolism[1]. FMOs bind to an FAD prosthetic group and interact with an NADPH cofactor to oxygenate substrates[2]. The FMO protein family is highly conserved both genetically and structurally from bacteria to humans[2,3]. Considering the conserved nature of FMOs, it is plausible that they share an endogenous, more ancient physiological role than detoxifying xenobiotics.

Through a screen of genes downstream the hypoxia-inducible factor-1 (HIF-1), a longevity-promoting transcription factor in *C. elegans*, flavin-containing monooxygenase-2 (*fmo-2*) was identified as necessary for the longevity and health benefits of both hypoxia and dietary restriction (DR)[4]. The *fmo-2* gene is also sufficient to confer these benefits on its own when overexpressed[4]. Recently, studies also suggest potential endogenous role(s) for mammalian FMOs, where changes in expression of multiple FMO proteins affect systemic metabolism[5–10]. Initial correlative reports also link FMOs to the aging process, showing that *Fmo* genes are frequently induced in long-lived mouse models, such as DR mice[5,6]. However, the mechanism(s)

for how *Fmo*s modulate endogenous metabolism and/or aging *in vivo* is unclear, as is their potential to benefit health and longevity in multiple species.

While frequently implicated in cancer cells, recent studies identify one carbon metabolism (OCM) as a common downstream target of multiple longevity pathways[11–14]. OCM is an important intermediate metabolic pathway and refers to a two-cycle metabolic network including the folate cycle and the methionine cycle[15]. OCM takes nutrient inputs, including glucose and vitamin B12, and utilizes them to synthesize intermediates for metabolic processes involved in growth and survival, including nucleotide metabolism, the transsulfuration and transmethylation pathways, and lipid metabolism[12,13,16]. In particular, suppressing expression of the methionine cycle gene *sams-1* by RNA-mediated interference (RNAi) extends the wild type worm lifespan, but fails to further extend the lifespan of the genetic DR model *eat-2* mutants[17].

Kynurenine synthesis from tryptophan and subsequent metabolism is another important metabolic pathway that can play a role in many processes, including longevity regulation. Knocking out tryptophan 2,3-dioxygenase (TDO), which catalyzes the first and rate-limiting step of this pathway, leads to lifespan extension in worms and flies[18,19]. Similarly, suppressing the kynurenine pathway by knocking down kynureninase (*kynu-1)* in worms also increases lifespan[20]. The kynurenine pathway competes for tryptophan with the serotonergic biosynthesis pathway and produces nicotinamide adenine dinucleotide (NAD) and other metabolites, including kynurenic acid and picolinic acid[21].

Given that 1) induction of Fmos correlates with increased longevity across species, 2) nematode *fmo-2* is necessary and sufficient to improve health and longevity downstream of metabolic perturbations, and 3) loss of Fmo expression can modify

aspects of metabolism, we hypothesized that Fmos affect aging by modifying one or more distinct metabolic processes. Therefore, we sought to determine the metabolic changes that occur when the expression of nematode *fmo-2* is perturbed to identify its mechanism of longevity regulation. Our resulting data support a model where *fmo-2* oxygenates tryptophan, leading to alteration of OCM components that confer longevity and healthspan benefits by reducing flux through methylation processes.

Results

Fmo-2 alters one carbon metabolism

Based on the conserved enzymatic mechanism[2,3] and our published data supporting a key role for nematode FMO-2 in regulating stress resistance, healthspan and longevity[4], we hypothesized that FMO-2 may significantly alter endogenous metabolism in *C. elegans*. To test if systemic metabolism was broadly altered by FMO-2, we used untargeted metabolomics analysis (**Data S3.1**) of three strains with varying *fmo-2* expression: the wild type reference strain (N2 Bristol), the *fmo-2(ok2147)* putative knockout strain (FMO-2 KO), and our previously published long-lived *fmo-2* overexpression (KAE9) strain (FMO-2 OE). The resulting principal component analysis (PCA) shows a substantial explained variance (65.3%) through principal components (PC) 1 and 2 (**Figure 3.1A**). Our untargeted metabolomics data suggest a distinct difference in the metabolome between the three strains, consistent with expression of nematode *fmo-2* being sufficient to modify endogenous metabolism (**Figure 3.1B**).

Having established broadly that *fmo-2* expression modifies metabolism, we next asked what key metabolic aspects are modified. Using p-value < 0.05 as our

significance threshold, we identified five metabolic pathways that are significantly altered by the overexpression of *fmo-2,* most of which are involved in amino acid metabolism (**Figure 3.1C, Table S3.1**). Of the five pathways, we observed the most significant enrichment in glycine, serine, and threonine metabolism (**Figure 3.1C**). Exogenous supplementation of glycine in worm diet is reported to extend lifespan by remodeling the methionine cycle[22], a component of one carbon metabolism (OCM) and another significantly enriched metabolic pathway from our analysis, cysteine and methionine metabolism (**Figure 1C, Table S3.1**). Indeed, OCM is a nexus of multiple metabolic pathways that are necessary for survival; OCM is implicated in multiple longevity pathways, including dietary restriction, insulin/IGF-1 signaling, and the metformin-induced longevity response[13,16,23]. Due to its relevance in multiple longevity pathways and the direct involvement of cysteine and methionine metabolism within this metabolic network, we postulated that *fmo-2* regulates longevity through its interactions with OCM.

To test whether *fmo-2* expression modifies OCM, we used targeted metabolomics analysis on a panel of metabolites involved in OCM and related pathways to determine whether their abundance levels were altered following *fmo-2* expression (**Data S3.3**). We hypothesized that the affected metabolites would have abundance levels that correlate with *fmo-2* expression level. To look for changes between groups, we initially compared the metabolite levels between the wild type and FMO-2 OE and also between the wild type and FMO-2 KO. In line with our hypothesis that OCM is altered by *fmo-2* expression, we observed significant changes in abundance levels of homocysteine, s-adenosylmethionine (SAM), and pyridoxal 5'-phosphate in FMO-2 OE,

and of methionine and cystine in FMO-2 KO, when compared to the wild type (**Table S3.2**). To test whether *fmo-2* expression levels statistically modulate OCM metabolites in correlation with *fmo-2* expression, we performed ANOVA trend analysis on the data from all three strains. We identified a significant change in levels of methionine, pyridoxal 5'-phosphate, homocysteine, and SAM in line with changes in the expression of *fmo-2* **(Figure 3.1D).** Furthermore, betaine, folic acid, serine, and cystathionine levels all show a trend with *fmo-2* expression, but they did not reach statistical significance below a 0.05 p-value (**Figure S3.1**). Taken together, our results are consistent with the hypothesis that the OCM pathway is modified by *fmo-2* expression.

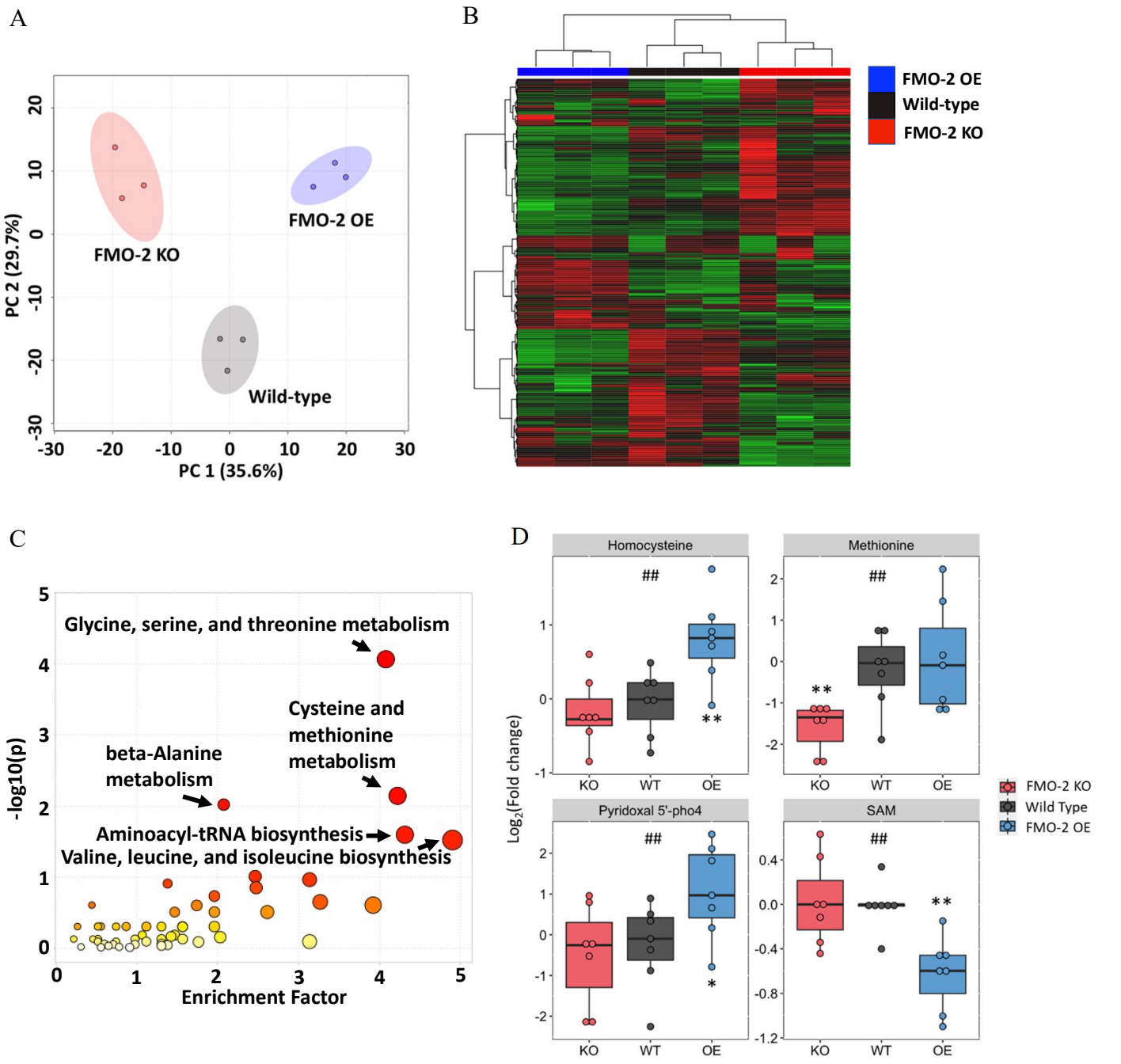
A
FMO-2 KO
FMO-2 OE
Wild-type
PC 2 (29.7%)
PC 1 (35.6%)
B
FMO-2 OE
Wild-type
FMO-2 KO
C
Glycine, serine, and threonine metabolism
Cysteine and methionine metabolism
beta-Alanine metabolism
Aminoacyl-tRNA biosynthesis
Valine, leucine, and isoleucine biosynthesis
-log10(p)
Enrichment Factor
D
Homocysteine
Methionine
Pyridoxal 5'-pho4
SAM
Log2(Fold change)
KO
WT
OE
FMO-2 KO
Wild Type
FMO-2 OE

Figure 3.1: One carbon metabolism is altered by *fmo-2* expression level. A) Principal component analysis of untargeted LC-MS metabolomics data of wild type, FMO-2 OE, and FMO-2 KO strains of *C. elegans*. B) Heatmap of untargeted LC-MS metabolomics data of the wild type, FMO-2 OE and FMO-2 KO. C) Pathway enrichment analysis using untargeted LC-MS metabolomics data of wild type and FMO-2 OE. D) Comparison of targeted metabolomics data of metabolites related to OCM between the wild type, FMO-2 OE and FMO-2 KO, normalized to the average of wild type intensity. pho4 = phosphate. SAM = s-adenosylmethionine. * represents $p < 0.05$, ** represents $p < 0.01$, and *** represents $p < 0.001$ using two-tailed Student's t-test. # represents $p < 0.05$ and ## represents $p < 0.01$ using one-way ANOVA trend analysis. Statistics are in Table S3.2. Figures 3.1A-C are generated using MetaboAnalyst. No notes = Not significant.

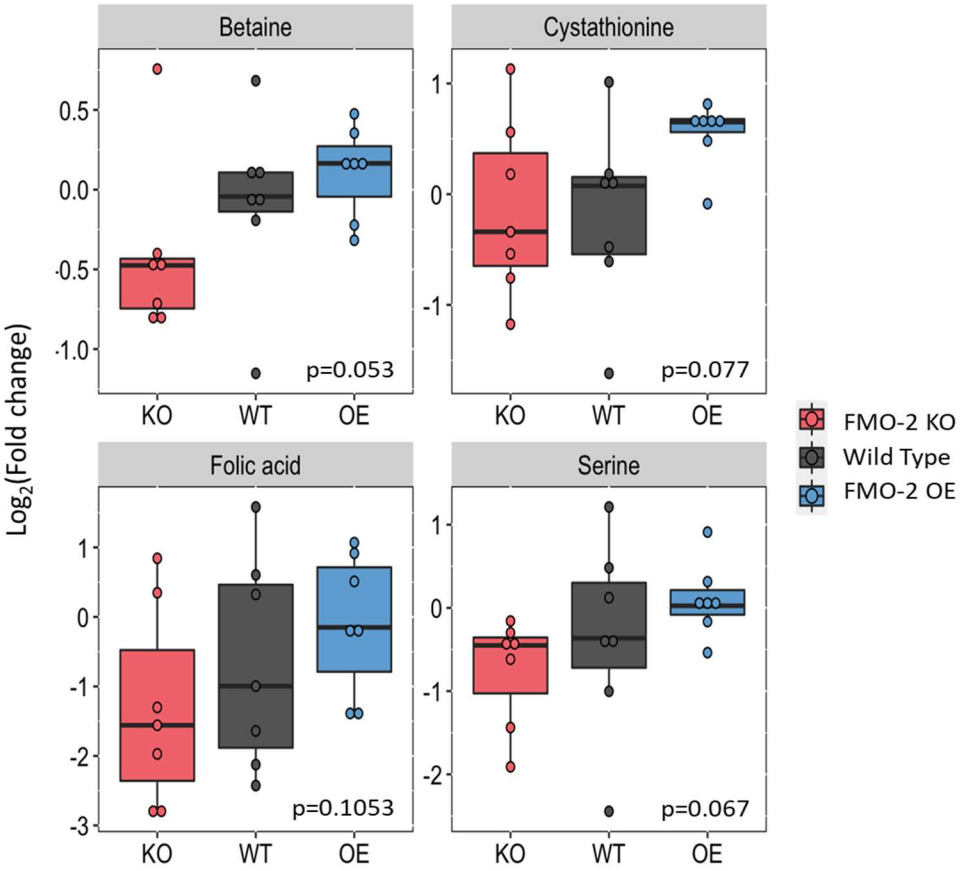

Figure S3.1: Comparison of targeted metabolomics data of metabolites related to OCM between the wild type, FMO-2 OE and FMO-2 KO. P-values are derived from one-way ANOVA trend analysis. Statistics are in Supplemental Table 2. No notes = Not significant

One carbon metabolism interacts with fmo-2 to regulate stress resistance and longevity

Having established that FMO-2 modifies endogenous metabolism broadly and OCM specifically, we next hypothesized that these metabolic changes are causal for longevity phenotypes. Previous studies identify increased stress resistance as a common phenotype shared by multiple long-lived organisms both within and between species[24–27]. To determine the functional interaction between *fmo-2* and OCM, we used RNAi to knockdown the expression of genes involved in OCM (**Figure 3.2A**) and tested for their role in promoting or repressing survival against the oxidative stressor paraquat. Of the eight genes that we tested, the individual knockdown of four genes, *sams-1*, *mel-32*, *mtrr-1*, and *Y106G6E.4*, exhibit altered stress resistance phenotypes for the wild type and FMO-2 OE (**Figure 3.2B-E**), as assessed using log-rank test with a cutoff threshold of $p < 0.05$ compared to the empty vector (EV) controls. Two of these genes, *sams-1*, and *mel-32*, show interaction with FMO-2 OE, as assessed by Cox regression analysis with p-value cutoff of 0.01 (**Table 3.1**). Interestingly, while *sams-1* knockdown extends worm lifespan[17], we find that knocking down *sams-1* decreases the stress resistance of the wild type and FMO-2 OE (**Figure 3.2B**), suggesting that the regulation of lifespan and stress resistance are uncoupled in this instance. This result is similar to previous work showing that *sams-1* knockdown is detrimental to survival under pathogen exposure[28]. We further find that *sams-1* knockdown interacts with FMO-2 OE, whereby it more severely decreases FMO-2 OE paraquat resistance compared to that of the wild type (**Figure 3.2B**). Conversely, we find that knocking down *mel-32* increases the resistance of both the wild type and FMO-2 OE, but it again shows an

interaction with FMO-2 OE, whereby FMO-2 OE has more modest extension compared to the wild type (**Figure 3.2C**).

We also find that knocking down *Y106G6E.4* and *mtrr-1* increase the stress resistance of both the wild type and FMO-2 OE without significant interaction with FMO-2 OE (**Figure 3.2D and 3.2E**), suggesting that the stress resistance conferred by the suppression of these genes is independent of *fmo-2*. Knocking down *atic-1*, *alh-3, cbs-1, and cth-2* yield inconsistent results in our experiments (**Table S3.3**). Overall, our data show that 2/8 of the genes that we tested interact with FMO-2 OE to modify paraquat resistance. While these results do not definitively prove that FMO-2 acts through OCM, they are consistent with the hypothesis that OCM is a regulator of stress resistance and that there is a genetic interaction between *fmo-2* and OCM in that regulation.

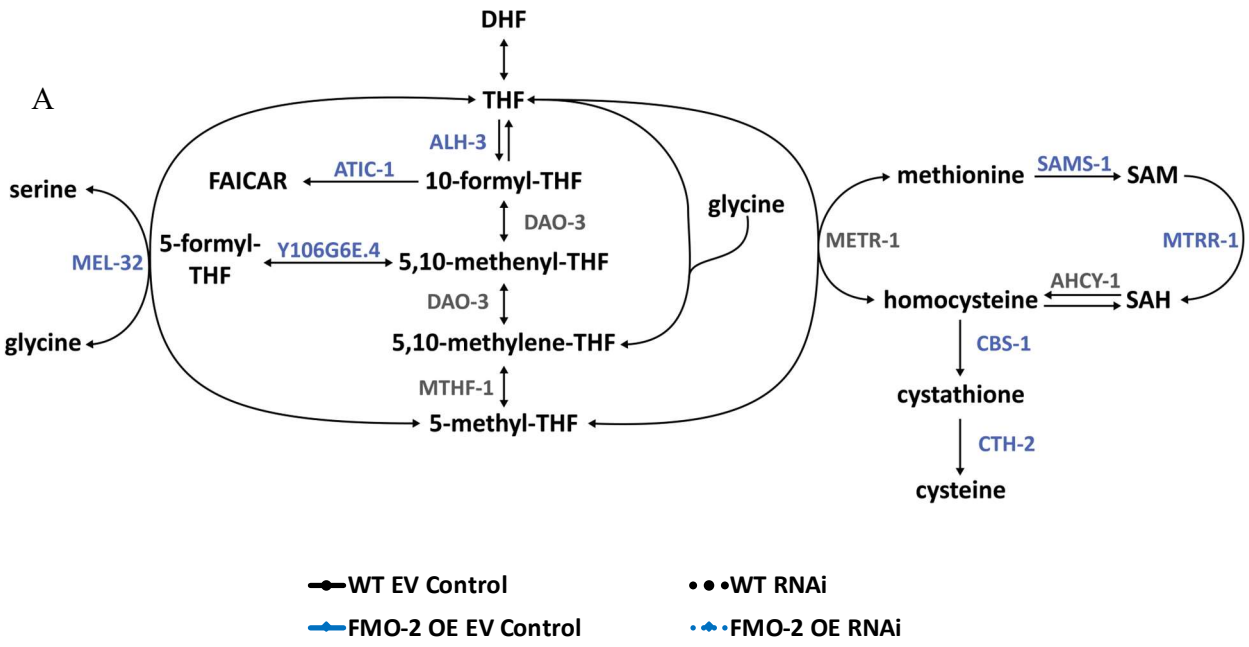
A
DHF
THF
ALH-3
FAICAR
ATIC-1
10-formyl-THF
DAO-3
serine
MEL-32
5-formyl-THF
Y106G6E.4
5,10-methenyl-THF
glycine
DAO-3
glycine
5,10-methylene-THF
MTHF-1
5-methyl-THF
methionine
SAMS-1
SAM
METR-1
MTRR-1
AHCY-1
homocysteine
SAH
CBS-1
cystathione
CTH-2
cysteine
WT EV Control
WT RNAi
FMO-2 OE EV Control
FMO-2 OE RNAi

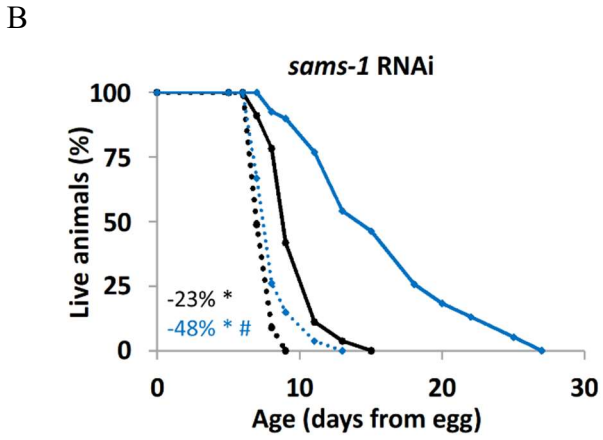
B
sams-1 RNAi
Live animals (%)
100
75
50
25
0
-23% *
-48% * #
0
10
20
30
Age (days from egg)

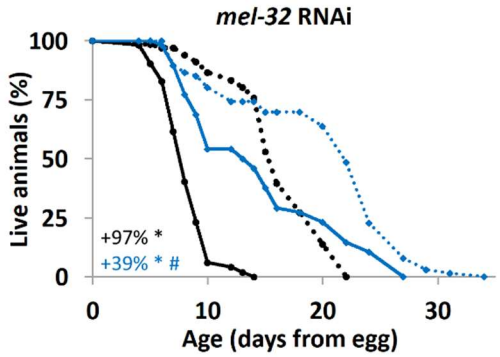
C
mel-32 RNAi
Live animals (%)
100
75
50
25
0
+97% *
+39% * #
0
10
20
30
Age (days from egg)

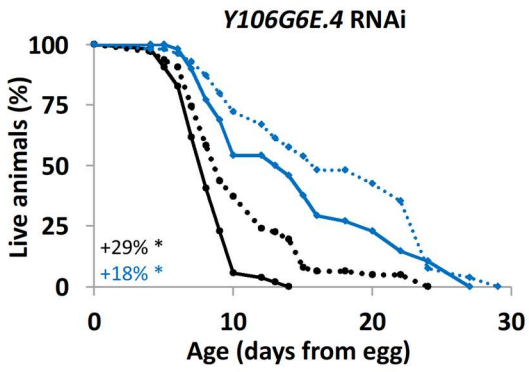
D
Y106G6E.4 RNAi
Live animals (%)
100
75
50
25
0
+29% *
+18% *
0
10
20
30
Age (days from egg)

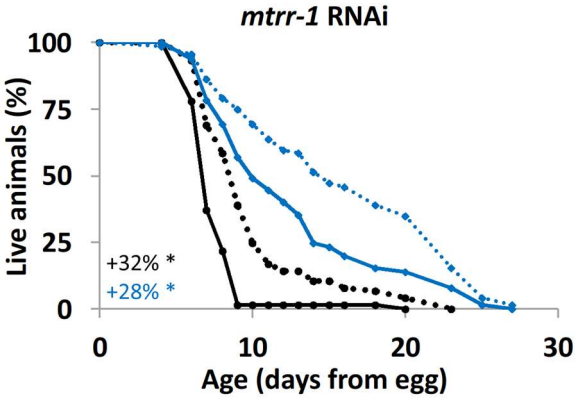
E
mtrr-1 RNAi
Live animals (%)
100
75
50
25
0
+32% *
+28% *
0
10
20
30
Age (days from egg)

Figure 3.2: *Fmo-2* interacts with OCM genes to regulate stress resistance. A) Diagram of OCM network. Genes included here are labeled in blue and genes not included are labeled in gray. 5 mM paraquat stress resistance assay comparing the wild type and FMO-2 OE on empty-vector (EV) and B) *sams-1* RNAi, C) *mel-32* RNAi, D) *Y106G6E.4* RNAi, and E) *mtrr-1* RNAi. Percent change in mean survival compared to their respective EV controls are shown in the left bottom corner of the figures. Black = wild type and blue = FMO-2 OE. * denotes significant change in mean survival at $p < 0.05$ using log-rank. # denotes significant interaction with the RNAi at $p < 0.01$ using Cox regression. Statistics are in Table S3.3 and Data S3.4.

Table 3.1. Cox regression analysis of OCM/tryptophan metabolism genes and *fmo-2* modified strains paraquat stress resistance data

	Experimental		FMO-2 OE		Interact with FMO-2 OE	
	Haz. Ratio	p-value	Haz. Ratio	p-value	Haz. Ratio	p-value
sams-1	1.630	<0.001	0.273	<0.001	2.982	<0.001
mel-32	0.299	<0.001	0.263	<0.001	1.593	0.002
mtrr-1	0.732	0.001	0.323	<0.001	0.874	0.310
Y106G6E.4	0.493	<0.001	0.309	<0.001	1.184	0.200
kmo-1	0.321	<0.001	0.243	<0.001	2.741	<0.001
tdo-2	1.721	<0.001	0.290	<0.001	1.477	<0.001
nkat-1	0.667	<0.001	0.302	<0.001	0.848	0.212

Experimental = effect of RNAi condition on worm stress resistance
FMO-2 OE = effect of overexpressing *fmo-2* on worm stress resistance
Interact with FMO-2 OE = interaction between RNAi and overexpressing *fmo-2* on worm stress resistance

Hazard ratio > 1 = decrease in stress resistance
Hazard ratio < 1 = increase in stress resistance

To test the interaction between *fmo-2* and OCM more directly, we performed lifespan experiments using RNAi knockdown of genes from our paraquat resistance screen (**Figures 3.3A-G**). We included FMO-2 KO in the lifespan analysis to determine if the interactions that we identify are dependent on *fmo-2* expression.

Multiple gene knockdowns show altered lifespan phenotypes for the wild type, FMO-2 OE, and FMO-2 KO that suggest interaction with FMO-2. Of the eight genes we tested, knockdown of two genes, *alh-3* and *atic-1*, suppress the lifespan extension of FMO-2 OE without affecting the lifespan of the wild type and FMO-2 KO (**Figure 3.3A and 3.3B**). Similar to our paraquat stress resistance experiments, we conclude this based on 1) log-rank test showing changes only in FMO-2 OE lifespan with a cutoff threshold of $p < 0.05$ compared to their respective empty vector (EV) controls, and 2) cox regression analysis (**Table S3.4, Table 3.2**) showing a differential interaction with FMO-2 OE and FMO-2 KO, using a cutoff threshold of $p < 0.01$. These results suggest that *alh-3* and *atic-1* are required for *fmo-2*-mediated lifespan extension and are consistent with previous reports that their expression levels are upregulated in long-lived worms[11,29]. *alh-3* is upregulated in *eat-2* mutants and *atic-1* is upregulated in both *eat-2* and *daf-2* mutants[11,29–31]. Thus, it is plausible that these genes are required for multiple longevity pathways, including FMO-2 overexpression.

In contrast to *alh-3* and *atic-1*, knockdown of *sams-1* increases the lifespan of the wild type, FMO-2 KO, and FMO-2 OE animals (**Figure 3.3C**). However, *sams-1* knockdown shows interactions with both FMO-2 KO and FMO-2 OE, whereby both strains show less extension under *sams-1* knockdown compared to the wild type, with FMO-2 OE showing a larger interaction effect size (**Table 3.2**). This suggests that there

is a functional overlap between *sams-1* and *fmo-2* in regulating longevity. Additionally, we find that knocking down *mel-32* only interacts with FMO-2 OE and extends its lifespan (**Table 3.2 and Figure 3.3D**). It is plausible that the metabolic alterations resulting from increased *fmo-2* expression are required for *mel-32* gene suppression to promote worm lifespan.

Knockdown of the remaining four genes, *cbs-1*, *cth-2*, *mtrr-1*, and Y106G6E.4, do not show interaction with FMO-2 KO and FMO-2 OE (**Table 3.2**). However, knocking down *cth-2* decreases the lifespan of all three strains, suggesting that this gene is generally required for worm health and survival (**Figure 3.3E**). Knocking down *mtrr-1* and Y106G6E.4 do not affect the lifespan of the worms in our experiments (**Figures 3.3F and 3.3G**) and knocking down *cbs-1* yields inconsistent results in our experiments (**Table S3.4**).

In total, our data show that half (4/8) of the genes tested interact with FMO-2 OE: two genes are required for FMO-2 OE lifespan extension (*alh-3* and *atic-1*), another gene interacts with FMO-2 OE and FMO-2 KO (*sams-1*), placing it in the same functional pathway with FMO-2, and one gene only extends the lifespan of FMO-2 OE when knocked down (*mel-32*). Together, our lifespan data, combined with our metabolomics results, support an interaction between *fmo-2* and genes involved with OCM in regulating worm lifespan.

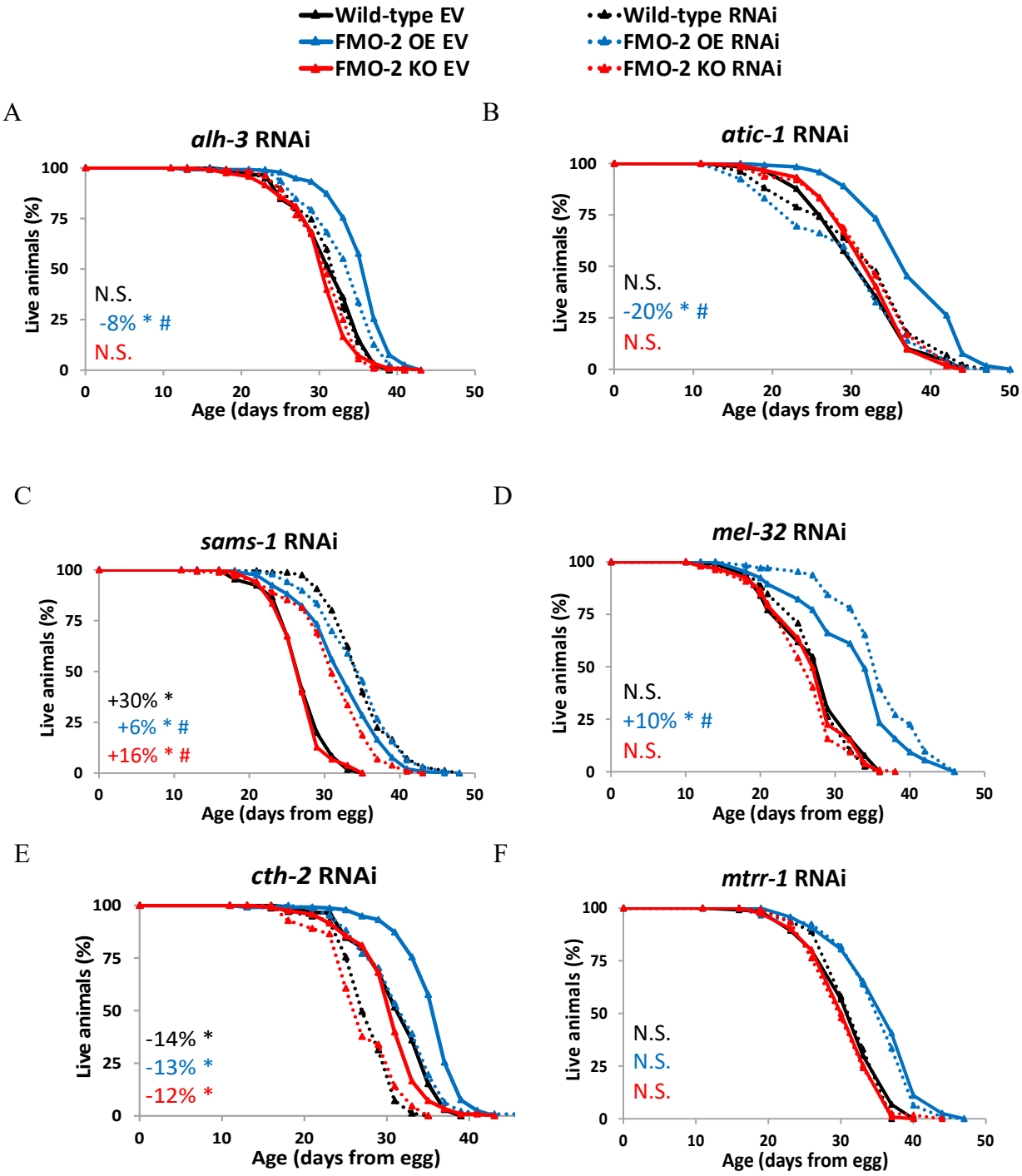
Wild-type EV
FMO-2 OE EV
FMO-2 KO EV
Wild-type RNAi
FMO-2 OE RNAi
FMO-2 KO RNAi
A
alh-3 RNAi
N.S.
-8% * #
N.S.
B
atic-1 RNAi
N.S.
-20% * #
N.S.
C
sams-1 RNAi
+30% *
+6% * #
+16% * #
D
mel-32 RNAi
N.S.
+10% * #
N.S.
E
cth-2 RNAi
-14% *
-13% *
-12% *
F
mtrr-1 RNAi
N.S.
N.S.
N.S.
Live animals (%)
Age (days from egg)

G

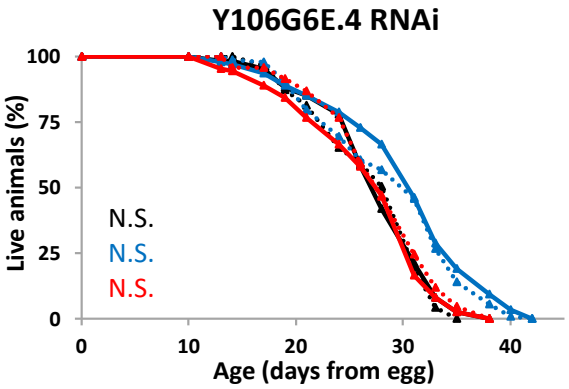

Figure 3.3: *Fmo-2* interacts with OCM genes to regulate lifespan. A) Diagram of OCM network. Genes included here are labeled in blue and genes not included are labeled in gray. Lifespan analysis comparing the wild type and FMO-2 OE on empty-vector (EV) and B) *alh-3* RNAi, C) *atic-1* RNAi, D) *sams-1* RNAi, E) *mel-32* RNAi, F) *cth-2* RNAi, G) *mtrr-1* RNAi, and H) Y106G6E.4 RNAi. Percent change in mean lifespan compared to their respective EV controls are shown in the left bottom corner of the figures. Black = wild type, blue = FMO-2 OE, and red = FMO-2 KO. * denotes significant change in mean lifespan at $p < 0.05$ using log-rank and # denotes significant interaction between the RNAi of interest and *fmo-2* genotype at $p < 0.01$ using Cox regression analysis. N.S. = not significant. Statistics are in Table S3.4 and Data S3.5.

Table 3.2. Cox regression analysis of OCM/tryptophan metabolism genes and *fmo-2* modified strains lifespan data

	Experimental		FMO-2 KO		FMO-2 OE		Interact with FMO-2 KO		Interact with FMO-2 OE	
	Haz. Ratio	p-value	Haz. Ratio	p-value	Haz. Ratio	p-value	Haz. Ratio	p-value	Haz. Ratio	p-value
alh-3	0.974	0.715	1.050	0.510	0.480	<0.001	1.088	0.413	1.333	0.005
atic-1	0.923	0.269	1.051	0.501	0.511	<0.001	0.898	0.302	1.641	<0.001
sams-1	0.298	<0.001	1.003	0.972	0.359	<0.001	1.632	<0.001	2.652	<0.001
mel-32	1.098	0.246	1.110	0.191	0.505	<0.001	0.891	0.307	0.455	<0.001
cth-2	1.619	<0.001	1.122	0.072	0.491	<0.001	1.183	0.058	0.932	0.417
mtrr-1	1.184	0.025	1.152	0.058	0.490	<0.001	0.963	0.718	1.089	0.421
Y106G6E.4	0.949	0.470	1.053	0.485	0.481	<0.001	0.848	0.118	1.079	0.456
kmo-1	3.160	<0.001	1.389	<0.001	0.513	<0.001	0.678	<0.001	0.798	0.038
tdo-2	0.306	<0.001	1.388	<0.001	0.510	<0.001	1.464	0.001	1.830	<0.001
nkat-1	1.090	0.221	1.298	<0.001	0.512	<0.001	0.836	0.067	0.785	0.015
Formate	0.623	<0.001	1.320	0.005	0.403	<0.001	1.231	0.156	1.625	0.001

Experimental = effect of experimental condition on worm lifespan
FMO-2 KO = effect of knocking out *fmo-2* on worm lifespan
FMO-2 OE = effect of overexpressing *fmo-2* on worm lifespan
Interact with FMO-2 KO = interaction between experimental condition and knocking out *fmo-2* on worm lifespan
Interact with FMO-2 OE = interaction between experimental condition and overexpressing *fmo-2* on worm lifespan

Hazard ratio > 1 = decrease in lifespan
Hazard ratio < 1 = increase in lifespan

Fmo-2 influences longevity by modulating the transmethylation pathway

Our data are consistent with a model where *fmo-2* interacts with OCM to regulate longevity and stress resistance. Previous studies identify multiple pathways that affect longevity and are also involved in OCM, including nucleotide metabolism, the transsulfuration pathway, and the transmethylation pathway[11,16,17]. Some of these pathways are also implicated in modifying longevity downstream of dietary restriction in multiple animal models[16,17,32], making it likely that one or more of these pathways are in the same functional pathway as *fmo-2*. However, the metabolic consequences of *fmo-2* expression on these pathways are not clear based on the changes observed in our targeted metabolomics analysis alone, as the data only show metabolic changes at a single time point and most of the metabolites within OCM are intermediate metabolites. The stress resistance and lifespan results further complicate interpretation as some genes do not affect these phenotypes and some have effects that are independent of *fmo-2*.

To help determine the biological relevance of the changes we observed in the OCM network following *fmo-2* expression, we applied a computational model (**Data S3.6**) to predict how enzyme expression (**Table S3.5**) changes may affect the output fluxes of OCM. The model assumes a steady-state mass balance of fluxes in the reactions illustrated in **Figure 3.4A**. This simple model includes eight reaction fluxes and five fluxes representing transport of methionine (met), tetrahydrofolate (thf), s-adenosylmethionine (sam), cysteine (cys), and 5,10-methylenetetrahydrofolate (5,10thf) into and out of the folate cycle and the methionine cycle. The model output fluxes represent important inputs for the nucleotide metabolism, the transsulfuration pathway,

and the transmethylation pathway, each of which are reported to be important for influencing the aging process[11,16,17] and are potential targets for the *fmo-2*-mediated longevity response. The stoichiometric coefficients for the reaction and transport processes in this system are stored in the matrix S (**Table S3.6**), where under steady-state conditions S***J** = **0**, where **J** is the vector of fluxes[33,34]. The entries in the vector **J** and matrix S are defined in **Figure 3.4A**. Vectors that satisfy the mass-balance relationship S***J** = **0** are said to belong to the nullspace of S. To predict how changes in the expression of genes for the enzymes catalyzing the reactions in this network may affect the output fluxes, we projected the gene expression data (**Table S3.5**) onto the nullspace of S (details provided in the Methods). This projection predicts an inverse correlation between *fmo-2* expression and flux through methylation reactions, where the methylation flux is predicted to be reduced in FMO-2 OE and increased in FMO-2 KO compared to wild type (**Figure 3.4B, Figure S3.2A-C**). This analysis does not predict correlative changes to flux through nucleotide metabolism or the transsulfuration pathway.

Based on this analysis, we hypothesized that artificially decreasing the flux through methylation should replicate FMO-2 OE longevity in the wild type and FMO-2 KO strains, while not affecting the FMO-2 OE worms. *sams-1* encodes for s-adenosylmethionine synthase and is involved in the conversion of methionine into s-adenosylmethionine (SAM). Suppression of *sams*-1 has been previously shown to decrease SAM level[35] and increase longevity[17]. Moreover, while *sams-1* has multiple orthologs, previous work has shown that knocking down sams-1 is sufficient to manipulate SAM levels in worms[35]. We find that *sams-1* RNAi recapitulates FMO-2 OE

lifespan extension in the wild type while interacting with FMO-2 OE, whose lifespan was significantly less affected **(Figure 3.3D, Table 3.2)**. Our data are consistent with previous studies showing that knockdown of *sams-1* fails to further extend the lifespan of the genetic DR model *eat-2* mutants[17], thereby placing *sams-1* knockdown in the same functional pathway as FMO-2 OE.

To validate the model metabolically, we used the abundance level of SAM and s-adenosylhomocysteine (SAH) from our targeted metabolomics analysis to calculate the SAM/SAH ratio. The SAM/SAH ratio is used as a biomarker for methylation potential, where a decrease in the ratio suggests a hypomethylated state and an increase suggests a hypermethylated state[36,37]. Consistent with our computational model prediction, we observed a significant reduction in the SAM/SAH ratio for FMO-2 OE (hypomethylation) and a significant trend in SAM/SAH ratio corresponding to *fmo*-2 expression by ANOVA trend analysis. (**Figure 3.4C**). In addition, we find that supplementing the worm diet with 2 mM SAM results in a reduction of FMO-2 OE lifespan (**Figure S3.2D**). Overall, our computational model prediction and experimental data support the hypothesis that *fmo-2* expression reduces flux through the transmethylation pathway, and that this reduction extends worm lifespan.

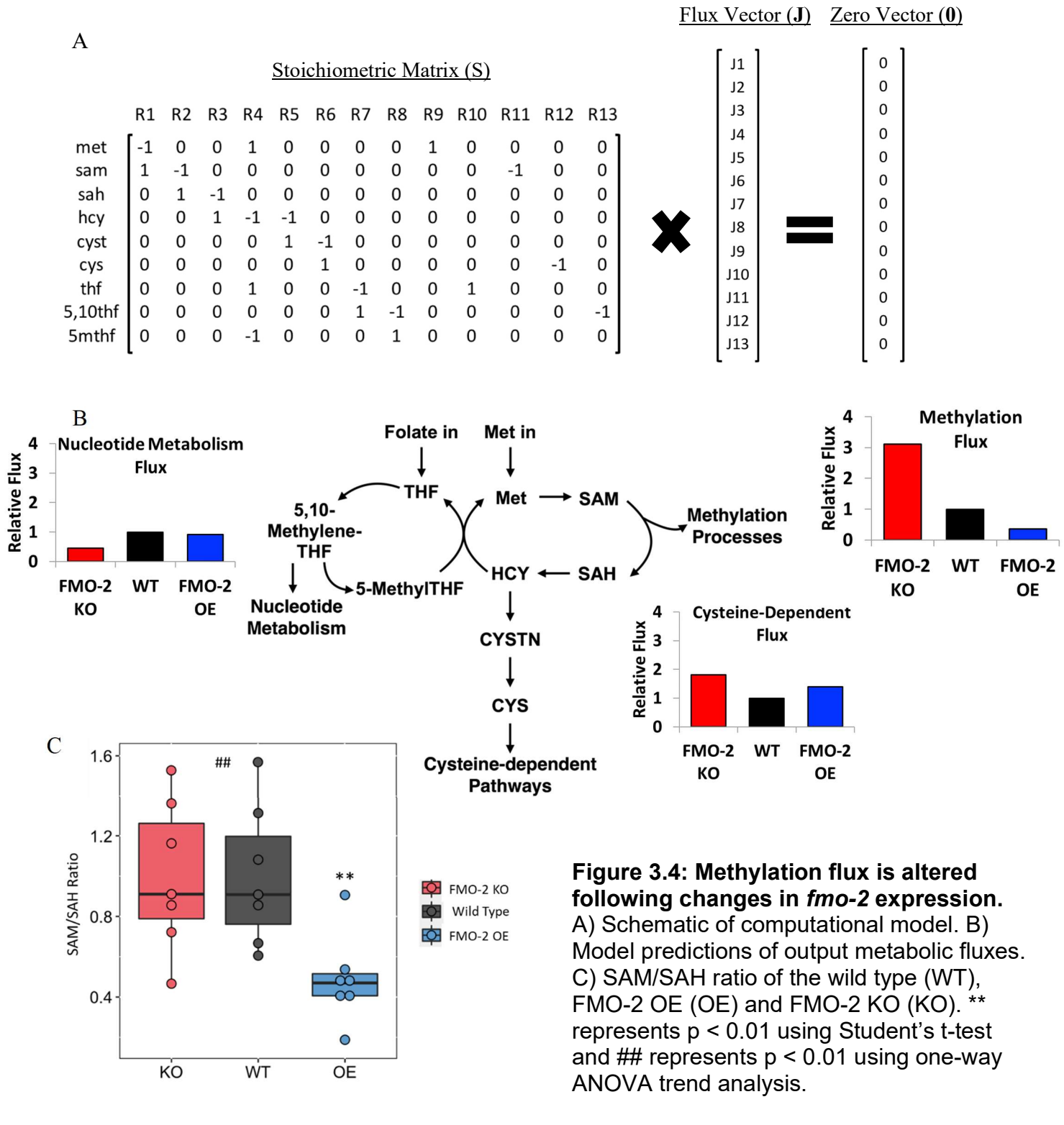

Figure 3.4: Methylation flux is altered following changes in *fmo-2* expression. A) Schematic of computational model. B) Model predictions of output metabolic fluxes. C) SAM/SAH ratio of the wild type (WT), FMO-2 OE (OE) and FMO-2 KO (KO). ** represents $p < 0.01$ using Student's t-test and ## represents $p < 0.01$ using one-way ANOVA trend analysis.

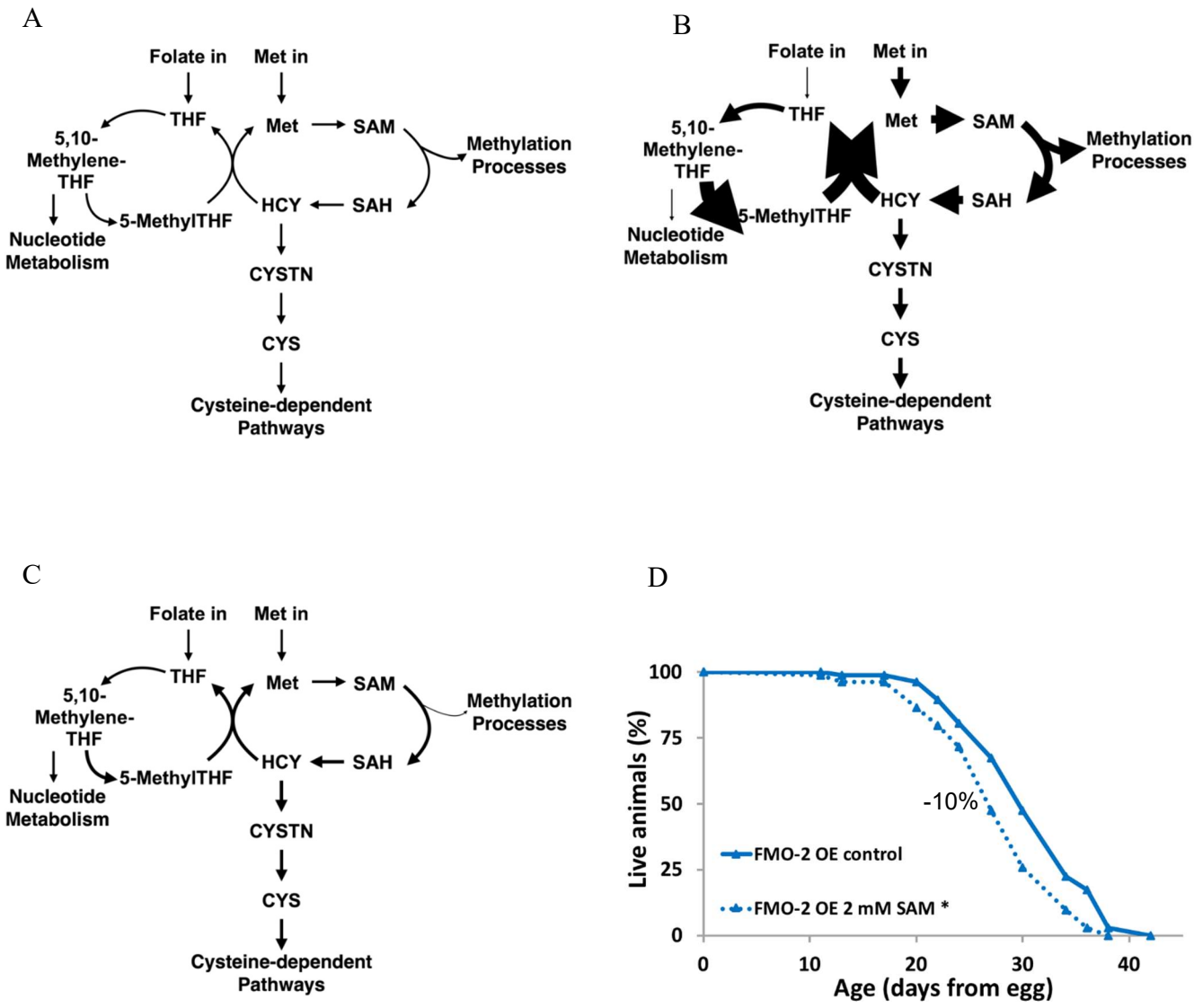

Figure S3.2: Computational model predicts reduced flux through methylation processes. Model predictions of OCM fluxes for A) the wild type, B) FMO-2 OE, and C) FMO-2 KO after normalization to the wild type. Arrow weights represent changes in each flux relative to the wild type, which is set to be equal to 1. D) Lifespan assay comparing the survival of FMO-2 OE on control and 2 mM s-adenosylmethionine supplementation conditions. * denotes significant change in mean lifespan at $p < 0.05$ using log-rank. Statistics are in Table S3.7.

Mammalian FMO metabolomics analysis reveals tryptophan as a substrate of FMO-2

Our data thus far suggest a model where *fmo-2* interacts with OCM to modulate the aging process. However, since FMOs are promiscuous enzymes that oxygenate many nucleophilic atoms, the mechanism by which *fmo-2* induction leads to changes in OCM is not readily evident. FMOs are known as xenobiotic metabolizing enzymes, with many known exogenous targets and few known endogenous targets[1]. Despite extensive knowledge on their enzymatic activity and recent data linking FMOs to endogenous metabolism, no link between specific and systemic metabolism has been made. We hypothesize that a limited number of FMO targets are causal in FMO-2's effects on OCM and, importantly, on the aging process.

Due to the high degree of conservation of catalytic residues between mouse FMOs and CeFMO-2 (**Figure 3.5A**), we referred to our previously published targeted metabolomics of mouse FMO overexpressing (OE) HepG2 cells to determine potential metabolic targets of FMO-2[10]. Using this previously published dataset, our selection criteria for putative substrates of FMO-2 included identifying metabolites that had decreased abundance in at least three of the five FMO OE cell lines to pDEST controls. We used this stringent criteria to identify the most well-conserved targets of FMOs, given that no data exist for CeFMO-2 targets. Using this approach, we identified tryptophan and phenylalanine as potential substrates of FMOs (**Figure 3.5B**). To determine if either of these are substrates of FMO-2, we measured the enzymatic activity of isolated FMO-2 protein in the presence of varying concentrations of tryptophan and phenylalanine. We find that FMO-2 is active toward tryptophan at a reasonable K_m and k_{cat} (K_m: 880 ± 430 μM; k_{cat}: 9.7 ± 1.5 sec^{-1}), suggesting that

tryptophan is a viable substrate of FMO-2 (**Figure 3.5C, Table S3.8**). In comparison, rat and invertebrate TDO enzymes with tryptophan demonstrate Km values of 221 uM and 276.5 uM, respectively, while mammalian IDO1 and IDO2 have Km values of 19.1-74 uM and 45.9 mM, respectively[38], putting the Km value of CeFMO-2 within the range of TDO and IDO proteins. FMO-2 was also active toward phenylalanine, but enzymatic activity did not become apparent until 10 mM, suggesting that phenylalanine is not likely a good endogenous substrate of FMO-2 (**Figure 3.5D**). Since FMO-2 has no previously reported activity toward tryptophan, we used LC-MS with 100, 250, and 500 μM tryptophan under the same enzymatic conditions to determine the product of tryptophan oxygenation. Our resulting data show increasing formation of N-formylkynurenine in a concentration dependent manner with increasing tryptophan in each of the samples. This result suggests that N-formylkynurenine is a product formed by FMO-2 activity toward tryptophan (**Figure 3.5E**). Consistent with these findings, we observe that tryptophan level is significantly reduced in FMO-2 OE compared to the wild type (**Figure 3.5F**). In addition, we find that tryptophan induces *fmo-2* gene expression in vivo, consistent with our hypothesis that tryptophan is a substrate of FMO-2 (**Figure S3.3**). The kinetic parameters of FMO-2 toward NADPH, methimazole, and tryptophan are summarized in **Figure 3.5G**. We also tested additional known substrates of mammalian FMOs, all of which were either poor substrates (e.g., cysteine, phenylalanine, and TMA) or non-substrates of FMO-2 (e.g., 2-heptanone). They are summarized with either the concentration of substrate at which FMO-2 activity is first detected or labeled not determined (N.D.) in **Table S3.8**. While we have observed that phenylalanine level is also significantly reduced in FMO-2 OE compared to the wild type (**Figure 3.5H**), we

believe the effect of FMO-2 on phenylalanine to be indirect as it is a poor substrate *in vitro* (**Figure 3.5D**).

Based on our initial data linking FMO-2 to OCM, it is important to note that in addition to being a key process in the kynurenine pathway, the conversion of tryptophan to N-formylkynurenine precedes the conversion of N-formylkynurenine to kynurenine by formamidase, a process that releases formate, which is also a carbon source for OCM[39]. Formate can enter OCM through the folate cycle, thus providing a connection between tryptophan metabolism, the kynurenine pathway, and OCM. Indeed, we observe a significant interaction between formate supplementation and FMO-2 OE, whereby supplementing the worm diet with formate extends the lifespan of the wild-type without further extending the lifespan of FMO-2 OE (**Figure 3.5I and Table 3.2**). Based on this knowledge, we hypothesize that the kynurenine pathway is a target of FMO-2 that leads to changes in OCM.

A

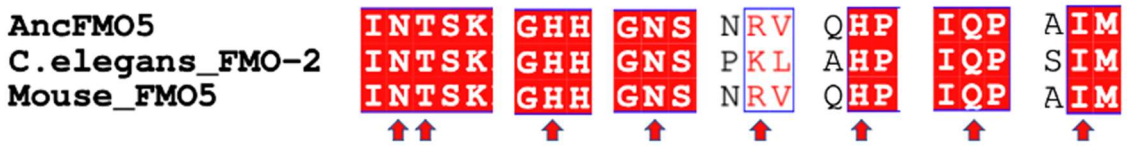
AncFMO5
C.elegans_FMO-2
Mouse_FMO5
INTSK GHH GNS NRV QHP IQP AIM
INTSK GHH GNS PKL AHP IQP SIM
INTSK GHH GNS NRV QHP IQP AIM

B

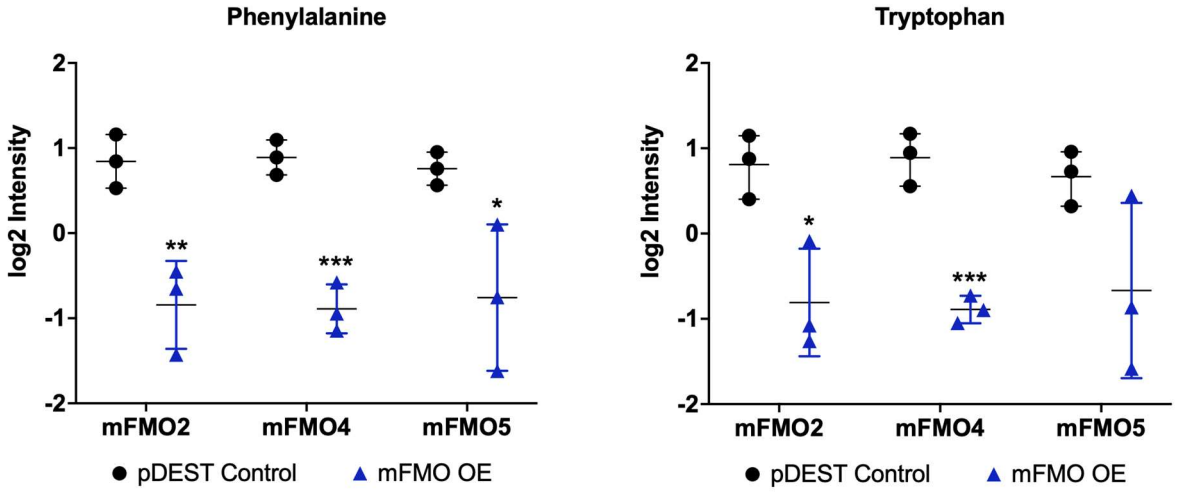
Phenylalanine
log2 Intensity
mFMO2
mFMO4
mFMO5
pDEST Control
mFMO OE
Tryptophan
log2 Intensity
mFMO2
mFMO4
mFMO5
pDEST Control
mFMO OE

C

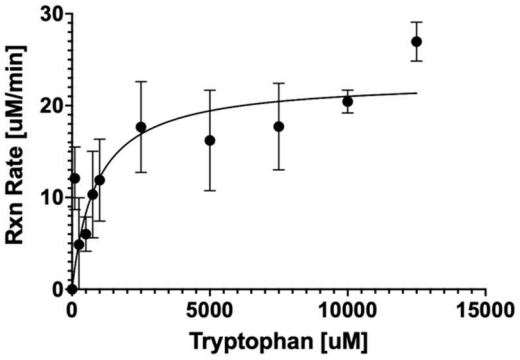
FMO-2 Enzyme Activity
Rxn Rate [uM/min]
Tryptophan [uM]

D

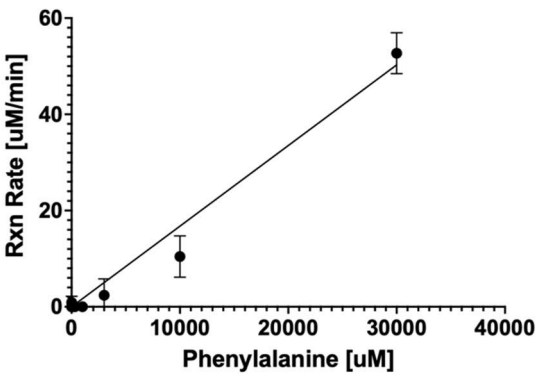
FMO-2 Enzyme Activity
Rxn Rate [uM/min]
Phenylalanine [uM]

E

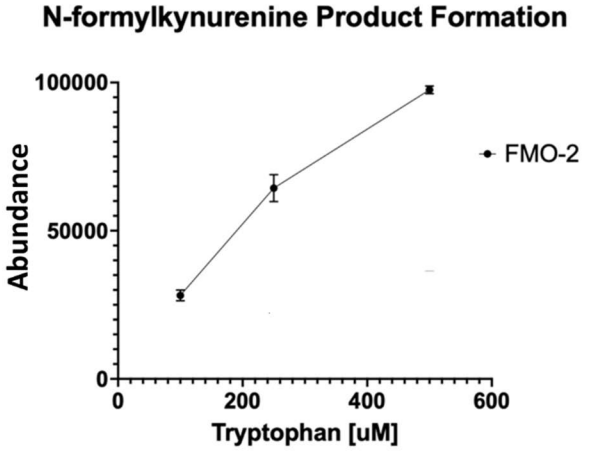
N-formylkynurenine Product Formation
Abundance
FMO-2
Tryptophan [uM]

F

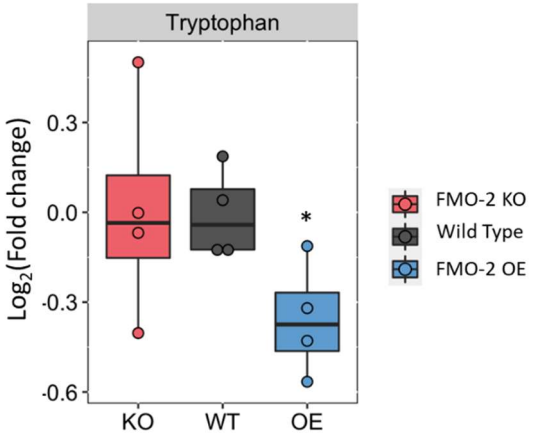
Tryptophan
Log2(Fold change)
KO
WT
OE
FMO-2 KO
Wild Type
FMO-2 OE

G

Substrate	K_m (mM)	k_{cat} (sec^{-1})	Catalytic Efficiency (sec^{-1} M^{-1})
NADPH	2.50 ± 1.24	264 ± 98	105000 ± 65000
Methimazole	1.92 ± 1.14	13.0 ± 6.0	6800 ± 5100
Tryptophan	0.88 ± 0.43	9.7 ± 1.5	11000 ± 5000

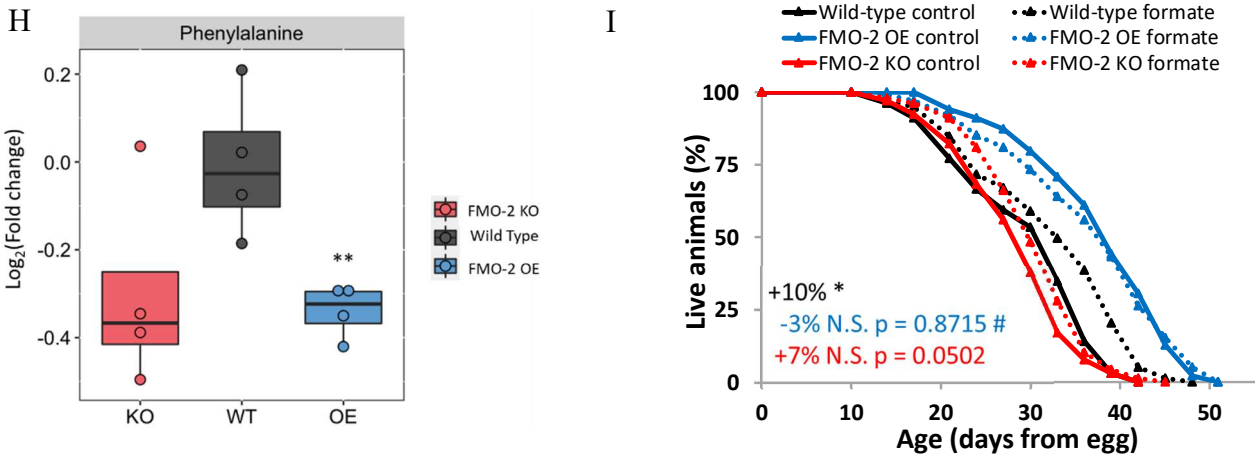

Figure 3.5: Mammalian FMO metabolomics analysis reveals the tryptophan/kynurenine pathway as a target of FMO-2. A) Conserved catalytic residues between CeFMO-2 and mFMO5 (indicated by red arrows). B) The level of phenylalanine and tryptophan present in HepG2 cells expressing pDEST control vector, mFMO2, mFMO4, and mFMO5. * represents $p < 0.05$ by two-tailed Student's t-test. C-D) The reaction rate by concentration for purified CeFMO-2 enzyme toward tryptophan and phenylalanine at 30°C. E) The abundance of N-formylkynurenine based on LC-MS analysis of CeFMO-2 activity toward 100, 250, and 500 µM tryptophan at 30°C. F) Comparison of targeted metabolomics data of tryptophan between the wild type, FMO-2 OE and FMO-2 KO, normalized to the average of wild type intensity. * = $p < 0.05$ using Student's t-test. G) Summary table of Michaelis-Menten parameters for CeFMO-2 cofactor and substrates. H) Comparison of targeted metabolomics data of phenylalanine between the wild type, FMO-2 OE and FMO-2 KO, normalized to the average of wild type intensity. ** = $p < 0.01$ using Student's t-test. I) Lifespan assay comparing the survival of the wild type, FMO-2 OE, and FMO-2 KO on control and 1 mM formate supplementation conditions. Black = wild type, blue = FMO-2 OE, and red = FMO-2 KO. * denotes significant change in mean lifespan at $p < 0.05$ using log-rank and # denotes significant interaction between the condition of interest and *fmo-2* genotype at $p < 0.01$ using Cox regression analysis. N.S. = not significant. Statistics are in Table S3.9 and Data S3.5.

A

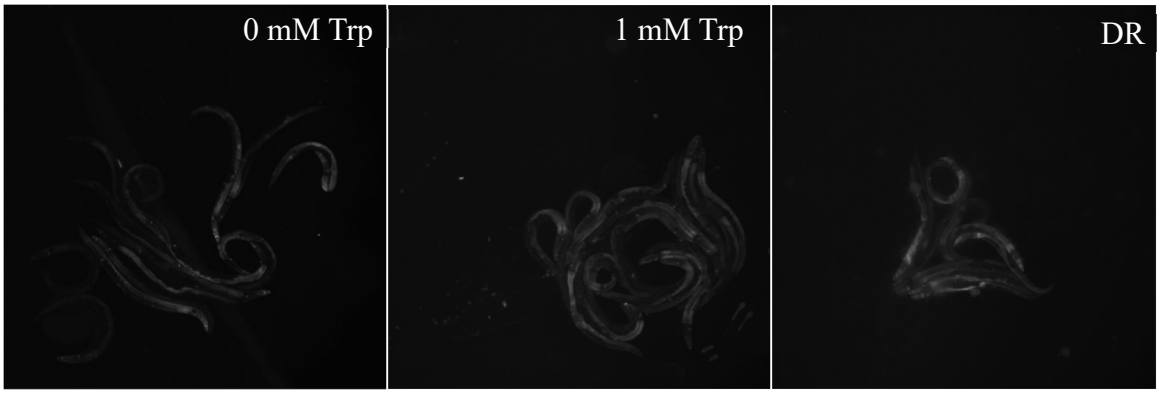

B

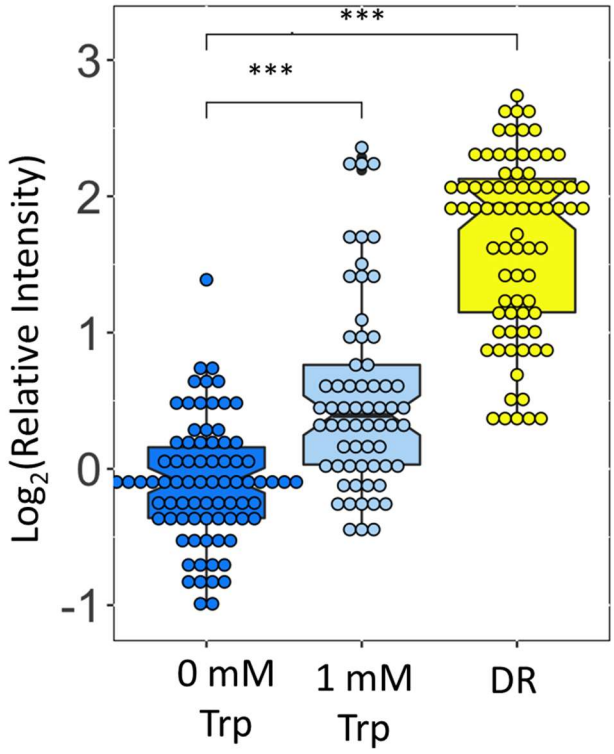

Figure S3.3: Tryptophan induces *fmo-2*. Fluorescence images (A) and quantification (B) of *fmo-2p::mCherry* transcriptional reporter strain under 0 mM tryptophan (fed, negative control), 1 mM tryptophan supplementation and dietary restriction (positive control) conditions. *** denotes p-value <0.0001 using one-way ANOVA.

To test this hypothesis, we assessed whether genes involved in tryptophan metabolism interact with FMO-2 (**Figure 3.6A**). Like our RNAi analyses of the OCM genes, we observe 1) changes in the stress resistance and lifespan of the wild type, FMO-2 OE, and FMO-2 KO worms following the knockdown of genes involved in the kynurenine pathway and 2) interactions between these genes and FMO-2 using the same parameters that we used for the OCM-related genes (**Figures 3.6B-6G, Tables 3.1 and 3.2**). Here, we again observed a separation between the regulation of stress resistance and lifespan under *kmo-1* and *tdo-2* knockdown. Knocking down *kmo-1* increases the stress resistance of the wild type and FMO-2 OE, but shows significant interaction with FMO-2 OE, whereby these worms are less affected by the RNAi compared to their wild type counterparts (**Figure 3.6B, Table 3.1**). Conversely, knocking down *kmo-1* decreases the lifespan of the wild type, FMO-2 OE, and FMO-2 KO (**Figure 3.6E**). However, this knockdown shows significant interaction with FMO-2 KO, whereby these worms are less affected by the RNAi compared to their wild type counterparts (**Table 3.2**). Knocking down *tdo-2* decreases the stress resistance of the wild type and FMO-2 OE but has a significant interaction with FMO-2 OE, whereby these worms are more affected by the RNAi compared to their wild type counterparts (**Figure 3.6C**, **Table 3.1**). Conversely, knocking down *tdo-2* extends the lifespan of the wild type, FMO-2 OE, and FMO-2 KO (**Figure 3.6F**). *Tdo-2* knockdown was previously reported to extend lifespan by inhibiting tryptophan degradation and thereby improving the regulation of proteotoxicity[19]. We find that *tdo-2* knockdown interacts with both FMO-2 KO and FMO-2 OE to modulate longevity, where both strains show reduced lifespan

extension compared to wild type animals (**Table 3.2**). Similar to *sams-1*, it is likely that there is a functional overlap between *tdo-2* and *fmo-2* in regulating worm lifespan.

Knocking down nkat-1 increases the stress resistance of the wild type and FMO-2 OE, but does not show a significant interaction with FMO-2 OE, consistent with it not acting in the same functional pathway as FMO-2 OE to regulate stress resistance (**Figure 3.6D, Table 3.1**). Knocking down *nkat-1* only extends the lifespan of FMO-2 OE but does not show an interaction with it below our statistical threshold (**Figure 3.6G, Table 3.2**). Knocking down *afmd-1* yields inconsistent results in our experiments (**Table S3.5**). In sum, our data support an interaction between multiple genes involved in the kynurenine pathway and FMO-2. Furthermore, our data again separate stress resistance and longevity, and are consistent with the possibility that FMO-2 confers stress resistance and longevity through separable mechanisms.

To prevent egg hatching, our stress resistance and lifespan experiments use 5-fluorodeoxyuridine (FUdR), which is a compound that inhibits a component of one-carbon metabolism, thymidylate synthase (TYMS-1)[40]. We tested whether this drug influences FMO-2 OE lifespan phenotype. We find that FMO-2 OE extends the worm lifespan even in the absence of FUdR (**Figure S3.4**), suggesting that FUdR does not have a major effect on FMO-2-mediated lifespan extension and consistent with published data showing that FUdR is also not required for decreased *sams-1* to extend lifespan[41].

A

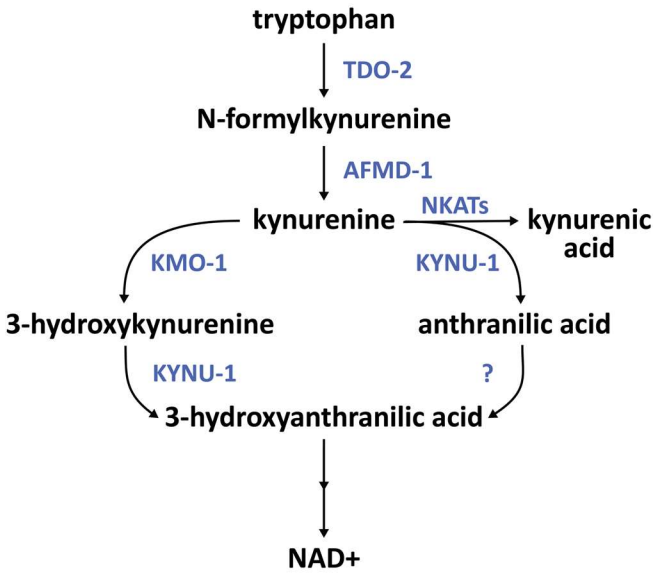
tryptophan
TDO-2
N-formylkynurenine
AFMD-1
kynurenine
NKATs
kynurenic acid
KMO-1
KYNU-1
3-hydroxykynurenine
anthranilic acid
KYNU-1
?
3-hydroxyanthranilic acid
NAD+


WT EV Control
WT RNAi
FMO-2 OE EV Control
FMO-2 OE RNAi

B

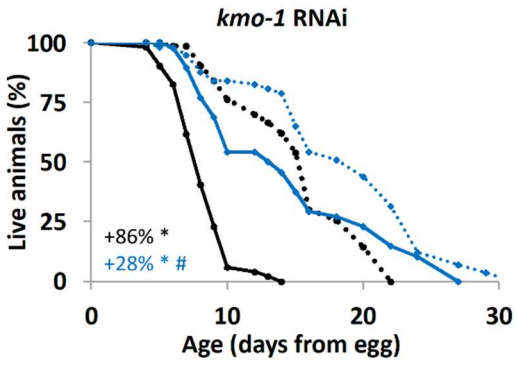
kmo-1 RNAi
Live animals (%)
100
75
50
25
0
+86% *
+28% * #
0
10
20
30
Age (days from egg)

C

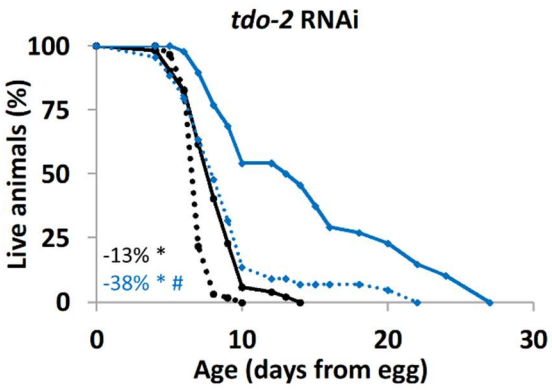
tdo-2 RNAi
Live animals (%)
100
75
50
25
0
-13% *
-38% * #
0
10
20
30
Age (days from egg)

D

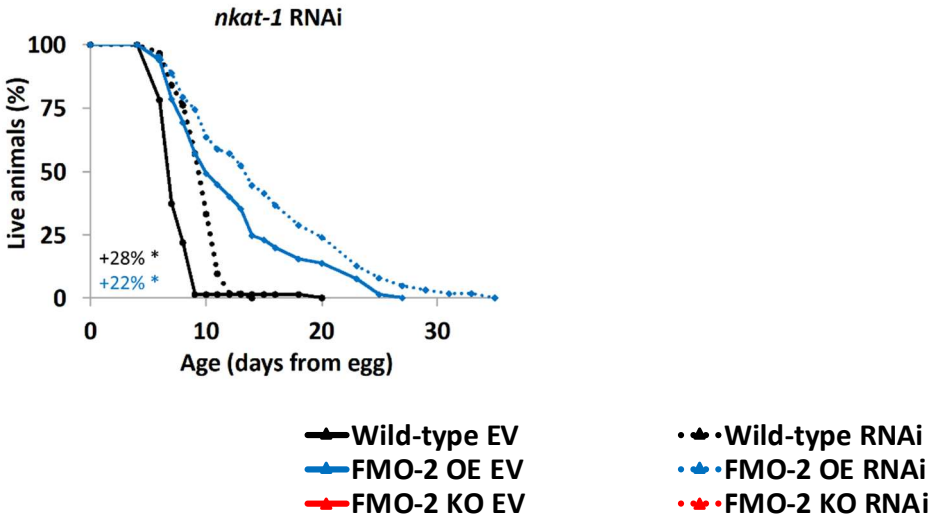
nkat-1 RNAi
Live animals (%)
100
75
50
25
0
+28% *
+22% *
0
10
20
30
Age (days from egg)
Wild-type EV
FMO-2 OE EV
FMO-2 KO EV
Wild-type RNAi
FMO-2 OE RNAi
FMO-2 KO RNAi

E

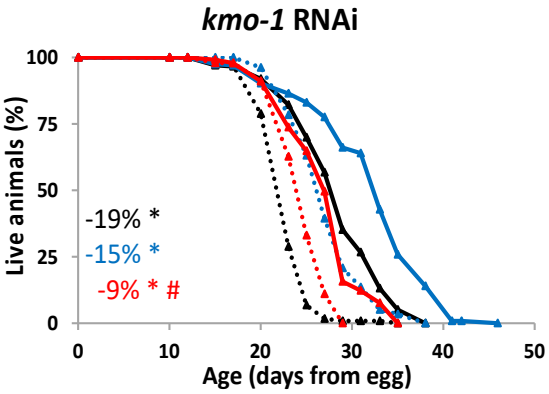
kmo-1 RNAi
Live animals (%)
100
75
50
25
0
-19% *
-15% *
-9% * #
0
10
20
30
40
50
Age (days from egg)

F

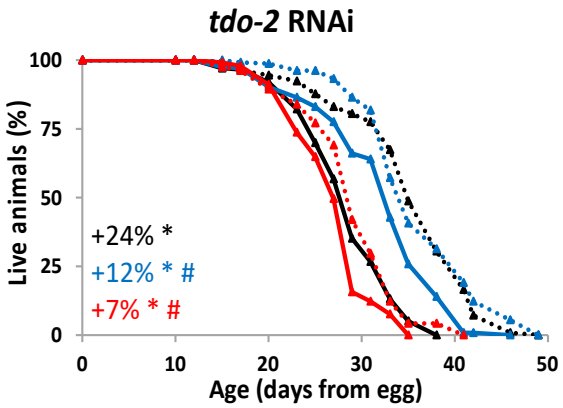
tdo-2 RNAi
Live animals (%)
100
75
50
25
0
+24% *
+12% * #
+7% * #
0
10
20
30
40
50
Age (days from egg)

G

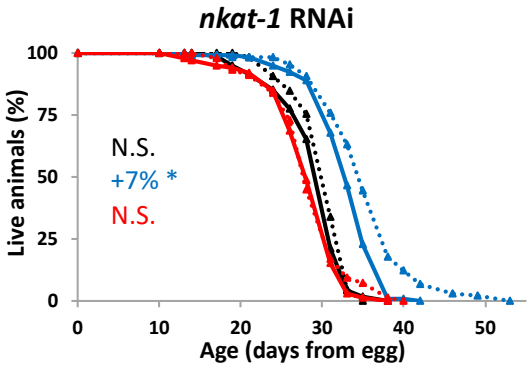
nkat-1 RNAi
Live animals (%)
100
75
50
25
0
N.S.
+7% *
N.S.
0
10
20
30
40
50
Age (days from egg)

Figure 3.6: *Fmo-2* interacts with kynurenine metabolism to regulate stress resistance and lifespan. A) Diagram of the kynurenine pathway. 5 mM paraquat stress resistance assay comparing the wild type and FMO-2 OE on empty-vector (EV) and B) *kmo1-1* RNAi, C) *tdo-2* RNAi and D) *nkat-1* RNAi. Lifespan assay comparing the survival of the wild type, FMO-2 OE, and FMO-2 KO on EV and E) *kmo-1* RNAi, F) *tdo-2* RNAi, and G) *nkat-1* RNAi. Percent change in mean lifespan compared to their respective EV controls are shown in the left bottom corner of the figures. Black = wild type, blue = FMO-2 OE, and red = FMO-2 KO. * denotes significant change in mean lifespan at $p < 0.05$ using log-rank and # denotes significant interaction between the RNAi of interest and *fmo-2* genotype at $p < 0.01$ using Cox regression analysis. N.S. = not significant. Statistics are in Tables S3.3, S3.4 and Data S3.4, S3.5.

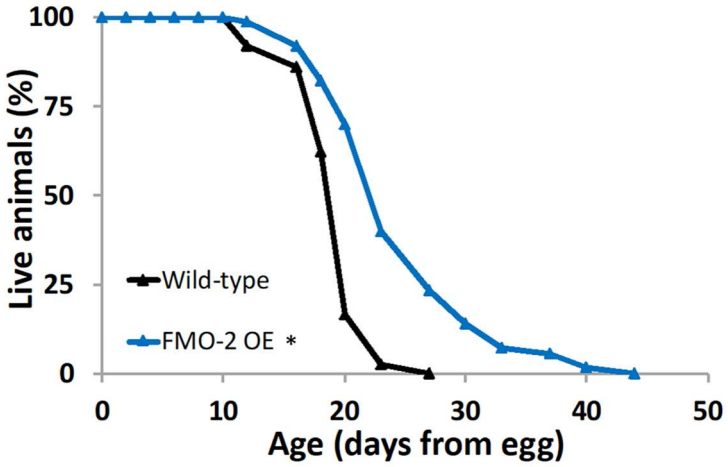

Figure S3.4: FMO-2 extends worm lifespan in the absence of FUdR. Lifespan assay comparing the survival of the wild type and FMO-2 OE in the absence of FUdR. * denotes significant change in mean lifespan at $p < 0.05$ using log-rank. Statistics are in Supplemental Table 10.

Discussion

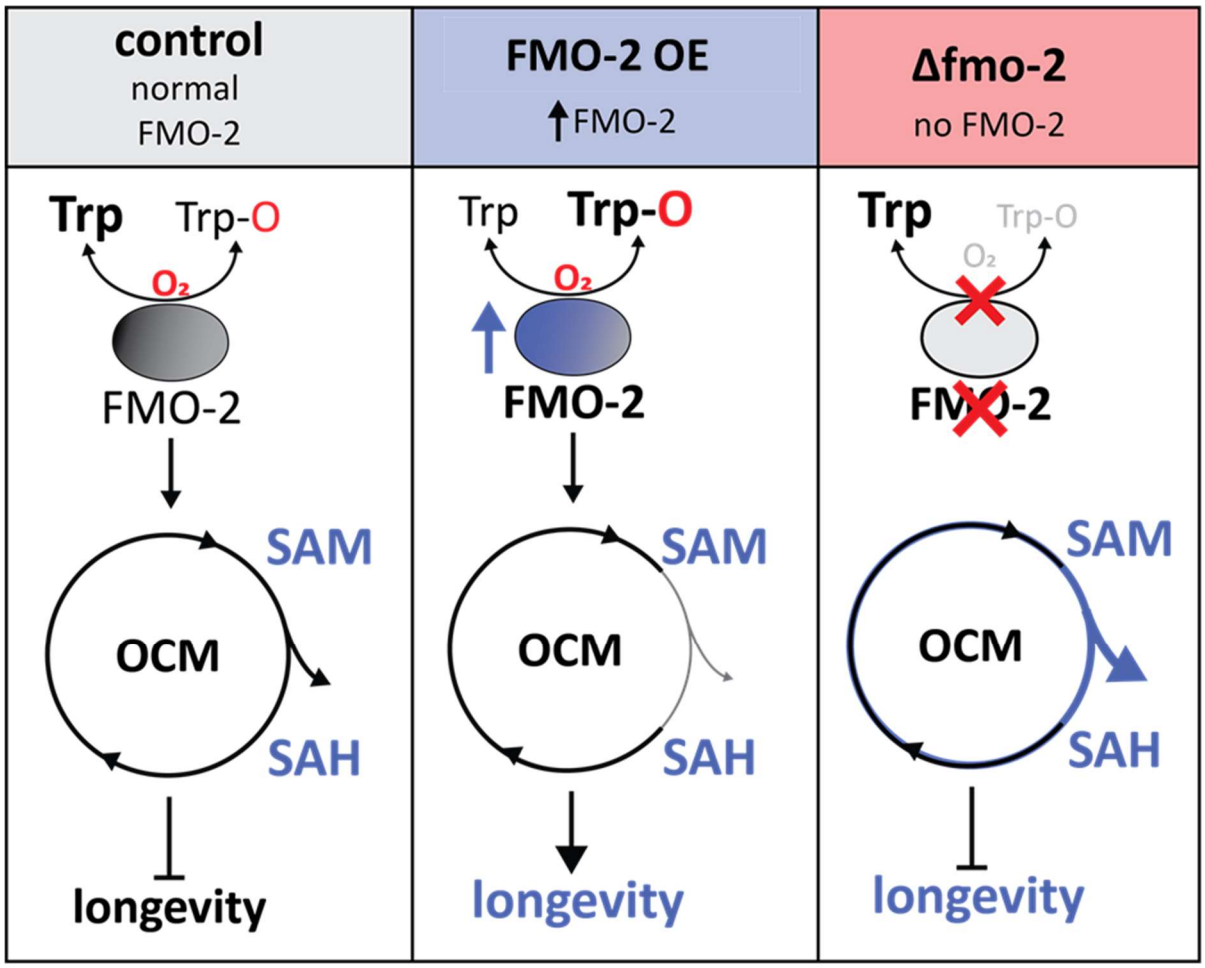

Figure 3.7: Proposed model. In control conditions, there is very low *fmo-2* expression, leading to low levels of tryptophan metabolism/kynurenine production through FMO-2, and maintaining normal flux through one carbon metabolism and normal lifespan. When *fmo-2* is induced, FMO-2 oxygenates tryptophan, leading to increased kynurenine production and decreased methylation output flux through OCM, thereby extending nematode lifespan. When *fmo-2* is absent, these metabolic changes do not occur, preventing an extension in lifespan. The gray line represents decreased flux and the blue line represents increased flux.

For half a century, FMOs have been primarily classified as xenobiotic enzymes. However, the mechanisms by which these enzymes affect endogenous metabolism are still not well studied, with the exception of human FMO1 (and FMO3) and mouse FMO1 converting hypotaurine to taurine[42]. Based on our data, we propose a model where overexpression of *fmo-2* to levels similar those observed under hypoxia and dietary restriction is sufficient to remodel metabolism in the nematode *C. elegans* (**Figure 3.7**). Here, we show that *Cefmo-2*, a regulator of longevity that is critical for lifespan extension and stress response under dietary restriction and hypoxia, interacts with both tryptophan and one-carbon metabolism to confer longevity and stress resistance benefits. We find that modulating the expression of a single oxygenating protein can cause a multitude of metabolic and physiological effects, similar to the activation of transcription factors and kinases. Our results suggest a broader, more significant role for FMO-2 than previously known.

Our data are consistent with a model where the reduction of flux through the methylation pathway leads to longevity benefits. By projecting gene expression data to a stoichiometric model for OCM metabolism, we predict that FMO overexpression results in a reduction in methylation flux. This model-based prediction based on gene expression data is experimentally validated, indicating that this approach can be a powerful tool to simplify the understanding of complex metabolic pathways and to study the biology of aging. Perturbation in the SAM/SAH ratio by either the supplementation of metformin or a mutation in *sams-1* also extends worm lifespan[13,17]. While multiple studies report that methionine restriction robustly extends lifespan across species, including worms, flies, and mice[13,43,44], others show that exogenous supplementation of

methionine is not detrimental to lifespan[45]. In our study, we observe a level of methionine that shows an increasing trend with increasing *fmo-2* expression level (**Figure 3.2**). Although SAM levels depend on methionine, there is precedent for SAM levels being low even when methionine levels are high[46]. Two potential reasons for these observations could be 1) FMO-2 blocks methionine to SAM conversion, which would increase methionine, or 2) there could be an increase in the fluxes of internal reactions within OCM. We hypothesize that #2 is more likely, since methionine is not an *in vitro* substrate for FMO-2 (**Table S3.8**). Taken together, these findings suggest that methionine utilization rather than methionine abundance is a key factor that influences the aging process.

Although suppressing *sams-1* expression phenocopies FMO-2 OE lifespan in the wild type and FMO-2 KO, doing so reduces the stress resistance of the worms against paraquat. This separation of lifespan and stress resistance is occasionally observed under other long-lived conditions[47]. It is unclear if simply reducing methylation is sufficient to promote longevity benefits, or if this mechanism requires suppression of specific methylation processes. It will be important for future studies to determine how cells regulate different methylation fluxes under *sams-1* knockdown and decreased overall methylation. One potential mechanism under this genetic condition could be that specific methyltransferases that are essential for survival will have higher affinity to methyl groups to outcompete other nonessential or deleterious methyltransferases.

We note that while our data suggest methylation as the key downstream effector of FMO-2, we have not excluded the possibility that the transsulfuration pathway may also be involved in this mechanism. The transsulfuration pathway is reported to be a

necessary and sufficient component of DR-mediated lifespan extension in flies[16]. It will be interesting to determine the mechanistic relationship between the transsulfuration and transmethylation pathways in regulating longevity. We also note that the stress resistance and lifespan experiments use FUdR. FUdR is a potential confounding influence, and while we do not believe it is greatly affecting our results, some influence has not been ruled out. We also note that we considered whether our findings could result from an artifact of and overexpression model of FMO-2. However, we believe this is unlikely based on our use of both KO and OE strains that trend in opposite directions, our previous work establishing FMO-2 as a regulator of longevity downstream of DR[4], and a more recently published work reporting that OCM is altered by the DR genetic model *eat-2* mutant[14].

Our data also support an interaction between *fmo-2* and tryptophan metabolism to influence longevity. These findings are particularly interesting because we identify a putative endogenous metabolic pathway of FMOs in relation to the aging process. Based on cell line metabolomics, enzyme kinetics, and LC-MS data, there are at least two plausible mechanisms for how oxygenation of tryptophan by FMO-2 can lead to the synthesis of N-formylkynurenine. First, FMOs across taxa are known to dimerize and form higher order oligomers[48,49]. Therefore, it is possible that FMO-2 dimerizes and dioxygenates tryptophan forming N-formyl-kynurenine, which is then converted to kynurenine by formamidase. Second, the same process could be involved in subsequent oxygenation by FMO-2 monomers, but it is unknown how stable a monooxygenated form of tryptophan would be within the cell, making the first mechanism more likely. To our knowledge this is the first example of the dioxygenation

of a substrate that could potentially require dimerized FMOs. The mechanism of this reaction and its potential requirement of dimerized FMOs will be a target of future research. Furthermore, the dioxygenation of tryptophan by FMOs is especially interesting considering only dioxygenases, such as *tdo-2*, *ido-1*, and *ido-2*, have been shown to mediate the conversion of tryptophan to N-formylkynurenine[19]. Regardless, our data implicate tryptophan as a *bona fide in vitro* and likely *in vivo* substrate of animal FMOs either through dioxygenating or monooxygenating mechanisms. Although we tested multiple conventional and unconventional FMO substrates, such as methimazole[48–50] and 2-heptanone[51] (**Table S3.8**), respectively, much work remains to fully establish the general FMO-2 substrate profile and how it compares to those of mammalian FMOs.

Our data support a model where the interaction between FMO-2 and tryptophan metabolism directly or indirectly modulates the metabolite profile of OCM, altering flux patterns that are consistent with our computational model predictions and subsequent genetic analyses. Further investigation is needed to understand the complete details of the *fmo-2*-mediated connection between OCM and tryptophan in regulating lifespan. Based on the knowledge we gained from this study and previous work, we propose the following two mechanisms may occur together or separately: 1) Oxygenation of tryptophan by FMO-2 alters OCM flux by increasing formate levels as a direct link between tryptophan metabolism and OCM. Formate is a single carbon-containing molecule that can enter the folate cycle as a carbon source[39], and we find that formate addition extends WT lifespan without affecting FMO-2 OE. Formate is generated as a byproduct when kynurenine is synthesized from N-formylkynurenine by formamidase[39].

It is possible that increased formate levels are causal in conferring stress resistance and longevity benefits under metabolically stressful conditions, such as DR or hypoxia. 2) FMO-2 interacts with the mechanistic target of rapamycin (mTOR). Dietary restriction leads to inhibition of mTOR signaling, which is a central regulator of lifespan and aging[52]. Interestingly, both DR- and rapamycin-mediated mTOR inhibition induce the expression of FMOs. A recent study shows that diaminodiphenyl sulfone (DDS) induces the expression of *fmo-2* and extends lifespan, but it does not further extend lifespan in combination with rapamycin[36]. This finding is consistent with the hypothesis that *fmo-2* interacts with mTOR inhibition to extend lifespan. We also show that *fmo-2* interacts with SAM and tryptophan metabolism, both of which are known to alter mTOR activity[53–55]. Thus, examination into the role of mTOR in *fmo*-2-mediated lifespan extension is warranted.

Taken together, our study expands the role of FMO-2 from a xenobiotic enzyme to a metabolic regulator of longevity that has global effects on the metabolome in worms. In particular, the identification of OCM as a target of FMO-2 has implications outside the aging field, considering that OCM remodeling has been studied under the context of cancer biology for more than 70 years[56]. Furthermore, through the identification of tryptophan as a putative substrate for CeFMO-2, this study highlights the conserved importance of FMOs in multiple contexts, including aging and many diseases where OCM and/or the kynurenine pathway play a role. These findings illustrate the potential for therapeutic targets of these proteins for treating age-related diseases and/or increasing longevity and healthspan. This exciting translational potential for the conserved roles of FMOs will be a target for future research.

Materials and Methods

Strains and Growth Conditions

Standard *C. elegans* cultivation procedures were used as previously described[4,57]. N2 wild type, KAE9 ((*eft-3p*::*fmo-2* + *h2b*::*gfp* + Cbr-*unc-119*(+)), and VC1668 (*fmo-2(ok2147*)) strains were maintained on solid nematode growth media (NGM) using *E. coli* OP50 throughout life except where RNAi (*E. coli* HT115) were used. All experiments were conducted at 20°C.

Metabolomics

OP50 bacteria were treated with 0.5% (v/v) paraformaldehyde as previously described[57] and seeded onto 100 mm NGM plates. Approximately 500 eggs were put on these plates and grown until they reached late L4 larval stage. The worms were washed off the plates with 10 mL of M9 buffer and were collected in 15 mL conical tubes. The worms were pelleted using a clinical centrifuge for 1 minute at 150 x g and the supernatant was vacuum aspirated. The worms were washed once with 10 mL of M9 buffer and then with 10 mL of 150 mM ammonium acetate to remove phosphates from M9, each time being centrifuged and the supernatant being aspirated. After these washing steps, the pellets were flash frozen in liquid nitrogen.

Metabolites were extracted from pellets by addition of 500 µL of ice-cold 9:1 methanol: chloroform, followed immediately by probe sonication for 30 seconds with a Branson 450 Sonicator. The resulting homogenates were kept on ice for 5 minutes and were then centrifuged for 10 minutes at 4000 x g at 4°C. Supernatant was then

transferred to autosampler vials for analysis. Hydrophilic interaction liquid chromatography-electrospray ionization mass spectrometry (HILIC-LC-ESI-MS) analysis was performed in negative ion mode using an Agilent 1200 LC system coupled to an Agilent 6220 time-of-flight mass spectrometer equipped with a Dual ESI source. Chromatography was performed as previously described[58,59], with the exception that the Phenomenex Luna NH2 column used had dimensions of 150 mm x 1.0 mm ID, the flow rate was 0.07 mL/min, and the injection volume was 10 µL. MS source and data acquisition parameters were as follows: drying gas temperature 350 °C, drying gas flow 10L/min, nebulizer pressure 20 psi, capillary voltage 3500V, fragmentor voltage 175V, MS scan range 50-1200 m/z, scan rate 1 spectrum/sec, reference mass correction enabled using 1.25 µM HP-0921 reference compound (Agilent, Santa Clara, CA). Untargeted peak detection and alignment was performed using XCMS[60] using the following parameters: peak finding method: centWave, maximum ppm deviation: 30, min/max peak width: 10/60 seconds, signal/noise threshold: 6, minimum m/z difference for peaks with overlapping retention time: 0.01, alignment bandwidth 10 sec. m/z slice width for peak grouping 0.025; remaining parameters were set at default values.

The resulting untargeted metabolomics data were analyzed using Metaboanalyst 4.0 (http://metaboanalyst.ca). Within Metaboanalyst, the data were median normalized, adjusted using auto scaling, and were then subjected to principal component analysis using default parameters. Pathway analysis was performed using Metaboanalyst's functional analysis module, which is an enhanced implementation of the original Mummichog pathway and network analysis algorithm. P-values and t-scores of each MS peak data were calculated between the wild type and FMO-2 OE (**Data S3.2**). Mass

tolerance was set to 10 parts per million (ppm) and mummichog algorithm p-value cutoff was set to 0.05. Default parameters were used for other settings and the analysis was done using the *C. elegans* pathway library. The mummichog algorithm produces putative compound annotation for interpretation at the pathway level. For individual features of interest, compound identities assigned by the algorithm were validated by targeted analysis using authentic standards as described below.

Targeted metabolomics analysis used the same LC-MS parameters as untargeted, but data analysis was performed using Agilent MassHunter Quantitative Analysis software. Metabolite identification was performed by matching accurate mass and retention time with authentic standards analyzed in-house on the same method. Statistical analysis for targeted metabolomics data was done using Metaboanalyst following median normalization and log transformation.

Stress resistance assay

Paraquat (Methyl viologen dichloride hydrate from Sigma-Aldrich) was used to induce oxidative stress. Worms were synchronized from eggs on RNAi plates seeded with *E. coli* HT115 strain expressing dsRNAi for a particular gene and at L4 stage 40 worms were transferred on RNAi-FUdR plates containing 5 mM paraquat. A minimum of two plates per strain per condition were used per replicate experiment. Worms were then scored every day and considered dead when they did not move in response to prodding under a dissection microscope. Worms that crawled off the plate were not considered, but ruptured worms were noted and considered as previously described[4].

Lifespans

Gravid adults were placed on NGM plates containing 1mM β-D-isothiogalactopyranoside (IPTG), 25 μg/ml carbenicillin, and the corresponding RNAi clone from the Vidal or Ahringer RNAi library. After 3 hours, the adults were removed, and the eggs were allowed to develop at 20°C until they reached late L4/young adult stage. From here, 40 to 90 worms were placed on each RNAi plate and transferred to fresh RNAi + FUdR plates on day 1, day 2, day 4, and day 6 of adulthood. A minimum of two plates per strain per condition were used per replicate experiment. Experimental animals were scored every 2-3 days and considered dead when they did not move in response to prodding under a dissection microscope. Worms that crawled off the plate were not considered, but ruptured worms were considered as previously described[4]. A similar method was used for formate and s-adenosylmethionine supplementation lifespan experiments, except either 1 mM formate or 2 mM s-adenosylmethionine was added to the NGM plates without IPTG. A similar method was also used for the non-FUdR lifespan experiments, except FUdR was not added to the plates and worms were fed *E. coli* OP50.

Cox Regression Methods

Supplementary Data 4 and 5 provide the results of Cox proportional hazards regression models, which were run in Stata 14. The model includes a categorical variable for strain, using Wild Type (N2) as the base category, and including dummy variables for FMO-2 OE and/or FMO-2 KO. It also includes a dummy variable for the individual RNAi versus empty vector (EV) control. Variables of particular interest for this

paper are the interactions between the RNAi dummy and the *fmo-2* mutant dummies, which capture the differential effect and interaction of various RNAi on *fmo-2* mutants versus control worms. To account for multiple testing, only interactions with a p-value < 0.01 were considered to be significant.

Computational Modeling

The computer model was generated by building a stoichiometric matrix S (10 reactants by 13 reactions), accounting for all reactions shown in Fig 4A. A steady-state approximation was used, as shown in Eq 1. In Eq. 1, S is the stoichiometric matrix and **J** is a vector of fluxes for each of the reactions.

Eq. 1

$$S \cdot \mathbf{J} = \mathbf{0}$$

To obtain a biologically relevant solution, we projected the expression data of genes involved in the reactions used in the model to the nullspace of S by solving for Eq. 2. Single genes were used as representative genes for each reaction to simplify the model. Gene expressions related to input fluxes were assumed to be one for all strains. Reactions used in the model and the relevant gene expression data are shown in **Table S3.6**. In Eq. 2, M is the nullspace of S, **b** is the vector of relative gene expression data from the wild type, FMO-2 OE or FMO-2 KO that have been normalized to the wild type, and **x** is a vector such that S**x** is the projection of **b** onto the column space of M, which gives us the vector of reaction fluxes, **J**, within the nullspace of S. To account for data

variability, expression level with greater than 0.5x or less than 1.5x fold changes were assumed to be equal to the wild type control. Eq. 2 was solved using the lsqminnorm function in MATLAB 2018a. The lsqminnorm function returns the minimum norm least-squares solution to M**x** = **b** by minimizing both the norm of M * **x** – **b** and the norm of **x**.

Eq. 2

$$\mathrm{M} \cdot \mathbf{x} = \mathbf{b}$$

The inner product of the resulting vector **x** and the nullspace matrix M was obtained to calculate the reaction flux predictions resulting from the gene expression projection as shown in Eq. 3. The calculated **J** for FMO-2 OE and FMO-2 KO were normalized to that of the wild type to obtain the relative fluxes.

Eq. 3

$$\mathrm{M} \cdot \mathbf{x} = \mathbf{J}$$

Quantitative PCR

RNA was isolated from day 1 adult worms following three rounds of freeze-thaw in liquid nitrogen using Invitrogen's Trizol extraction method and 1 µg of RNA was reverse transcribed to cDNA using SuperScript™ II Reverse Transcriptase (Invitrogen). Gene expression levels were measured using 1 µg of cDNA and SYBR™ Green PCR Mastermix (Applied Biosystems) and primers at 10 µM concentration. mRNA levels were normalized using previously published housekeeping gene controls, *tba-1* and *pmp-3*[61]. List of primers used are in **Table S3.11**.

Enzyme Kinetic Assays

Oxygenation activity of FMO-2 was characterized using the method previously described[62]. Briefly, oxygenation of substrates was determined by spectrophotometrically following the consumption of NADPH at 340 nm using the molar extinction coefficient 6.22 $mM^{-1}cm^{-1}$. Components of the assay buffer included 25 mM sodium phosphate buffer (pH 8.5), 0.5 mM diethylenetriaminepentaacetic acid (DETAPAC), 0.5 mM NADPH, and 0.04 µM FMO-2 (0.4 µM FMO5) with excess FAD. The final substrate concentrations for tryptophan were 100, 250, 500, 750 µM and 1, 2.5, 5, 7.5, and 10 mM. The final substrate concentrations for MMI were 100, 300, and 600 µM and 1, 3, 5, 7, 10, and 30 mM. To determine the rate of oxidation of NADPH by FMO, NADPH concentrations of 10, 30, 100, 300, 500, and 700 µM and 1 and 1.5 mM were used. Experiments were conducted at 30^{o}C while shaking. Kinetic parameters (i.e k_{cat} and K_m) were determined by fitting plots of the rate of turnover vs the substrate concentration to the Michaelis-Menten equation using GraphPad Prism (version 9.1.0; GraphPad Software Inc., San Diego, CA.). Purified FMO-2 protein was purchased from GenScript. Purified FMO5 protein, NADPH, FAD, MMI, L-tryptophan, and all other substrates were purchased from Sigma Aldrich (St. Louis, MO). DETAPAC and sodium phosphate buffer were purchased from Fisher (Waltham, MA).

In vitro studies LC-MS

Analysis of samples from *in vitro* studies with purified FMO2 and FMO5 protein was performed using LC-MS with untargeted feature detection. Samples contained 100,

250, or 500 µM tryptophan in the same conditions as the enzymatic assays with either FMO-2 or FMO5 proteins. 100 µL of conditioned media were vortexed with 400 µL of 1:1:1 methanol:acetonitrile:acetone to precipitate protein. The extract was centrifuged for 10 minutes at 16,000 x g and 200 µL of supernatant were transferred to a clean autosampler vial with insert and dried under a stream of nitrogen gas. The dried extract was reconstituted in 50 µL of 85/15 acetonitrile/water and analyzed by HILIC-TOF-MS on an Agilent 1290 Infinity II / Agilent 6545 QTOF. Chromatography was performed on a Waters BEH Amide column (2.1 mm ID x 10 cm, 1.7 µm particle diameter) with mobile phase prepared as described previously[63] except that mobile phase A contained 5% acetonitrile. The flow rate was 0.3mL/min, the column temperature 55 ^{o}C , and the gradient was as follows: 0-0.70 min 100%B, 0.7-6.7 min 100-85%B, 6.7-8.7 min 85%B, 8.7-16 min 85-28%B, 16-16.7 min 28%B, 16.7-16.8 28-0%B. Total run time was 22 min. Ion polarity was positive, gas temp was 320 ^{o}C , drying gas was 8L/min, nebulizer was 35 psi, sheath gas temp and flow were 350 ^{o}C and 11 L/min, capillary voltage 3500V. The instrument was operated in full scan mode at 2 spectra/sec and a mass range of 50-1200 Da. Feature detection and alignment was performed using XCMS. Potential reaction products were detected by computationally examining the data for features present in each sample set. Identification of potential reaction products was performed using MS/MS data acquired from a pooled sample.

<u>*Fmo-2* induction experiment</u>

Synchronized L4 *fmo-2p::mCherry* transcriptional reporter strain animals were incubated overnight in S-media enriched with OP50 with and without 1 mM tryptophan

in a 96-well plate. Some worms were also incubated overnight in S-media without OP50 as a positive control to induce *fmo-2* expression under dietary restriction.

Microscopy

Images were acquired with the LASx software and Leica scope at 6.3x magnification with more than 15 worms per treatment. Prior to imaging, worms were anesthetized with 0.5M sodium azide (NaN3) on a 2% agarose pad. Fluorescence mean comparisons were calculated using ImageJ software.

Statistical analyses

Log-rank test was used to derive p-value for lifespan and paraquat survival assays using $p < 0.05$ cut-off threshold compared to EV controls. Unpaired Student's t-test was used to derive p-values for targeted metabolomics data using $p < 0.05$ cut-off threshold compared to the wild type. Using one-way ANOVA for trend analysis, p-values were calculated for *fmo-2* expression levels that affect OCM metabolite levels. Unpaired Student's t-test was used to derive p-values for comparing the metabolomics data of HepG2 pDEST control and FMO2, FMO4, and FMO5 OE cell lines using $p < 0.05$ cut-off threshold.

Acknowledgments

We thank Stephanie Leiser for input on and analysis of Cox Hazards ratios. This work was funded by the Glenn Foundation for Medical Research, NIH grant F31AG067634 to HSC, and NIH grants R21AG059117 and R01AG075061 to SFL.

Author Contributions

Conceptualization: HSC, SFL

Methodology: HSC, AB, MBH, LJ, DAB, CRE, SFL

Investigation: HSC, AB, MBH, MLS, RC, SH, SB, HAM, AMT, JM, LJ, CRE, SFL

Visualization: HSC, AB, MBH, ESD, SFL

Supervision: DAB, SFL

Writing—original draft: HSC, AB, MBH, SFL

Writing—review & editing: HSC, AB, MBH, MLS, RC, SH, SB, HAM, AMT, JM, ESD, DAB, CRE, SFL

***** Data S3.1-S3.7 were too large to be included in the thesis. They are available on request and will be made available publicly online once the manuscript is published.

Table S3.1: Pathway enrichment analysis of metabolites in the wild-type and FMO-2 OE

Wild-type vs FMO-2 OE	Pathway total	Hits.total	Hits.sig	Expected	FET (p-value)	EASE	Gamma	Emp.Hits	Empirical	Pathway Number
Glycine, serine and threonine metabolism	25	13	13	3.183	8.70E-05	0.001	0.003	0	0	P1
Cysteine and methionine metabolism	34	10	9	4.329	0.010	0.049	0.004	0	0	P2
beta-Alanine metabolism	13	7	7	1.655	0.007	0.058	0.004	0	0	P3
Aminoacyl-tRNA biosynthesis	20	14	11	2.546	0.026	0.079	0.004	0	0	P4
Valine, leucine and isoleucine biosynthesis	8	5	5	1.019	0.030	0.181	0.006	0	0	P5
Valine, leucine and isoleucine degradation	35	16	11	4.456	0.099	0.212	0.006	0	0	P6
Alanine, aspartate and glutamate metabolism	20	11	8	2.546	0.110	0.263	0.007	2	0.02	P7
Propanoate metabolism	19	8	6	2.419	0.143	0.355	0.009	7	0.07	P8
Amino sugar and nucleotide sugar metabolism	27	9	6	3.438	0.254	0.494	0.013	10	0.1	P9
Butanoate metabolism	12	7	5	1.528	0.227	0.495	0.013	0	0	P10
Pantothenate and CoA biosynthesis	16	5	4	2.037	0.187	0.495	0.013	5	0.05	P11
Inositol phosphate metabolism	17	3	3	2.164	0.125	0.496	0.013	0	0	P12
Fructose and mannose metabolism	16	4	3	2.037	0.314	0.686	0.025	0	0	P13
Sphingolipid metabolism	9	4	3	1.146	0.314	0.686	0.025	6	0.06	P14
Terpenoid backbone biosynthesis	12	4	3	1.528	0.314	0.686	0.025	0	0	P15
Glyoxylate and dicarboxylate metabolism	30	11	6	3.820	0.507	0.726	0.029	9	0.09	P16
Synthesis and degradation of ketone bodies	4	2	2	0.509	0.251	0.749	0.032	0	0	P17

D-Arginine and D-ornithine metabolism	4	2	2	0.509	0.251	0.749	0.032	0	0	P18
N-Glycan biosynthesis	35	2	2	4.456	0.251	0.749	0.032	0	0	P19
Mucin type O-glycan biosynthesis	4	2	2	0.509	0.251	0.749	0.032	0	0	P20
Galactose metabolism	15	5	3	1.910	0.505	0.813	0.042	38	0.38	P21
Arginine and proline metabolism	27	15	7	3.438	0.710	0.854	0.051	6	0.06	P22
Pentose phosphate pathway	21	3	2	2.674	0.504	0.875	0.056	35	0.35	P23
Histidine metabolism	8	3	2	1.019	0.504	0.875	0.056	0	0	P24
Glycerophospholipid metabolism	12	3	2	1.528	0.504	0.875	0.056	4	0.04	P25
Glycolysis / Gluconeogenesis	22	6	3	2.801	0.663	0.892	0.062	39	0.39	P26
Pyruvate metabolism	16	6	3	2.037	0.663	0.892	0.062	39	0.39	P27
Pyrimidine metabolism	40	21	9	5.093	0.828	0.913	0.071	52	0.52	P28
Sulfur metabolism	11	4	2	1.401	0.693	0.938	0.085	18	0.18	P29
Tyrosine metabolism	21	5	2	2.674	0.819	0.970	0.115	29	0.29	P30
Tryptophan metabolism	30	5	2	3.820	0.819	0.970	0.115	0	0	P31
D-Glutamine and D-glutamate metabolism	5	5	2	0.637	0.819	0.970	0.115	0	0	P32
Nicotinate and nicotinamide metabolism	14	5	2	1.782	0.819	0.970	0.115	5	0.05	P33
Glutathione metabolism	17	9	3	2.164	0.917	0.982	0.137	5	0.05	P34
Citrate cycle (TCA cycle)	16	6	2	2.037	0.896	0.985	0.145	29	0.29	P35
Folate biosynthesis	22	6	2	2.801	0.896	0.985	0.145	23	0.23	P36
Purine metabolism	60	23	7	7.639	0.988	0.996	0.203	72	0.72	P37
Pentose and glucuronate interconversions	14	6	1	1.782	0.986	1.000	1.000	39	0.39	P38
Ascorbate and aldarate metabolism	6	4	1	0.764	0.941	1.000	1.000	59	0.59	P39

Fatty acid biosynthesis	6	2	1	0.764	0.754	1.000	1.000	0	0	P40
Fatty acid elongation	29	1	1	3.692	0.502	1.000	1.000	0	0	P41
Fatty acid degradation	35	2	1	4.456	0.754	1.000	1.000	0	0	P42
Arginine biosynthesis	6	3	1	0.764	0.879	1.000	1.000	0	0	P43
Lysine degradation	15	2	1	1.910	0.754	1.000	1.000	0	0	P44
Selenocompound metabolism	14	1	1	1.782	0.502	1.000	1.000	21	0.21	P45
Starch and sucrose metabolism	10	5	1	1.273	0.971	1.000	1.000	39	0.39	P46
Mannose type O-glycan biosynthesis	9	1	1	1.146	0.502	1.000	1.000	0	0	P47
Glycerolipid metabolism	7	1	1	0.891	0.502	1.000	1.000	35	0.35	P48
Arachidonic acid metabolism	12	4	1	1.528	0.941	1.000	1.000	16	0.16	P49
One carbon pool by folate	8	2	1	1.019	0.754	1.000	1.000	23	0.23	P50
Porphyrin and chlorophyll metabolism	17	2	1	2.164	0.754	1.000	1.000	13	0.13	P51
Nitrogen metabolism	5	2	1	0.637	0.754	1.000	1.000	0	0	P52
Drug metabolism - cytochrome P450	13	3	1	1.655	0.879	1.000	1.000	0	0	P53
Drug metabolism - other enzymes	25	5	1	3.183	0.971	1.000	1.000	0	0	P54
Phosphatidylinositol signaling system	15	1	1	1.910	0.502	1.000	1.000	0	0	P55

FET = Fisher's exact test
EASE = Expression Analysis Systematic Explorer

The analysis was done using the untargeted metabolomics data from Supplementary Data 1. Statistics used for the pathway analysis is in Supplementary Data 2.

Table S3.2: Statistics for targeted metabolomics analysis of wild-type, FMO-2 OE, and FMO-2 KO

Metabolite	**n**	**Fold change**			**Unpaired t-test (p-value)**			**ANOVA: Test for Trend**
		WT	OE	KO	WT vs OE	OE vs KO	WT vs KO	p-value
Biotin	7	1	0.844	0.768	0.498	0.633	0.258	0.613
Pantothenic acid	7	1	0.831	0.832	0.367	0.897	0.365	0.914
Nicotinic acid	7	1	0.909	1.200	0.994	0.174	0.354	0.317
Choline	7	1	1.592	0.973	0.173	0.143	0.951	0.157
Riboflavin	7	1	1.441	1.043	0.758	0.801	0.934	0.770
Betaine	7	1	1.098	0.807	0.427	0.043	0.277	0.054
Thiamine	7	1	1.096	0.891	0.976	0.693	0.459	0.660
Methionine	7	1	1.559	0.354	0.640	0.011	0.006	0.006
Pyridoxal 5'-phosphate	7	1	2.659	0.934	0.045	0.032	0.713	0.021
Folic acid	7	1	1.131	0.622	0.424	0.090	0.426	0.105
Dihydrofolic acid	7	1	1.710	1.168	0.727	0.811	0.929	0.796
Serine	7	1	1.115	0.640	0.368	0.015	0.437	0.067
5-methyltetrahydrofolate	7	1	1.572	1.090	0.202	0.304	0.787	0.332
S-adenosylhomocysteine	7	1	1.472	1.065	0.123	0.211	0.838	0.167
Methylcobalamin	7	1	1.310	1.447	0.738	0.405	0.478	0.320
Homocysteine	7	1	1.866	0.926	0.009	0.004	0.611	0.002
S-adenosylmethionine	7	1	0.664	1.049	0.001	0.006	0.832	0.001
Cystathionine	7	1	1.490	1.044	0.045	0.056	0.906	0.078
Cystine	7	1	1.886	0.450	0.899	0.298	0.062	0.234
SAM/SAH	7	1.189	0.490	1.579	0.006	0.008	0.997	0.007

SAM/SAH ratio was calculated from the s-adenosylmethionine and s-adenosylhomocysteine data.

Targeted metabolomics data is in Supplementary Data 3.

Table S3.3: Stress resistance analyses against 5 mM paraquat

Strain	Experiment	Food	n	Median	Mean	p-value	% change median	% change mean
KAE9	2	afmd-1 (RNAi)	48	10	13.1	0.058	0%	26%
KAE9	6	afmd-1 (RNAi)	49	13	15.0	0.339	-13%	-7%
KAE9	7	afmd-1 (RNAi)	56	9	12.5	0.631	-18%	-7%
KAE9	8	afmd-1 (RNAi)	92	14	16.3	0.000	40%	30%
KAE9	9	afmd-1 (RNAi)	64	19	17.0	0.011	58%	21%
Wild-type/Control	2	afmd-1 (RNAi)	88	7	6.8	0.001	17%	15%
Wild-type/Control	6	afmd-1 (RNAi)	42	9	10.1	0.802	0%	3%
Wild-type/Control	7	afmd-1 (RNAi)	53	8	7.8	0.227	0%	-5%
Wild-type/Control	8	afmd-1 (RNAi)	74	9	10.4	0.000	29%	38%
Wild-type/Control	9	afmd-1 (RNAi)	70	8	9.5	0.636	0%	4%
KAE9	4	alh-3 (RNAi)	65	6	6.9	0.000	-40%	-29%
KAE9	5	alh-3 (RNAi)	49	4	5.3	0.069	-33%	-13%
KAE9	10	alh-3 (RNAi)	103	18	18.7	0.498	-14%	-2%
Wild-type/Control	4	alh-3 (RNAi)	16	5	5.1	0.000	-17%	-23%
Wild-type/Control	5	alh-3 (RNAi)	31	5	5.5	0.000	0%	16%
Wild-type/Control	10	alh-3 (RNAi)	81	11	12.1	0.206	0%	8%
KAE9	1	atic-1 (RNAi)	50	6	6.2	0.000	-25%	-34%
KAE9	2	atic-1 (RNAi)	67	10	12.4	0.028	0%	19%
KAE9	7	atic-1 (RNAi)	66	6	8.4	0.000	-45%	-37%
KAE9	8	atic-1 (RNAi)	64	12	13.9	0.205	20%	11%
KAE9	9	atic-1 (RNAi)	67	19	17.3	0.004	58%	24%
Wild-type/Control	1	atic-1 (RNAi)	53	5	4.7	0.003	0%	-7%
Wild-type/Control	2	atic-1 (RNAi)	64	6	6.3	0.210	0%	6%
Wild-type/Control	7	atic-1 (RNAi)	33	6	6.7	0.000	-25%	-18%
Wild-type/Control	8	atic-1 (RNAi)	57	7	7.6	0.604	0%	1%
Wild-type/Control	9	atic-1 (RNAi)	57	9	10.0	0.358	13%	10%
KAE9	1	cbs-1 (RNAi)	37	7	7.1	0.001	-13%	-24%
KAE9	4	cbs-1 (RNAi)	43	8	7.7	0.000	-20%	-21%
KAE9	5	cbs-1 (RNAi)	34	6	6.2	0.417	0%	2%
Wild-type/Control	1	cbs-1 (RNAi)	52	6	6.3	0.000	20%	25%

Wild-type/Control	4	cbs-1 (RNAi)	41	7	6.8	0.110	17%	4%
Wild-type/Control	5	cbs-1 (RNAi)	39	6	5.5	0.000	20%	17%
KAE9	1	cth-2 (RNAi)	62	6	6.4	0.000	-25%	-33%
KAE9	4	cth-2 (RNAi)	42	8	7.8	0.000	-20%	-20%
KAE9	5	cth-2 (RNAi)	41	7	7.6	0.000	17%	25%
KAE9	10	cth-2 (RNAi)	76	16	17.5	0.064	-24%	-8%
Wild-type/Control	1	cth-2 (RNAi)	36	6	6.1	0.000	20%	21%
Wild-type/Control	4	cth-2 (RNAi)	73	5	5.2	0.000	-17%	-21%
Wild-type/Control	5	cth-2 (RNAi)	46	5	5.3	0.000	0%	12%
Wild-type/Control	10	cth-2 (RNAi)	81	16	16.9	0.000	45%	50%
KAE9	1	EV (RNAi)	22	8	9.4	N/A	0%	0%
KAE9	2	EV (RNAi)	42	10	10.4	N/A	0%	0%
KAE9	3	EV (RNAi)	48	13	14.5	N/A	0%	0%
KAE9	4	EV (RNAi)	49	10	9.8	N/A	0%	0%
KAE9	5	EV (RNAi)	34	6	6.1	N/A	0%	0%
KAE9	6	EV (RNAi)	39	15	16.1	N/A	0%	0%
KAE9	7	EV (RNAi)	34	11	13.4	N/A	0%	0%
KAE9	8	EV (RNAi)	65	10	12.5	N/A	0%	0%
KAE9	9	EV (RNAi)	75	12	14.0	N/A	0%	0%
KAE9	10	EV (RNAi)	91	21	19.1	N/A	0%	0%
Wild-type/Control	1	EV (RNAi)	61	5	5.0	N/A	0%	0%
Wild-type/Control	2	EV (RNAi)	73	6	5.9	N/A	0%	0%
Wild-type/Control	3	EV (RNAi)	52	8	8.1	N/A	0%	0%
Wild-type/Control	4	EV (RNAi)	66	6	6.6	N/A	0%	0%
Wild-type/Control	5	EV (RNAi)	24	5	4.7	N/A	0%	0%
Wild-type/Control	6	EV (RNAi)	55	9	9.8	N/A	0%	0%
Wild-type/Control	7	EV (RNAi)	56	8	8.2	N/A	0%	0%
Wild-type/Control	8	EV (RNAi)	78	7	7.5	N/A	0%	0%
Wild-type/Control	9	EV (RNAi)	44	8	9.1	N/A	0%	0%
Wild-type/Control	10	EV (RNAi)	72	11	11.2	N/A	0%	0%
KAE9	2	kmo-1 (RNAi)	36	12	11.7	0.038	20%	12%
KAE9	3	kmo-1 (RNAi)	57	20	18.6	0.006	54%	28%
KAE9	7	kmo-1 (RNAi)	45	15	13.6	0.956	36%	2%
KAE9	10	kmo-1 (RNAi)	95	21	20.6	0.922	0%	8%

Wild-type/Control	2	kmo-1 (RNAi)	61	7	7.1	0.000	17%	19%
Wild-type/Control	3	kmo-1 (RNAi)	63	16	15.2	0.000	100%	86%
Wild-type/Control	7	kmo-1 (RNAi)	58	9	9.7	0.001	13%	19%
Wild-type/Control	10	kmo-1 (RNAi)	99	21	20.5	0.000	91%	83%
KAE9	1	mel-32 (RNAi)	37	9	9.1	0.243	13%	-3%
KAE9	3	mel-32 (RNAi)	66	22	20.1	0.000	69%	39%
KAE9	4	mel-32 (RNAi)	36	7	8.1	0.000	-30%	-17%
KAE9	8	mel-32 (RNAi)	36	23	19.8	0.000	130%	59%
Wild-type/Control	1	mel-32 (RNAi)	51	6	5.6	0.000	20%	12%
Wild-type/Control	3	mel-32 (RNAi)	66	16	16.0	0.000	100%	97%
Wild-type/Control	4	mel-32 (RNAi)	36	7	7.2	0.000	17%	9%
Wild-type/Control	8	mel-32 (RNAi)	88	15	14.9	0.000	114%	99%
KAE9	2	mtrr-1 (RNAi)	61	12	14.9	0.001	20%	43%
KAE9	7	mtrr-1 (RNAi)	44	9	11.0	0.054	-18%	-18%
KAE9	8	mtrr-1 (RNAi)	72	15	16.0	0.003	50%	28%
KAE9	9	mtrr-1 (RNAi)	70	21	19.0	0.000	75%	36%
Wild-type/Control	2	mtrr-1 (RNAi)	77	7	6.6	0.007	17%	11%
Wild-type/Control	7	mtrr-1 (RNAi)	39	7	7.6	0.104	-13%	-8%
Wild-type/Control	8	mtrr-1 (RNAi)	77	9	9.9	0.000	29%	32%
Wild-type/Control	9	mtrr-1 (RNAi)	42	8	9.8	0.312	0%	7%
KAE9	2	nkat-1 (RNAi)	39	12	12.2	0.017	20%	16%
KAE9	7	nkat-1 (RNAi)	71	13	14.9	0.143	18%	12%
KAE9	8	nkat-1 (RNAi)	63	14	15.2	0.019	40%	22%
KAE9	9	nkat-1 (RNAi)	73	23	21.3	0.000	92%	52%
Wild-type/Control	2	nkat-1 (RNAi)	79	6	6.8	0.001	0%	15%
Wild-type/Control	7	nkat-1 (RNAi)	49	7	7.5	0.034	-13%	-8%
Wild-type/Control	8	nkat-1 (RNAi)	63	10	9.6	0.000	43%	28%
Wild-type/Control	9	nkat-1 (RNAi)	79	9	10.6	0.044	13%	16%
KAE9	3	sams-1 (RNAi)	66	8	7.9	0.000	-38%	-45%
KAE9	6	sams-1 (RNAi)	27	8	8.3	0.000	-47%	-48%
KAE9	10	sams-1 (RNAi)	106	11	9.8	0.000	-48%	-49%
Wild-type/Control	3	sams-1 (RNAi)	72	7	7.4	0.000	-13%	-10%

Wild-type/Control	6	sams-1 (RNAi)	45	7	7.6	0.000	-22%	-23%
Wild-type/Control	10	sams-1 (RNAi)	111	11	9.5	0.000	0%	-16%
KAE9	3	tdo-2 (RNAi)	44	8	9.0	0.000	-38%	-38%
KAE9	8	tdo-2 (RNAi)	49	8	9.5	0.002	-20%	-24%
KAE9	10	tdo-2 (RNAi)	79	11	11.6	0.000	-48%	-39%
Wild-type/Control	3	tdo-2 (RNAi)	64	7	7.1	0.000	-13%	-13%
Wild-type/Control	8	tdo-2 (RNAi)	81	6	5.9	0.000	-14%	-21%
Wild-type/Control	10	tdo-2 (RNAi)	65	11	9.2	0.000	0%	-18%
KAE9	2	Y106G6E.4 (RNAi)	65	12	13.6	0.003	20%	30%
KAE9	3	Y106G6E.4 (RNAi)	54	16	17.1	0.059	23%	18%
KAE9	7	Y106G6E.4 (RNAi)	67	13	13.9	0.730	18%	4%
KAE9	9	Y106G6E.4 (RNAi)	96	21	21.3	0.000	75%	52%
Wild-type/Control	2	Y106G6E.4 (RNAi)	77	7	6.8	0.002	17%	14%
Wild-type/Control	3	Y106G6E.4 (RNAi)	62	9	10.5	0.000	13%	29%
Wild-type/Control	7	Y106G6E.4 (RNAi)	52	7	7.4	0.005	-13%	-10%
Wild-type/Control	9	Y106G6E.4 (RNAi)	80	19	16.2	0.000	138%	77%

KAE9 = FMO-2 OE

Cox regression analysis is in Supplementary Data 4.

Table S3.4: Lifespan analyses

Strain	Experiment	Food	n	Median	Mean	p-value	% change median	% change mean
KAE9	6	afmd-1 (RNAi)	130	29	29.4	0.017	-12%	-9%
KAE9	7	afmd-1 (RNAi)	114	35	33.9	0.019	6%	2%
KAE9	13	afmd-1 (RNAi)	85	28	26.7	0.016	0%	-6%
VC1668	6	afmd-1 (RNAi)	93	27	27.2	0.861	0%	0%
VC1668	7	afmd-1 (RNAi)	105	31	28.8	0.441	11%	1%
VC1668	13	afmd-1 (RNAi)	103	22	23.6	0.016	-12%	-5%
Wild-type/Control	6	afmd-1 (RNAi)	132	29	28.0	0.241	0%	-1%
Wild-type/Control	7	afmd-1 (RNAi)	127	31	30.6	0.001	0%	4%
Wild-type/Control	13	afmd-1 (RNAi)	100	28	25.7	0.091	0%	-4%
KAE9	1	alh-3 (RNAi)	131	31	28.9	0.000	0%	-5%
KAE9	4	alh-3 (RNAi)	118	37	38.0	0.168	0%	-1%
KAE9	8	alh-3 (RNAi)	129	35	34.2	0.000	-10%	-8%
VC1668	1	alh-3 (RNAi)	131	28	27.3	0.306	0%	1%
VC1668	4	alh-3 (RNAi)	107	33	32.5	0.514	0%	-1%
VC1668	8	alh-3 (RNAi)	129	31	30.9	0.524	0%	1%
Wild-type/Control	1	alh-3 (RNAi)	134	26	26.4	0.000	-7%	-5%
Wild-type/Control	4	alh-3 (RNAi)	124	33	34.1	0.051	0%	7%
Wild-type/Control	8	alh-3 (RNAi)	137	33	31.9	0.915	0%	1%
KAE9	1	atic-1 (RNAi)	124	31	28.7	0.029	0%	-6%
KAE9	4	atic-1 (RNAi)	117	33	30.6	0.000	-11%	-20%
KAE9	8	atic-1 (RNAi)	141	33	32.6	0.012	-15%	-13%
VC1668	1	atic-1 (RNAi)	129	31	28.5	0.003	11%	6%
VC1668	4	atic-1 (RNAi)	112	33	33.4	0.262	0%	2%
VC1668	8	atic-1 (RNAi)	109	33	31.4	0.020	6%	3%
Wild-type/Control	1	atic-1 (RNAi)	137	28	26.4	0.135	0%	-5%

Wild-type/Control	4	atic-1 (RNAi)	108	33	32.5	0.107	0%	2%
Wild-type/Control	8	atic-1 (RNAi)	137	33	31.7	0.168	0%	0%
KAE9	1	cbs-1 (RNAi)	66	33	32.6	0.046	6%	7%
KAE9	3	cbs-1 (RNAi)	101	37	35.5	0.874	0%	-2%
KAE9	8	cbs-1 (RNAi)	135	35	37.1	0.689	-10%	0%
VC1668	1	cbs-1 (RNAi)	129	26	25.9	0.057	-7%	-4%
VC1668	3	cbs-1 (RNAi)	118	33	33.2	0.001	10%	6%
VC1668	8	cbs-1 (RNAi)	140	33	31.9	0.011	6%	4%
Wild-type/Control	1	cbs-1 (RNAi)	128	31	29.6	0.004	11%	6%
Wild-type/Control	3	cbs-1 (RNAi)	115	30	31.5	0.861	-9%	-1%
Wild-type/Control	8	cbs-1 (RNAi)	138	33	34.9	0.000	0%	10%
KAE9	1	cth-2 (RNAi)	131	31	29.8	0.211	0%	-2%
KAE9	3	cth-2 (RNAi)	109	33	34.3	0.046	-11%	-6%
KAE9	8	cth-2 (RNAi)	144	33	32.3	0.000	-15%	-13%
KAE9	9	cth-2 (RNAi)	142	29	27.8	0.000	-12%	-15%
VC1668	1	cth-2 (RNAi)	127	24	22.8	0.000	-14%	-16%
VC1668	3	cth-2 (RNAi)	114	30	27.6	0.000	0%	-12%
VC1668	8	cth-2 (RNAi)	109	26	26.8	0.000	-16%	-12%
VC1668	9	cth-2 (RNAi)	135	25	23.8	0.000	-7%	-12%
Wild-type/Control	1	cth-2 (RNAi)	145	26	25.1	0.000	-7%	-10%
Wild-type/Control	3	cth-2 (RNAi)	110	33	31.4	0.743	0%	-2%
Wild-type/Control	8	cth-2 (RNAi)	157	26	27.3	0.000	-21%	-14%
Wild-type/Control	9	cth-2 (RNAi)	172	25	23.8	0.000	-7%	-12%
KAE9	1	EV (RNAi)	128	31	30.4	N/A	0%	0%
KAE9	2	EV (RNAi)	130	34	32.9	N/A	0%	0%
KAE9	3	EV (RNAi)	118	37	36.3	N/A	0%	0%
KAE9	4	EV (RNAi)	119	37	38.3	N/A	0%	0%
KAE9	5	EV (RNAi)	110	31	29.9	N/A	0%	0%
KAE9	6	EV (RNAi)	124	33	32.2	N/A	0%	0%

KAE9	7	EV (RNAi)	118	33	33.3	N/A	0%	0%
KAE9	8	EV (RNAi)	134	39	37.2	N/A	0%	0%
KAE9	9	EV (RNAi)	145	33	32.7	N/A	0%	0%
KAE9	10	EV (RNAi)	56	29	29.4	N/A	0%	0%
KAE9	11	EV (RNAi)	76	30	28.6	N/A	0%	0%
KAE9	12	EV (RNAi)	118	31	30.2	N/A	0%	0%
KAE9	13	EV (RNAi)	99	28	28.4	N/A	0%	0%
VC1668	1	EV (RNAi)	128	28	27.0	N/A	0%	0%
VC1668	2	EV (RNAi)	140	27	27.0	N/A	0%	0%
VC1668	3	EV (RNAi)	110	30	31.3	N/A	0%	0%
VC1668	4	EV (RNAi)	114	33	32.9	N/A	0%	0%
VC1668	5	EV (RNAi)	123	28	26.6	N/A	0%	0%
VC1668	6	EV (RNAi)	91	27	27.1	N/A	0%	0%
VC1668	7	EV (RNAi)	99	28	28.3	N/A	0%	0%
VC1668	8	EV (RNAi)	116	31	30.6	N/A	0%	0%
VC1668	9	EV (RNAi)	134	27	27.1	N/A	0%	0%
VC1668	10	EV (RNAi)	68	29	28.1	N/A	0%	0%
VC1668	11	EV (RNAi)	79	28	26.7	N/A	0%	0%
VC1668	12	EV (RNAi)	112	27	26.4	N/A	0%	0%
VC1668	13	EV (RNAi)	106	25	24.9	N/A	0%	0%
Wild-type/Control	1	EV (RNAi)	127	28	27.8	N/A	0%	0%
Wild-type/Control	2	EV (RNAi)	123	29	27.4	N/A	0%	0%
Wild-type/Control	3	EV (RNAi)	104	33	31.9	N/A	0%	0%
Wild-type/Control	4	EV (RNAi)	122	33	32.0	N/A	0%	0%
Wild-type/Control	5	EV (RNAi)	118	31	28.3	N/A	0%	0%
Wild-type/Control	6	EV (RNAi)	139	29	28.4	N/A	0%	0%
Wild-type/Control	7	EV (RNAi)	141	31	29.4	N/A	0%	0%
Wild-type/Control	8	EV (RNAi)	139	33	31.7	N/A	0%	0%
Wild-type/Control	9	EV (RNAi)	132	27	27.2	N/A	0%	0%
Wild-type/Control	10	EV (RNAi)	63	29	27.5	N/A	0%	0%
Wild-type/Control	11	EV (RNAi)	79	28	25.9	N/A	0%	0%
Wild-type/Control	12	EV (RNAi)	121	27	26.4	N/A	0%	0%
Wild-type/Control	13	EV (RNAi)	101	28	26.7	N/A	0%	0%

KAE9	6	kmo-1 (RNAi)	125	27	27.4	0.000	-18%	-15%
KAE9	7	kmo-1 (RNAi)	122	31	28.4	0.000	-6%	-15%
KAE9	13	kmo-1 (RNAi)	186	25	25.0	0.000	-11%	-12%
VC1668	6	kmo-1 (RNAi)	91	25	24.8	0.000	-7%	-9%
VC1668	7	kmo-1 (RNAi)	92	26	25.6	0.000	-7%	-10%
VC1668	13	kmo-1 (RNAi)	96	20	21.3	0.000	-20%	-15%
Wild-type/Control	6	kmo-1 (RNAi)	133	23	23.1	0.000	-21%	-19%
Wild-type/Control	7	kmo-1 (RNAi)	135	26	25.5	0.000	-16%	-13%
Wild-type/Control	13	kmo-1 (RNAi)	96	20	21.3	0.000	-29%	-20%
KAE9	2	mel-32 (RNAi)	63	36	36.1	0.008	6%	10%
KAE9	5	mel-32 (RNAi)	97	35	33.0	0.000	13%	10%
KAE9	10	mel-32 (RNAi)	60	38	38.8	0.000	31%	32%
VC1668	2	mel-32 (RNAi)	129	27	26.3	0.187	0%	-3%
VC1668	5	mel-32 (RNAi)	114	28	27.8	0.226	0%	5%
VC1668	10	mel-32 (RNAi)	66	29	28.0	0.718	0%	0%
Wild-type/Control	2	mel-32 (RNAi)	130	29	27.6	0.456	0%	1%
Wild-type/Control	5	mel-32 (RNAi)	121	31	28.0	0.653	0%	-1%
Wild-type/Control	10	mel-32 (RNAi)	63	26	25.9	0.009	-10%	-6%
KAE9	2	mtrr-1 (RNAi)	127	32	30.0	0.000	-6%	-9%
KAE9	3	mtrr-1 (RNAi)	114	37	35.6	0.234	0%	-2%
KAE9	5	mtrr-1 (RNAi)	123	31	29.1	0.232	0%	-3%
VC1668	2	mtrr-1 (RNAi)	129	27	26.0	0.000	0%	-4%
VC1668	3	mtrr-1 (RNAi)	117	30	31.3	0.933	0%	0%
VC1668	5	mtrr-1 (RNAi)	112	26	25.4	0.030	-7%	-5%
Wild-type/Control	2	mtrr-1 (RNAi)	132	27	26.7	0.002	-7%	-3%
Wild-type/Control	3	mtrr-1 (RNAi)	109	33	32.4	1.000	0%	2%
Wild-type/Control	5	mtrr-1 (RNAi)	123	28	26.4	0.001	-10%	-7%

KAE9	6	nkat-1 (RNAi)	125	35	34.4	0.016	6%	7%
KAE9	7	nkat-1 (RNAi)	108	35	35.6	0.000	6%	7%
KAE9	11	nkat-1 (RNAi)	75	32	30.7	0.037	7%	8%
KAE9	13	nkat-1 (RNAi)	92	28	27.6	0.162	0%	-3%
VC1668	6	nkat-1 (RNAi)	109	27	27.6	0.894	0%	2%
VC1668	7	nkat-1 (RNAi)	100	28	28.8	0.432	0%	2%
VC1668	11	nkat-1 (RNAi)	77	28	27.6	0.098	0%	3%
VC1668	13	nkat-1 (RNAi)	115	25	25.2	0.828	0%	1%
Wild-type/Control	6	nkat-1 (RNAi)	131	27	27.5	0.027	-7%	-3%
Wild-type/Control	7	nkat-1 (RNAi)	65	31	30.5	0.097	0%	4%
Wild-type/Control	11	nkat-1 (RNAi)	67	28	27.7	0.005	0%	7%
Wild-type/Control	13	nkat-1 (RNAi)	102	28	25.4	0.025	0%	-5%
KAE9	12	sams-1 (RNAi)	55	31	30.8	0.584	0%	2%
KAE9	9	sams-1 (RNAi)	146	35	34.8	0.001	6%	6%
KAE9	11	sams-1 (RNAi)	70	28	28.5	0.517	-13%	0%
VC1668	9	sams-1 (RNAi)	135	31	31.5	0.000	15%	16%
VC1668	11	sams-1 (RNAi)	81	28	27.5	0.052	0%	3%
VC1668	12	sams-1 (RNAi)	113	27	28.2	0.002	0%	7%
Wild-type/Control	9	sams-1 (RNAi)	151	35	35.3	0.000	30%	30%
Wild-type/Control	11	sams-1 (RNAi)	59	30	29.2	0.000	7%	12%
Wild-type/Control	12	sams-1 (RNAi)	119	29	30.0	0.000	7%	14%
KAE9	6	tdo-2 (RNAi)	131	35	36.1	0.000	6%	12%
KAE9	7	tdo-2 (RNAi)	139	38	38.1	0.000	15%	14%
KAE9	13	tdo-2 (RNAi)	96	37	36.6	0.000	32%	29%
VC1668	6	tdo-2 (RNAi)	74	29	29.0	0.003	7%	7%
VC1668	7	tdo-2 (RNAi)	100	35	33.5	0.000	25%	18%
VC1668	13	tdo-2 (RNAi)	102	28	26.1	0.001	12%	5%

Wild-type/Control	6	tdo-2 (RNAi)	129	35	35.3	0.000	21%	24%
Wild-type/Control	7	tdo-2 (RNAi)	137	38	37.3	0.000	23%	27%
Wild-type/Control	13	tdo-2 (RNAi)	101	33	31.1	0.000	18%	16%
KAE9	1	Y106G6E.4 (RNAi)	131	31	29.4	0.190	0%	9%
KAE9	4	Y106G6E.4 (RNAi)	126	37	38.2	0.504	0%	0%
KAE9	8	Y106G6E.4 (RNAi)	122	39	36.5	0.584	0%	-2%
VC1668	1	Y106G6E.4 (RNAi)	69	28	28.2	0.291	0%	4%
VC1668	4	Y106G6E.4 (RNAi)	123	33	33.0	0.926	0%	0%
VC1668	8	Y106G6E.4 (RNAi)	122	33	31.4	0.024	6%	3%
Wild-type/Control	1	Y106G6E.4 (RNAi)	149	31	27.6	0.644	11%	-1%
Wild-type/Control	4	Y106G6E.4 (RNAi)	119	33	33.8	0.030	0%	6%
Wild-type/Control	8	Y106G6E.4 (RNAi)	119	33	31.4	0.477	0%	-1%

KAE9 = FMO-2 OE
VC1668 = FMO-2 KO

Cox regression analysis in Supplementary Data 5.

Table S3.5: Gene expression data used in the computational model

	Reactions	Genes used in the model projection	RT-PCR fold change in FMO-2 OE (normalized to the wild-type)	RT-PCR fold change in FMO-2 KO (normalized to the wild-type)
Reaction 1 (R1):	met --> sam	*sams-1*	1.20	6.80
Reaction 2 (R2):	sam --> sah	*mtrr-1*	1.22	1.61
Reaction 3 (R3):	sah --> hcy	*ahcy-1*	2.05	4.48
Reaction 4 (R4):	hcy + 5mthf --> met + thf	*metr-1*	1.62	3.46
Reaction 5 (R5):	hcy --> cyst	*cbs-1*	1.22	1.14
Reaction 6 (R6):	cyst --> cys	*cth-2*	1.95	3.36
Reaction 7 (R7):	thf --> 5,10thf	*mel-32*	1.13	2.37
Reaction 8 (R8):	5,10thf --> 5mthf	*mthf-1*	1.31	2.64
Reaction 9 (R9):	met input (methionine transport)	n/a (fold change assumed to be 1)	1.00	1.00
Reaction 10 (R10):	thf input (folate transport)	n/a (fold change assumed to be 1)	1.00	1.00
Reaction 11 (R11):	sam output	*set-2*	0.99	0.89
Reaction 12 (R12):	cys output	*gcs-1*	1.25	1.32
Reaction 13 (R13):	5,10thf output	*tyms-1*	0.68	0.45

met = methionine
sam = s-adenosylmethionine
sah = s-adenosylhomocysteine
hcy = homocysteine
cyst = cystathionine
cys = cysteine
thf = tetrahydrofolate
5,10thf = 5,10-methylenetetrahydrofolate
5mthf = 5-methyltetrahydrofolate

Table S3.6: Stoichiometric matrix for computational model

	R1	R2	R3	R4	R5	R6	R7	R8	R9	R10	R11	R12	R13
met	-1	0	0	1	0	0	0	0	1	0	0	0	0
sam	1	-1	0	0	0	0	0	0	0	0	-1	0	0
sah	0	1	-1	0	0	0	0	0	0	0	0	0	0
hcy	0	0	1	-1	-1	0	0	0	0	0	0	0	0
cyst	0	0	0	0	1	-1	0	0	0	0	0	0	0
cys	0	0	0	0	0	1	0	0	0	0	0	-1	0
thf	0	0	0	1	0	0	-1	0	0	1	0	0	0
5,10thf	0	0	0	0	0	0	1	-1	0	0	0	0	-1
5mthf	0	0	0	-1	0	0	0	1	0	0	0	0	0

met = methionine
sam = s-adenosylmethionine
sah = s-adenosylhomocysteine
hcy = homocysteine
cyst = cystathionine
cys = cysteine
thf = tetrahydrofolate
5,10thf = 5,10-methylenetetrahydrofolate
5mthf = 5-methyltetrahydrofolate

R = reaction

Table S3.7: S-adenosylmethionine (SAM) supplementation lifespan analyses

Strain	Experiment	Food	n	Median	Mean	p-value	% change median	% change mean
KAE9	1	Control	76	30	30.8	N/A	0%	0%
KAE9	2	Control	100	27	27.2	N/A	0%	0%
KAE9	1	2 mM SAM	74	27	27.9	0.001	-10%	-10%
KAE9	2	2 mM SAM	100	27	25.3	0.000	0%	-7%

Table S3.8: FMO-2 enzyme kinetics analyses

Substrate	Km (mM)	kcat (sec-1)	Catalytic Efficiency (sec-1 M-1)
NADPH	2.50 ± 1.24	264 ± 98	105000 ± 65000
Methimazole	1.92 ± 1.14	13.0 ± 6.0	6800 ± 5100
Tryptophan	0.88 ± 0.43	9.7 ± 1.5	11000 ± 5000
Aspartic Acid	N.D.	N.D.	N.D. (Activity starts at 1 mM)
Glutamine	N.D.	N.D.	N.D. (Activity starts at 3 mM)
TMA	N.D.	N.D.	N.D. (Activity starts at 10 mM)
Cysteine	N.D.	N.D.	N.D. (Activity starts at 10 mM)
Phenylalanine	N.D.	N.D.	N.D. (Activity starts at 10 mM)
L-Methionine	N.D.	N.D.	N.D. (Activity starts at 20 mM)
Valine	N.D.	N.D.	N.D. (Activity starts at 30 mM)
β-alanine	N.D.	N.D.	N.D.
uracil	N.D.	N.D.	N.D.
2-heptanone	N.D.	N.D.	N.D.

N.D. = not determined

Table S3.9: Formate supplementation lifespan analyses

Strain	Experiment	Food	n	Median	Mean	p-value	% change median	% change mean
KAE9	1	1 mM formate	64	31	31.9	0.102	-6%	-4%
KAE9	2	1 mM formate	100	39	37.1	0.872	0%	-3%
VC1668	1	1 mM formate	105	29	28.3	0.000	12%	7%
VC1668	2	1 mM formate	100	30	30.7	0.050	0%	7%
Wild-type/Control	1	1 mM formate	54	31	30.6	0.001	7%	8%
Wild-type/Control	2	1 mM formate	99	33	32.6	0.000	0%	10%
KAE9	1	Control	99	33	33.4	N/A	0%	0%
KAE9	2	Control	102	39	38.2	N/A	0%	0%
VC1668	1	Control	105	26	26.6	N/A	0%	0%
VC1668	2	Control	106	30	28.7	N/A	0%	0%
Wild-type/Control	1	Control	97	29	28.2	N/A	0%	0%
Wild-type/Control	2	Control	101	33	29.8	N/A	0%	0%

KAE9 = FMO-2 OE
VC1668 = FMO-2 KO

Table S3.10: Non-FUdR lifespan analysis

Strain	Experiment	Food	n	Median	Mean	p-value	% change median	% change mean
KAE9	1	OP50	73	23	24.7	0.000	15%	29%
KAE9	2	OP50	81	23	25.3	0.000	15%	19%
Wild-type/Control	1	OP50	85	20	19.2	N/A	0%	0%
Wild-type/Control	2	OP50	100	20	21.2	N/A	0%	0%

Table S3.11: qRT-PCR primers.

Genes	Forward Primers (5'-3')	Reverse Primers (5'-3')
sams-1	CAAATTTCTGACGCCGTTCTC	TCCGCAGAGCATAACCATAC
mtrr-1	GGAACTGGAGTCTCGGTATTTC	ACGACATCCAAAGAAGAGAACA
ahcy-1	TGAGACTCTTACTGCTCTCG	GGAGAAGATGTTGCAGGAAG
metr-1	GTCGAAGTGGTCTGATTCTT	GCCATCTCTTCAGGAGTTTC
cbs-1	GCCATCTCATACGCAACA	CAGGGTATGCAAGACAGTATC
cth-2	AGAACCAGAGCAATGGGATATG	GGGTTTCCAGCACGAGAATAA
mel-32	GTACACCAACAACGAGAACA	CAGCCTTGCTTGTGAAGT
mthf-1	CGGTTGTCGAGGAGAAGATAAC	GACAAATCGAGGTGGGAAGAA
set-2	GAAGAAGCAGAAACCGAGAA	CCTCTTCAGATCGTGGTTTG
gcs-1	GGAGGAAAGAGGATTGGAAC	GTAGCCAACAGAACATGGAT
tyms-1	GAGAAGGAACACGAAGAGATG	CGTGGTAAGCAACGGAAT

References

1. Rossner R, Kaeberlein M, Leiser SF. Flavin-containing monooxygenases in aging and disease: Emerging roles for ancient enzymes. J Biol Chem. 2017. doi:10.1074/jbc.R117.779678

2. Ziegler DM. An overview of the mechanism, substrate specificities, and structure of FMOs. In: Drug Metabolism Reviews. ; 2002. doi:10.1081/DMR-120005650

3. Krueger SK, Williams DE. Mammalian flavin-containing monooxygenases: Structure/function, genetic polymorphisms and role in drug metabolism. Pharmacol Ther. 2005. doi:10.1016/j.pharmthera.2005.01.001

4. Leiser SF, Miller H, Rossner R, et al. Cell nonautonomous activation of flavin-containing monooxygenase promotes longevity and health span. Science (80-). 2015. doi:10.1126/science.aac9257

5. Steinbaugh MJ, Sun LY, Bartke A, Miller RA. Activation of genes involved in xenobiotic metabolism is a shared signature of mouse models with extended lifespan. Am J Physiol Metab. 2012. doi:10.1152/ajpendo.00110.2012

6. Swindell WR. Genes and gene expression modules associated with caloric restriction and aging in the laboratory mouse. BMC Genomics. 2009. doi:10.1186/1471-2164-10-585

7. Bennett CF, Kwon JJ, Chen C, et al. Transaldolase inhibition impairs mitochondrial respiration and induces a starvation-like longevity response in Caenorhabditis elegans. PLoS Genet. 2017. doi:10.1371/journal.pgen.1006695

8. Veeravalli S, Omar BA, Houseman L, et al. The phenotype of a flavin-containing monooyxgenase knockout mouse implicates the drug-metabolizing enzyme FMO1 as a novel regulator of energy balance. Biochem Pharmacol. 2014. doi:10.1016/j.bcp.2014.04.007

9. Scott F, Gonzalez Malagon SG, O'Brien BA, et al. Identification of flavin-containing monooxygenase 5 (FMO5) as a regulator of glucose homeostasis and a potential sensor of gut bacteria. Drug Metab Dispos. 2017. doi:10.1124/dmd.117.076612

10. Huang S, Howington MB, Dobry CJ, Evans CR, Leiser SF. Flavin-Containing Monooxygenases Are Conserved Regulators of Stress Resistance and Metabolism. Front Cell Dev Biol. 2021;9. doi:10.3389/fcell.2021.630188

11. Gao AW, Smith RL, van Weeghel M, Kamble R, Janssens GE, Houtkooper RH. Identification of key pathways and metabolic fingerprints of longevity in C. elegans. Exp Gerontol. 2018;113:128-140. doi:10.1016/J.EXGER.2018.10.003

12. Menendez JA, Joven J. One-carbon metabolism: An aging-cancer crossroad for

the gerosuppressant metformin. Aging (Albany NY). 2012.

13. Cabreiro F, Au C, Leung KY, et al. Metformin retards aging in C. elegans by altering microbial folate and methionine metabolism. Cell. 2013. doi:10.1016/j.cell.2013.02.035

14. Annibal A, George Tharyan R, Fides Schonewolff M, et al. Regulation of the one carbon folate cycle as a shared metabolic signature of longevity. doi:10.1038/s41467-021-23856-9

15. Locasale JW. Serine, glycine and one-carbon units: Cancer metabolism in full circle. Nat Rev Cancer. 2013. doi:10.1038/nrc3557

16. Kabil H, Kabil O, Banerjee R, Harshman LG, Pletcher SD. Increased transsulfuration mediates longevity and dietary restriction in Drosophila. Proc Natl Acad Sci. 2011. doi:10.1073/pnas.1102008108

17. Hansen M, Hsu A-L, Dillin A, Kenyon C. New Genes Tied to Endocrine, Metabolic, and Dietary Regulation of Lifespan from a Caenorhabditis elegans Genomic RNAi Screen. Kim S, ed. PLoS Genet. 2005;1(1):e17. doi:10.1371/journal.pgen.0010017

18. Oxenkrug GF. The extended life span of Drosophila melanogaster eye-color (white and vermilion) mutants with impaired formation of kynurenine. J Neural Transm. 2010. doi:10.1007/s00702-009-0341-7

19. Van Der Goot AT, Zhu W, Vázquez-Manrique RP, et al. Delaying aging and the aging-associated decline in protein homeostasis by inhibition of tryptophan degradation. Proc Natl Acad Sci U S A. 2012. doi:10.1073/pnas.1203083109

20. Sutphin GL, Backer G, Sheehan S, et al. Caenorhabditis elegans orthologs of human genes differentially expressed with age are enriched for determinants of longevity. Aging Cell. 2017. doi:10.1111/acel.12595

21. Badawy AAB. Kynurenine pathway of tryptophan metabolism: Regulatory and functional aspects. Int J Tryptophan Res. 2017;10(1). doi:10.1177/1178646917691938

22. Liu YJ, Janssens GE, McIntyre RL, et al. Glycine promotes longevity in caenorhabditis elegans in a methionine cycle-dependent fashion. PLoS Genet. 2019. doi:10.1371/journal.pgen.1007633

23. Depuydt G, Xie F, Petyuk VA, et al. LC-MS proteomics analysis of the insulin/IGF-1-deficient caenorhabditis elegans daf-2(e1370) mutant reveals extensive restructuring of intermediary metabolism. J Proteome Res. 2014. doi:10.1021/pr401081b

24. Johnson TE, Cypser J, De Castro E, et al. Gerontogenes mediate health and

longevity in nematodes through increasing resistance to environmental toxins and stressors. In: Experimental Gerontology. ; 2000. doi:10.1016/S0531-5565(00)00138-8

25. Finkel T, Holbrook NJ. Oxidants, oxidative stress and the biology of ageing. Nature. 2000. doi:10.1038/35041687

26. Johnson TE, Henderson S, Murakami S, et al. Longevity genes in the nematode Caenorhabditis elegans also mediate increased resistance to stress and prevent disease. J Inherit Metab Dis. 2002. doi:10.1023/A:1015677828407

27. Miller RA. Cell stress and aging: New emphasis on multiplex resistance mechanisms. In: Journals of Gerontology - Series A Biological Sciences and Medical Sciences. ; 2009. doi:10.1093/gerona/gln072

28. Ding W, Smulan LJ, Hou NS, Taubert S, Watts JL, Walker AK. s-Adenosylmethionine Levels Govern Innate Immunity through Distinct Methylation-Dependent Pathways. Cell Metab. 2015;22:633-645. doi:10.1016/j.cmet.2015.07.013

29. Lee HJ, Noormohammadi A, Koyuncu S, et al. Prostaglandin signals from adult germline stem cells delay somatic ageing of Caenorhabditis elegans. Nat Metab. 2019;1(8):790-810. doi:10.1038/s42255-019-0097-9

30. Hine C, Harputlugil E, Zhang Y, et al. Endogenous hydrogen sulfide production is essential for dietary restriction benefits. Cell. 2015;160(1-2):132-144. doi:10.1016/j.cell.2014.11.048

31. Wei Y, Kenyon C. Roles for ROS and hydrogen sulfide in the longevity response to germline loss in Caenorhabditis elegans. Proc Natl Acad Sci U S A. 2016;113(20):E2832-E2841. doi:10.1073/pnas.1524727113

32. Obata F, Miura M. Enhancing S-adenosyl-methionine catabolism extends Drosophila lifespan. Nat Commun. 2015;6(1):1-9. doi:10.1038/ncomms9332

33. Orth JD, Thiele I, Palsson BO. What is flux balance analysis? Nat Biotechnol. 2010. doi:10.1038/nbt.1614

34. Singh S, Samal A, Giri V, Krishna S, Raghuram N, Jain S. Flux-based classification of reactions reveals a functional bow-tie organization of complex metabolic networks. Phys Rev E - Stat Nonlinear, Soft Matter Phys. 2013. doi:10.1103/PhysRevE.87.052708

35. Walker AK, Jacobs RL, Watts JL, et al. A conserved SREBP-1/phosphatidylcholine feedback circuit regulates lipogenesis in metazoans. Cell. 2011. doi:10.1016/j.cell.2011.09.045

36. Choi H, Cho SC, Ha YW, et al. DDS promotes longevity through a microbiome-

mediated starvation signal. Transl Med Aging. 2019;3:64-69. doi:10.1016/j.tma.2019.07.001

37. Yi P, Melnyk S, Pogribna M, Pogribny IP, Hine RJ, James SJ. Increase in plasma homocysteine associated with parallel increases in plasma S-adenosylhomocysteine and lymphocyte DNA hypomethylation. J Biol Chem. 2000;275(38):29318-29323. doi:10.1074/jbc.M002725200

38. Yuasa HJ, Ball HJ. Efficient tryptophan-catabolizing activity is consistently conserved through evolution of TDO enzymes, but not IDO enzymes. J Exp Zool B Mol Dev Evol. 2015;324(2):128-140. doi:10.1002/jez.b.22608

39. Brosnan ME, Brosnan JT. Formate: The Neglected Member of One-Carbon Metabolism. 2016. doi:10.1146/annurev-nutr-071715-050738

40. Santi D V, Mchenry CS. 5-Fluoro-2'-Deoxyuridylate: Covalent Complex with Thymidylate Synthetase (Affinity Labeling/Enzyme Mechanism/Inhibition/Fluorinated Pyrimidines). Vol 69.; 1972. https://www.pnas.org.

41. Lim C-Y, Lin H-T, Kumsta C, et al. SAMS-1 coordinates HLH-30/TFEB and PHA-4/FOXA activities through histone methylation to mediate dietary restriction-induced autophagy and longevity. Autophagy. May 2022:1-17. doi:10.1080/15548627.2022.2068267

42. Veeravalli S, Phillips IR, Freire RT, Varshavi D, Everett JR, Shephard EA. Flavin-Containing Monooxygenase 1 Catalyzes the Production of Taurine from Hypotaurine s. DRUG Metab Dispos Drug Metab Dispos. 2020;48:378-385. doi:10.1124/dmd.119.089995

43. Sun L, Sadighi Akha AA, Miller RA, Harper JM. Life-span extension in mice by preweaning food restriction and by methionine restriction in middle age. Journals Gerontol - Ser A Biol Sci Med Sci. 2009. doi:10.1093/gerona/glp051

44. Lee BC, Kaya A, Ma S, et al. Methionine restriction extends lifespan of Drosophila melanogaster under conditions of low amino-acid status. Nat Commun. 2014. doi:10.1038/ncomms4592

45. Parkhitko AA, Binari R, Zhang N, Asara JM, Demontis F, Perrimon N. Tissue-specific down-regulation of S-adenosyl-homocysteine via suppression of dAhcyL1/dAhcyL2 extends health span and life span in Drosophila. Genes Dev. 2016. doi:10.1101/gad.282277.116

46. Maddocks ODK, Labuschagne CF, Adams PD, Vousden KH. Serine Metabolism Supports the Methionine Cycle and DNA/RNA Methylation through De Novo ATP Synthesis in Cancer Cells. Mol Cell. 2016;61(2):210-221. doi:10.1016/j.molcel.2015.12.014

47. Dues DJ, Andrews EK, Senchuk MM, Van Raamsdonk JM. Resistance to Stress Can Be Experimentally Dissociated From Longevity. Journals Gerontol Ser A. 2019;74(8):1206-1214. doi:10.1093/gerona/gly213

48. Reddy RR, Ralph EC, Motika MS, Zhang J, Cashman JR. Characterization of human flavin-containing monooxygenase (FMO) 3 and FMO5 expressed as maltose-binding protein fusions. Drug Metab Dispos. 2010. doi:10.1124/dmd.110.033639

49. Lončar N, Fiorentini F, Bailleul G, et al. Characterization of a thermostable flavin-containing monooxygenase from Nitrincola lacisaponensis (NiFMO). Appl Microbiol Biotechnol. 2019;103(4):1755-1764. doi:10.1007/s00253-018-09579-w

50. Chen Y, Patel NA, Crombie A, Scrivens JH, Murrell JC. Bacterial flavin-containing monooxygenase is trimethylamine monooxygenase. Proc Natl Acad Sci. 2011. doi:10.1073/pnas.1112928108

51. Fiorentini F, Geier M, Binda C, et al. Biocatalytic Characterization of Human FMO5: Unearthing Baeyer-Villiger Reactions in Humans. ACS Chem Biol. 2016;11(4):1039-1048. doi:10.1021/acschembio.5b01016

52. Kapahi P, Kaeberlein M, Hansen M. Dietary restriction and lifespan: Lessons from invertebrate models. Ageing Res Rev. 2017;39:3-14. doi:10.1016/j.arr.2016.12.005

53. Gu X, Orozco JM, Saxton RA, et al. SAMTOR is an S-adenosylmethionine sensor for the mTORC1 pathway. Science (80-). 2017;358(6364):813-818. doi:10.1126/science.aao3265

54. Metz R, Rust S, DuHadaway JB, et al. IDO inhibits a tryptophan sufficiency signal that stimulates mTOR: A novel IDO effector pathway targeted by D-1-methyl-tryptophan. Oncoimmunology. 2012;1(9):1460-1468. doi:10.4161/onci.21716

55. Wang H, Ji Y, Wu G, et al. L-Tryptophan activates mammalian target of rapamycin and enhances expression of tight junction proteins in intestinal porcine epithelial cells. J Nutr. 2015;145(6):1156-1162. doi:10.3945/jn.114.209817

56. Newman AC, Maddocks ODK. One-carbon metabolism in cancer. Br J Cancer. 2017;116(12):1499-1504. doi:10.1038/bjc.2017.118

57. Beydoun S, Choi HS, Dela-Cruz G, et al. An alternative food source for metabolism and longevity studies in Caenorhabditis elegans. Commun Biol. 2021;4(1). doi:10.1038/s42003-021-01764-4

58. Overmyer KA, Thonusin C, Qi NR, Burant CF, Evans CR. Impact of anesthesia and euthanasia on metabolomics of mammalian tissues: Studies in a C57BL/6J mouse model. PLoS One. 2015. doi:10.1371/journal.pone.0117232

59. Overmyer KA, Thonusin C, Qi NR, et al. Maximal oxidative capacity during exercise is associated with skeletal muscle fuel selection and dynamic changes in mitochondrial protein acetylation. PLoS One. 2015. doi:10.1016/j.cmet.2015.02.007

60. Smith CA, Want EJ, O'Maille G, Abagyan R, Siuzdak G. XCMS: Processing mass spectrometry data for metabolite profiling using nonlinear peak alignment, matching, and identification. Anal Chem. 2006. doi:10.1021/ac051437y

61. Zhang Y, Chen D, Smith MA, Zhang B, Pan X. Selection of reliable reference genes in caenorhabditis elegans for analysis of nanotoxicity. PLoS One. 2012;7(3):31849. doi:10.1371/journal.pone.0031849

62. Motika MS, Zhang J, Zheng X, Riedler K, Cashman JR. Novel variants of the human flavin-containing monooxygenase 3 (FMO3) gene associated with trimethylaminuria. Mol Genet Metab. 2009;97(2):128-135. doi:10.1016/j.ymgme.2009.02.006

63. Blaženović I, Kind T, Sa MR, et al. Structure Annotation of All Mass Spectra in Untargeted Metabolomics. Anal Chem. 2019;91(3):2155-2162. doi:10.1021/acs.analchem.8b04698

Chapter IV

FMO-2 Interacts with Phosphatidylcholine Synthesis and The UPR^{ER} to Promote Longevity

Foreword

This work is based on our findings in Chapter III that FMO-2 and reduced methylation flux are in the same functional pathway in regulating longevity. This work was initiated by Dr. Bhat and me with our initial hypothesis that FMO-2 reduces phosphatidylcholine (PC) synthesis downstream of methylation, which in turn activates the endoplasmic reticulum unfolded protein response (UPR^{ER}) to regulate longevity. This hypothesis is based in part on the information presented in Chapter I. While the manuscript for this work is not yet completed, it is consistent with our initial hypothesis and presents a mechanism by which FMO-2 may regulate PC synthesis and the UPR^{ER} to regulate longevity. The results from this chapter identify key components of FMO-2-mediated longevity regulation downstream of methylation, which we find to be a critical output of metabolic changes caused by FMO-2 within one-carbon metabolism. The data shown were obtained primarily by Dr. Bhat and me with the help from a fellow graduate student Angela Tuckowski.

Abstract

Cellular response to environmental and internal stresses is a key component of homeostasis and longevity regulation. In *C. elegans*, *flavin-containing monooxygenase-2* (*fmo-2*) is induced under two separate environmental stresses, hypoxia and dietary restriction, and is necessary and sufficient to promote longevity benefits in response. However, little is known about the molecular mechanisms by which FMO-2 promotes these benefits. We previously identified the reduction in transmethylation as a potential mechanism of FMO-2. Using transcriptomics analysis and follow-up supplementation and gene-knockdown approaches, here we identify the phosphatidylcholine synthesis pathway to be downstream of *fmo-2* and its reduction of methylation flux. We further find that the IRE-1-dependent UPR (UPR^{ER}) is necessary for *fmo-2* longevity benefits. Our data are consistent with previous studies showing that perturbations in phosphatidylcholine synthesis regulate the UPR^{ER} and suggest a model where *fmo-2* regulates cellular lipid balance to regulate a major component of the stress response pathway to influence longevity.

Introduction

Flavin-containing monooxygenases (FMOs) are enzymes that oxygenate substrates. While studied primarily as xenobiotic-metabolizing enzymes, FMOs can also metabolize endogenous metabolic substrates. FMOs are bound to an FAD prosthetic group and commonly oxygenate substrates with nucleophilic centers, such as nitrogen and sulfur,

in the presence of NADPH and oxygen. These enzymes are highly conserved genetically and structurally across taxa, suggesting a more ancient role than simply metabolizing xenobiotics[1]. Considering their conservation, it is likely that the mechanisms that we identify in worms will be translatable to humans and other mammals.

A plausible role of FMOs is the regulation of endogenous metabolic processes. Mouse FMOs are involved in multiple endogenous metabolic pathways[2–8] and in regulating stress resistance against multiple stressors, likely through metabolic modulation[9]. In humans, a mutation in FMO3 that prevents the conversion of trimethylamine (TMA) into trimethylamine oxide (TMAO), causes a condition known as trimethylaminuria, or fish odor syndrome[1,6,7,10]. More recently, our lab finds that *C. elegans fmo-2* is induced downstream of multiple longevity pathways, including hypoxia and dietary restriction (DR)[11]. *Fmo-2* is also necessary and sufficient to promote health and longevity benefits downstream of these two pathways[11]. Our data implicate one-carbon metabolism and tryptophan metabolism as downstream effectors of *fmo-2* (Chapter III). The resulting model from our work suggests that *fmo-2* influences longevity by reducing methylation flux in a similar manner to knocking down *sams-1* (Chapter III), which encodes for S-adenosylmethionine synthase that is responsible for converting methionine into S-adenosylmethione (SAM), a major methyl donor. Therefore, it is likely that FMOs regulate the aging process by modifying endogenous metabolic processes.

There are multiple methylation reactions that occur in cells. These reactions are catalyzed by methyltransferases that transfer a methyl group from a methyl donor, like SAM, to a methyl recipient substrate. Several methyltransferases reportedly affect the aging process. Knockdown of *set-2*, a histone methyltransferase, and *fib-1*, which is involved in pre-rRNA processing and modification and histone modification, increase worm lifespan[12,13]. Taken together, these data raise a possibility that specific methyltransferases are important in the context of longevity regulation.

Another methylation process that may be important for longevity regulation is phosphatidylcholine (PC) metabolism. In the context of methylation, a methyl group from SAM is transferred to phosphatidylethanolamine by *pmt-1* to form phosphocholine, which is then converted into PC through a further series of chemical reactions. Alternatively, PC can also be synthesized independent of SAM through the conversion of choline into phospholipid by *ckb-2*[14]. Recent evidence suggest that PC imbalance can activate the UPR^{ER}, a stress response mechanism that induces the expression of genes involved in the regulation of protein folding and autophagy[15], through the activation of IRE-1[14], which is discussed in Chapter I. IRE-1 and its target transcription factor XBP-1 are required for multiple longevity pathways, including dietary restriction[16] (DR) and insulin signaling[17]. While the UPR^{ER} activation is commonly linked to proteotoxic insults, these findings suggest that PC synthesis is another regulator of this response that can influence longevity.

Given that 1) PC synthesis is downstream of methylation, 2) a perturbation in PC synthesis activates the UPR^{ER}, 3) The UPR^{ER} is required downstream of multiple

longevity pathways, including DR, and 4) *fmo-2* regulates longevity downstream of DR and affects methylation, we hypothesized that *fmo-2* promotes longevity by reducing PC synthesis, which in turn activates the UPR^{ER}. Our resulting data support a model where FMO-2 interacts with components of the PC synthesis to regulate stress resistance and lifespan and requires the UPR^{ER} to extend lifespan in worms. Taken together, our model is consistent with previous studies that show a link between phospholipid metabolism and the UPR^{ER} activation, and positions *fmo-2* as a regulator of these processes.

Results

FMO-2 interacts with PC synthesis genes to regulate stress resistance

To determine the downstream mechanisms of *fmo-2*, we first examined the interaction between *fmo-2* and lipid metabolism downstream of methylation. While other methyltransferases are involved in longevity regulation as mentioned above, we focused on lipids as *fmo-2* has previously been implicated in the regulation of fatty acid metabolism[18] and thus would be a more likely downstream effector of *fmo-2*. In particular, we were interested in the phosphatidylcholine (PC) synthesis pathway because of its mechanistic proximity to methylation. During PC synthesis, phosphatidylethanolamine is converted into phosphocholine by *pmt-1* in the presence of S-adenosylmethionine (SAM). Phosphocholine can also be synthesized in a SAM-independent manner through the conversion of choline into phosphocholine by *ckb-2*. Phosphocholine is then converted into PC through a series of downstream reactions[14]

(**Figure 4.1A**). Since the reduction in methylation is implicated in *fmo-2*-mediated longevity regulation, we hypothesized that PC synthesis may also be involved in this mechanism downstream of methylation. To determine the interaction between PC synthesis and *fmo-2*, we knocked down *pmt-1* in *fmo-2* overexpression (FMO-2 OE) and wild-type (WT) animals and assessed their stress resistance, which is a common phenotype observed in multiple long-lived organisms, as mentioned in Chapter III. We have used paraquat to assess the stress resistance of the worms as we observed that FMO-2 OE is resistant against paraquat (Chapter III). We find that knocking down *pmt-1* increases the stress resistance of WT without changing the stress resistance of FMO-2 OE (**Figure 4.1B**), suggesting that the knockdown of *pmt-1* is in the same functional pathway as FMO-2 in conferring stress resistance against paraquat.

Next, tested if the reduction in PC is sufficient to confer stress resistance. We also knocked down *ckb-2*, which is involved in the methylation-independent PC synthesis through the synthesis of phosphocholine from choline instead of using a methyl donor. Similar to *pmt-1*, knocking down *ckb-2* also conferred stress resistance in WT without further increasing the stress resistance of FMO-2 against paraquat (**Figure 4.1C**). Taken together, our data suggest that a reduction in PC synthesis leads to changes in stress resistance.

A

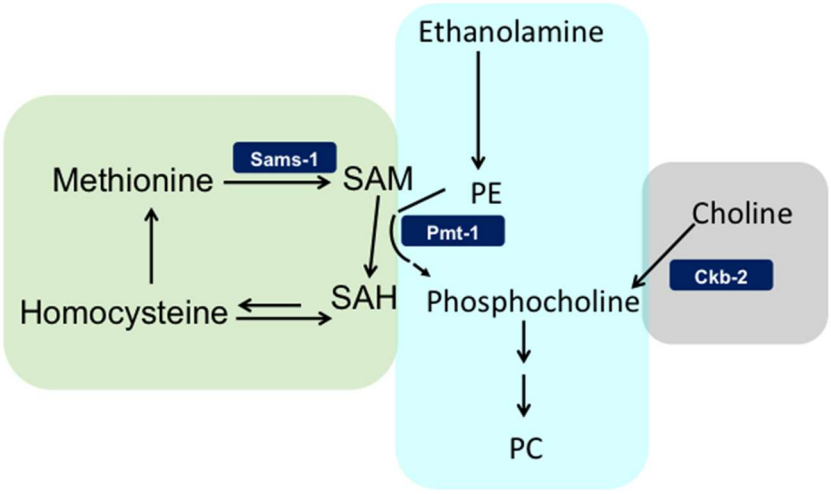

B

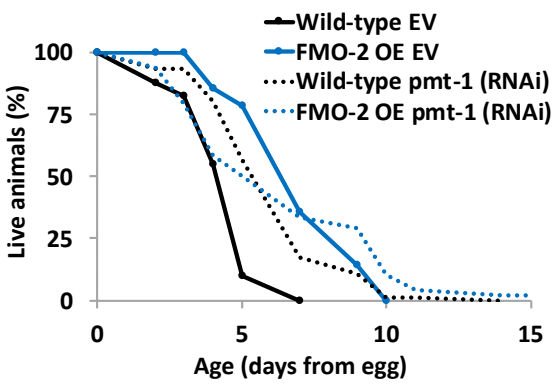

C

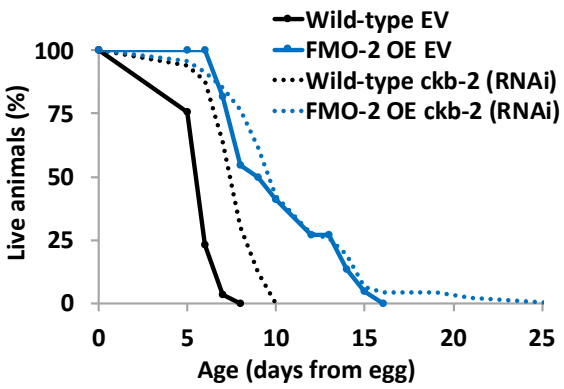

Figure 4.1: FMO-2 interacts with genes involved in the PC synthesis pathways to regulate stress resistance. A) Diagram of the PC synthesis pathways. SAM = S-adenosylmethionine, SAH = S-adenosylhomocysteine, and PC = phosphatidylcholine. 5 mM paraquat stress resistance assay comparing the wild-type and FMO-2 OE on empty-vector (EV) and B) *pmt-1* RNAi and C) *ckb-2* RNAi. Statistics are in Table 4.1.

FMO-2 interacts with PC synthesis substrates to regulate longevity

If the reduction of PC synthesis is necessary for FMO-2-mediated longevity benefits, we hypothesized that supplementing worms with the substrates of PC synthesis, which would increase PC levels, would reduce the lifespan extension in FMO-2 OE. To test this hypothesis, we supplemented the worm diet with two substrates: 1) ethanolamine, which is a precursor molecule for phosphatidylethanolamine that is also involved in the SAM-dependent synthesis of PC, and 2) choline, which is involved in the SAM-independent synthesis of PC. Since these substrates are precursor molecules for PC synthesis, we hypothesized that supplementing the worm diet with them would increase PC levels, thereby decreasing FMO-2 OE lifespan extension. Consistent with this hypothesis, we find that the choline supplementation reduces the lifespan of FMO-2 OE more severely than that of WT (**Figure 4.2A**), suggesting a negative interaction between FMO-2 and choline. However, supplementing with ethanolamine does not change the lifespan of WT and FMO-2 OE (**Figure 4.2B**). The finding that the ethanolamine supplementation does not reduce FMO-2 OE lifespan is consistent with our previous data suggesting that methylation flux is reduced in FMO-2 OE and our finding that SAM supplementation reduces lifespan in FMO-2 OE. In the SAM-dependent PC synthesis, ethanolamine is converted into phosphatidylcholine, which then receives a methyl group from SAM to produce phosphocholine[14]. Since FMO-2 OE has a reduced SAM availability (Chapter III), it is plausible that increasing ethanolamine level does not affect PC synthesis. In sum, our data are consistent with a model where a reduction in PC synthesis is required for FMO-2-mediated lifespan extension.

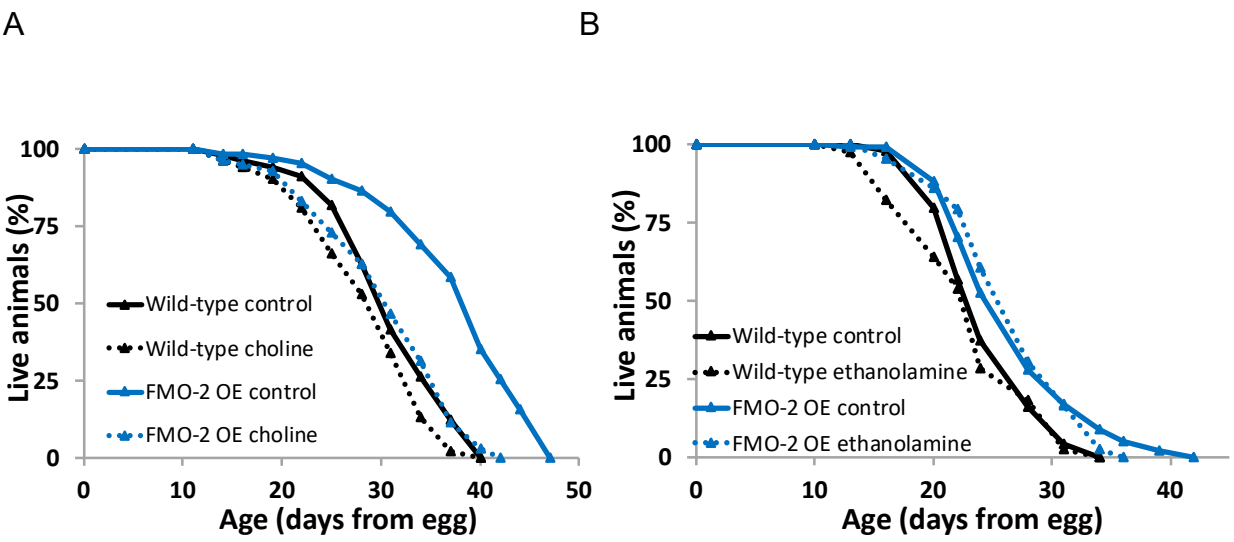

Figure 4.2: FMO-2 interacts with substrates involved in PC synthesis to regulate longevity. Lifespan assay comparing the survival of the wild-type and FMO-2 OE on control and A) 10 mM choline and B) 30 mM ethanolamine supplementation conditions. Statistics are in Table 4.2.

FMO-2 requires components of the UPR^{ER} to regulate longevity

Previous studies have shown that the components of IRE-1-mediated UPR^{ER} are necessary to extend lifespan under dietary restriction[16]. Additionally, recent evidence supports that the reduction of PC synthesis via PMT1 deletion leads to lifespan extension in yeast[19]. Based on these findings and our finding that *fmo-2* interacts with genes and substrates of PC synthesis to influence stress resistance and longevity, we hypothesized that the components of the UPR^{ER} are also required for FMO-2-mediated lifespan extension. To test this hypothesis, we knocked down *ire-1* and its downstream transcription factor *xbp-1*. We find that the knockdown of either of these genes

abrogates the lifespan extension of FMO-2 OE (**Figure 4.3**). While the *xbp-1* knockdown rescues the wildtype lifespan phenotype in FMO-2 OE (**Figure 4.3A**), *ire-1* knockdown decreases both the lifespan of WT and FMO-2 OE with a more severe effect on FMO-2 OE (**Figure 4.3B**). Since *ire-1* affects other genes besides *xbp-1* that are important for survival[20], we hypothesize that knocking down *ire-1* has detrimental effect on lifespan that is not observed with *xbp-1* knockdown. In sum, our data suggest that the UPR^{ER} is indeed a necessary downstream target of FMO-2 and places *fmo-2* within the mechanism of longevity regulation by DR and the UPR^{ER}.

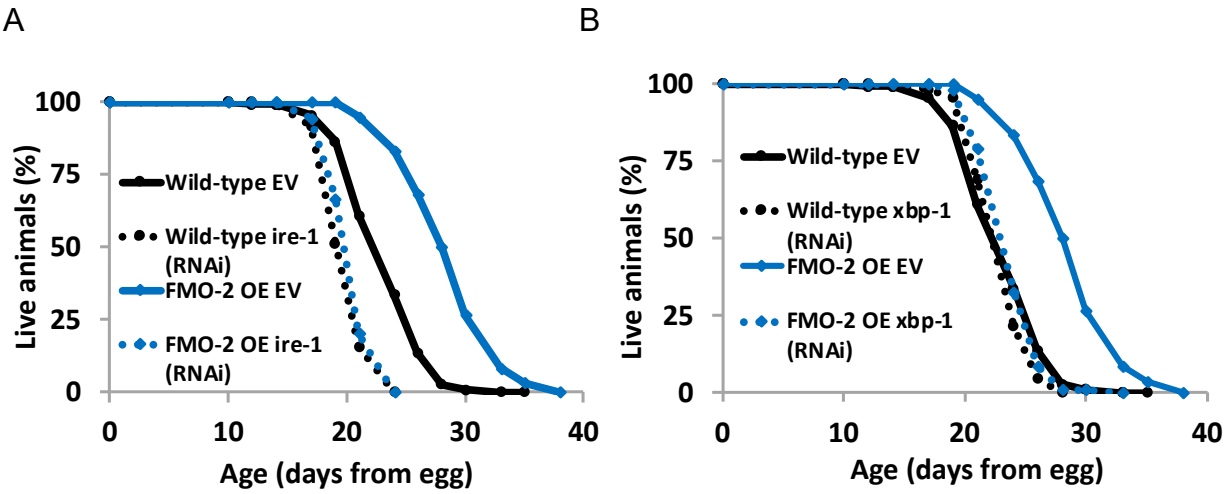

Figure 4.3: FMO-2 requires components of the UPR^{ER} to regulate longevity. Lifespan assay comparing the survival of the wild type and FMO-2 OE on EV and A) ire-1 RNAi and B) xbp-1 RNAi. Statistics are in Table 4.2.

Discussion

Here, we show that *C. elegans fmo-2* interacts with genes and substrates of PC synthesis to regulate stress resistance and longevity and that *fmo-2* requires components of the UPR^{ER} to extend lifespan. Our data are consistent with a model where the induction of *fmo-2* leads to reduced methylation through *pmt-1*, which leads to reduced PC synthesis that activates the UPR^{ER} to promote longevity and health benefits in worms.

However, we have not directly measured and compared the level of PC in FMO-2 OE and WT. It will be interesting to measure it using a lipidomics approach to directly test the hypothesis that FMO-2 induction leads to reduced PC synthesis. In addition, while stress resistance and lifespan tend to be directly correlated, there are instances of separation of these two phenotypes, as we ourselves have reported previously (Chapter III). Therefore, it will be of interest to assess the lifespan of FMO-2 OE and WT under *pmt-1* and *ckb-2* knockdown similar to how we tested for stress resistance against paraquat. Likewise, it should also be tested if supplementing substrates of PC synthesis would affect the stress resistance of the worms in the same direction as their lifespan.

Previously, we observed that knocking down *sams-1* leads to a reduction in stress resistance against paraquat (Chapter III). Conversely, we find here that knocking down *pmt-1*, a gene that is downstream of *sams-1*, confers stress resistance. We hypothesize that this is because knocking down *sams-1* likely alters other methyltransferases as

well, which may result in deleterious effects, such as reducing stress resistance. This suggests that the reduction of flux through specific methylation reactions rather than a global reduction in methylation is important for longevity regulation. While we have tested p*mt-1*, there could be other methyltransferases that are also important for *fmo-2*-mediated longevity regulation, including *set-2* and *fib-1*. It would be interesting to do a genetic screen of methyltransferases to determine if there are any other enzymes that are in the same functional pathway as FMO-2. Moreover, if global methylation is indeed detrimental to aspects of healthspan but specific methylation is beneficial, it would be important to determine how FMO-2 selectively modulates changes in these specific methylation reactions.

In addition, while we determine that the components of the UPR^{ER} is required for *fmo-2* longevity regulation, we have not tested if the UPR^{ER} is activated under *fmo-2* induction and if so, whether this activation is due to the reduction in PC synthesis. It will be important to test for the UPR^{ER} activation (e.g., measuring the level of IRE-1 phosphorylation using western blot) following *fmo-2* expression under the genetic and supplementary conditions tested above to determine the relationship between *fmo-2*, PC synthesis, and the UPR^{ER}.

Taken together, these results further the understanding of the downstream mechanism of FMO-2-mediated longevity regulation. In particular, we identify the PC synthesis pathway and the IRE-1-mediated UPR^{ER} as the key effectors of longevity within this regulatory process. While additional work is needed to determine if/how these pathways

are linked to one another mechanistically, the finding that FMO-2 interacts with the components of the PC synthesis pathway and the UPR^{ER} are consistent with previous studies showing that mammalian FMOs regulate endogenous metabolic processes and that the UPR^{ER} is necessary for DR-mediated longevity benefits. Thus, these findings highlight the potential of targeting the PC synthesis pathway to modulate health and longevity in humans.

Materials and Methods

C elegans maintenance

Standard *C. elegans* maintenance procedures were used as previously described[11,21]. N2 wild type, KAE9 ((*eft-3p*::*fmo-2* + *h2b*::*gfp* + Cbr-*unc-119*(+)), and VC1668 (*fmo-2(ok2147*)) strains were grown on solid nematode growth media (NGM) using *E. coli* OP50 throughout life except where RNAi (*E. coli* HT115) were used. All experiments were conducted at 20°C.

Stress resistance assay

Paraquat (Methyl viologen dichloride hydrate from Sigma-Aldrich) was used to induce oxidative stress. Worms were synchronized from eggs on RNAi plates seeded with *E. coli* HT115 strain expressing dsRNAi for a particular gene and at L4 stage 40 worms were transferred on RNAi-FUDR plates containing 5 mM paraquat. A minimum of two

plates per strain per condition were used per replicate experiment. Worms were then scored every day and considered dead when they did not move in response to prodding under a dissection microscope. Worms that crawled off the plate were not considered, but ruptured worms were noted and considered as previously described[11].

Lifespan assays

Gravid adults were placed on NGM plates containing 1mM β-D-isothiogalactopyranoside (IPTG), 25 μg/ml carbenicillin, and the corresponding RNAi clone from the Vidal or Ahringer RNAi library. After 3 hours, the adults were removed, and the eggs were allowed to develop at 20°C until they reached late L4/young adult stage. From here, 40 to 90 worms were placed on each RNAi plate and transferred to fresh RNAi + FUDR plates on day 1, day 2, day 4, and day 6 of adulthood. A minimum of two plates per strain per condition were used per replicate experiment. Experimental animals were scored every 2-3 days and considered dead when they did not move in response to prodding under a dissection microscope. Worms that crawled off the plate were not considered, but ruptured worms were considered as previously described[11]. A similar method was used for supplementation lifespan experiments, except either 30 mM ethanolamine or 10 mM choline was added to the NGM plates without IPTG. Log-rank test was used to derive p-value for lifespan and paraquat survival assays using $p < 0.05$ cut-off threshold compared to controls.

Table 4.1: Stress resistance analyses against 5 mM paraquat

Strain	Experiment	Food	n	Median	Mean	p-value	% change median	% change mean
KAE9	1	ckb-2 (RNAi)	47	9	10.1	0.478	13%	7%
KAE9	1	EV (RNAi)	22	8	9.4	N/A	0%	0%
Wild-type/Control	1	ckb-2 (RNAi)	33	7	6.9	0.000	40%	37%
Wild-type/Control	1	EV (RNAi)	61	5	5.0	N/A	0%	0%
KAE9	2	pmt-1 (RNAi)	48	7	6.5	0.990	0%	-11%
KAE9	2	EV (RNAi)	14	7	7.3	N/A	0%	0%
Wild-type/Control	2	pmt-1 (RNAi)	76	7	6.3	0.000	29%	29%
Wild-type/Control	2	EV (RNAi)	40	5	4.5	N/A	0%	0

Table 4.2: Lifespan analyses

Strain	Experiment	Food	n	Median	Mean	p-value	% change median	% change mean
Wild-type/Control	1	0 mM choline	99	31	31.1	N/A	0%	0%
Wild-type/Control	1	10 mM choline	100	31	28.9	0.006	0%	-7%
KAE9	1	0 mM choline	103	40	37.8	N/A	0%	0%
KAE9	1	10 mM choline	99	31	30.8	0.000	-23%	-19%
Wild-type/Control	2	0 mM ethanolamine	99	24	24.8	N/A	0%	0%
Wild-type/Control	2	30 mM ethanolamine	39	24	23.3	0.354	0%	-6%
KAE9	2	0 mM ethanolamine	101	28	26.9	N/A	0%	0%
KAE9	2	30 mM ethanolamine	43	28	27.0	0.879	0%	0%
Wild-type/Control	3	EV (RNAi)	110	24	23.5	N/A	0%	0%
Wild-type/Control	3	ire-1 (RNAi)	121	21	20.3	0.000	-13%	-13%
Wild-type/Control	3	xbp-1 (RNAi)	107	24	23.4	0.254	0%	0%
KAE9	3	EV (RNAi)	60	30	29.0	N/A	0%	0%
KAE9	3	ire-1 (RNAi)	108	21	20.8	0.000	-30%	-28%
KAE9	3	xbp-1 (RNAi)	104	24	24.2	0.000	-20%	-16%

KAE9 = FMO-2 OE

References

1. Rossner R, Kaeberlein M, Leiser SF. Flavin-containing monooxygenases in aging and disease: Emerging roles for ancient enzymes. J Biol Chem. 2017. doi:10.1074/jbc.R117.779678

2. Swindell WR. Genes and gene expression modules associated with caloric restriction and aging in the laboratory mouse. BMC Genomics. 2009. doi:10.1186/1471-2164-10-585

3. Steinbaugh MJ, Sun LY, Bartke A, Miller RA. Activation of genes involved in xenobiotic metabolism is a shared signature of mouse models with extended lifespan. Am J Physiol Metab. 2012. doi:10.1152/ajpendo.00110.2012

4. Scott F, Gonzalez Malagon SG, O'Brien BA, et al. Identification of flavin-containing monooxygenase 5 (FMO5) as a regulator of glucose homeostasis and a potential sensor of gut bacteria. Drug Metab Dispos. 2017. doi:10.1124/dmd.117.076612

5. Veeravalli S, Omar BA, Houseman L, et al. The phenotype of a flavin-containing monooyxgenase knockout mouse implicates the drug-metabolizing enzyme FMO1 as a novel regulator of energy balance. Biochem Pharmacol. 2014. doi:10.1016/j.bcp.2014.04.007

6. Petalcorin MIR, Joshua GW, Agapow P-M, Dolphin CT. The fmo genes of Caenorhabditis elegans and C. briggsae: characterisation, gene expression and comparative genomic analysis. Gene. 2005;346:83-96. doi:10.1016/J.GENE.2004.09.021

7. Miao J, Ling A V., Manthena P V., et al. Flavin-containing monooxygenase 3 as a potential player in diabetes-associated atherosclerosis. Nat Commun. 2015;6. doi:10.1038/ncomms7498

8. Dever JT, Elfarra AA. In vivo metabolism of L-methionine in mice: Evidence for stereoselective formation of methionine-d-sulfoxide and quantitation of other major metabolites. Drug Metab Dispos. 2006;34(12):2036-2043. doi:10.1124/dmd.106.012104

9. Huang S, Howington MB, Dobry CJ, Evans CR, Leiser SF. Flavin-Containing Monooxygenases Are Conserved Regulators of Stress Resistance and Metabolism. Front Cell Dev Biol. 2021;9. doi:10.3389/fcell.2021.630188

10. Schugar RC, Shih DM, Warrier M, et al. The TMAO-Producing Enzyme Flavin-Containing Monooxygenase 3 Regulates Obesity and the Beiging of White Adipose Tissue. Cell Rep. 2017;19(12):2451-2461. doi:10.1016/j.celrep.2017.05.077

11. Leiser SF, Miller H, Rossner R, et al. Cell nonautonomous activation of flavin-

containing monooxygenase promotes longevity and health span. Science (80-). 2015. doi:10.1126/science.aac9257

12. Greer EL, Maures TJ, Hauswirth AG, et al. Members of the H3K4 trimethylation complex regulate lifespan in a germline-dependent manner in C. elegans. Nature. 2010;466(7304):383-387. doi:10.1038/nature09195

13. Lim C-Y, Lin H-T, Kumsta C, et al. SAMS-1 coordinates HLH-30/TFEB and PHA-4/FOXA activities through histone methylation to mediate dietary restriction-induced autophagy and longevity. Autophagy. May 2022:1-17. doi:10.1080/15548627.2022.2068267

14. Hou NS, Gutschmidt A, Choi DY, et al. Activation of the endoplasmic reticulum unfolded protein response by lipid disequilibrium without disturbed proteostasis in vivo. Proc Natl Acad Sci U S A. 2014;111(22):E2271-80. doi:10.1073/pnas.1318262111

15. Lee SK. Endoplasmic Reticulum Homeostasis and Stress Responses in Caenorhabditis elegans. Prog Mol Subcell Biol. 2021;59:279-303. doi:10.1007/978-3-030-67696-4_13

16. Chen D, Thomas EL, Kapahi P. HIF-1 Modulates Dietary Restriction-Mediated Lifespan Extension via IRE-1 in Caenorhabditis elegans. Mango SE, ed. PLoS Genet. 2009;5(5):e1000486. doi:10.1371/journal.pgen.1000486

17. Henis-Korenblit S, Zhang P, Hansen M, et al. Insulin/IGF-1 signaling mutants reprogram ER stress response regulators to promote longevity. Proc Natl Acad Sci U S A. 2010;107(21):9730-9735. doi:10.1073/pnas.1002575107

18. Goh GYS, Winter JJ, Bhanshali F, et al. NHR-49/HNF4 integrates regulation of fatty acid metabolism with a protective transcriptional response to oxidative stress and fasting. Aging Cell. 2018;17(3):e12743. doi:10.1111/acel.12743

19. Cui H-J, Liu X-G, McCormick M, et al. PMT1 deficiency enhances basal UPR activity and extends replicative lifespan of Saccharomyces cerevisiae. Age (Omaha). 2015;37(3):46. doi:10.1007/s11357-015-9788-7

20. Quwaider D, Corchete LA, Martín-Izquierdo M, et al. RNA sequencing identifies novel regulated IRE1-dependent decay targets that affect multiple myeloma survival and proliferation. Exp Hematol Oncol. 2022;11(1):18. doi:10.1186/s40164-022-00271-4

21. Beydoun S, Choi HS, Dela-Cruz G, et al. An alternative food source for metabolism and longevity studies in Caenorhabditis elegans. Commun Biol. 2021;4(1). doi:10.1038/s42003-021-01764-4

Chapter V

Conclusions

Summary of Findings and Overall Model

This work began with the goal of understanding the downstream molecular mechanisms by which FMO-2 regulates longevity and health in *C. elegans*. Given the structural conservation of FMOs[1,2] and recent findings that suggest their role in regulating endogenous metabolism[3], my initial hypothesis was that FMO-2 regulates the aging process by rewiring key metabolic pathways.

The first challenge of my thesis was to develop a method to stop bacterial metabolism. In *C. elegans* metabolism studies, bacterial metabolic activity is a major confounding factor as the worms obtain nutrients from bacterial food source[4]. There have been multiple attempts to remove this variable, such as heat killing, antibiotic treatment, and UV irradiation, which either only stop bacterial growth, inconsistently suppress bacterial metabolism, or negatively affect worm development[4]. Therefore, the first goal of my thesis was to develop a method to consistently stop bacterial replication and metabolism because studying the worm metabolism was a crucial part of my thesis in understanding the metabolic mechanism of FMO-2. For Chapter II, I worked with my co-

authors to develop such a method using a low concentration of PFA[4]. We found that treating bacterial strains with PFA stops bacterial growth and metabolic activity without having a severe effect on the worm phenotype[4].

This new method allowed me to proceed with the study presented in Chapter III, where my co-authors and I determined the mechanism of metabolic regulation of longevity and stress resistance by FMO-2. Using the PFA-killing method developed in Chapter II, we determined the metabolic changes that occur following *fmo-2* expression level using untargeted and targeted metabolomics approaches. The resulting data suggest that FMO-2 modifies one-carbon metabolism. Using the RNAi gene knockdown approach, we showed that FMO-2 interacts on a functional level with key enzymes involved in one-carbon metabolism. Using computer model and subsequent experimental validations, we identified the flux through methylation processes as a potential effector of longevity downstream of FMO-2. Taken together, our data suggest that an increase in *fmo-2* expression leads to changes in OCM that suppresses methylation to promote longevity.

In addition, using the previously published data on the metabolic changes caused by mouse FMOs from our lab, along with *in vitro* enzymatic experiments, we identified tryptophan as a *bona fide* endogenous substrate of FMO-2. Similar to FMO-2's interaction with OCM genes, we also saw interactions between FMO-2 and genes involved in the kynurenine pathway. In addition, we found that the supplementation of formate is sufficient to increase the lifespan of the wildtype animals without further extending the lifespan of FMO-2 OE, suggesting that an increase in formate level is in

the same functional pathway as FMO-2. Taken together, these results are consistent with my current model that increasing oxygenation of tryptophan by FMO-2 leads to an increased production of formate, which can then modify OCM to regulate longevity.

In chapter IV, I looked further into the FMO-2 mechanism of longevity regulation downstream of reduced methylation flux. While the data presented in this chapter are preliminary and will need further optimization and additional biological replicates, they show that genes involved in the SAM-dependent and SAM-independent phosphatidylcholine synthesis are in the same functional pathway as FMO-2 in regulating stress resistance. Moreover, the results from the supplementation of phosphatidylcholine synthesis pathway substrates support my hypothesis, whereby these substrates suppress the lifespan of FMO-2 OE under conditions that would increase PC levels. Lastly, our data suggest that the major components of IRE-1-mediated UPR^{ER} are required for FMO-2-mediated lifespan extension. These data, in conjunction with what is already known about the connection between PC synthesis and the UPR^{ER}, as mentioned in Chapter I, support the hypothesis that FMO-2 overexpression leads to reduced PC synthesis by suppressing methylation flux, which in turn activates the IRE-1-mediated UPR^{ER} to promote longevity.

Based on the work and ideas presented in my thesis, I propose the following model:

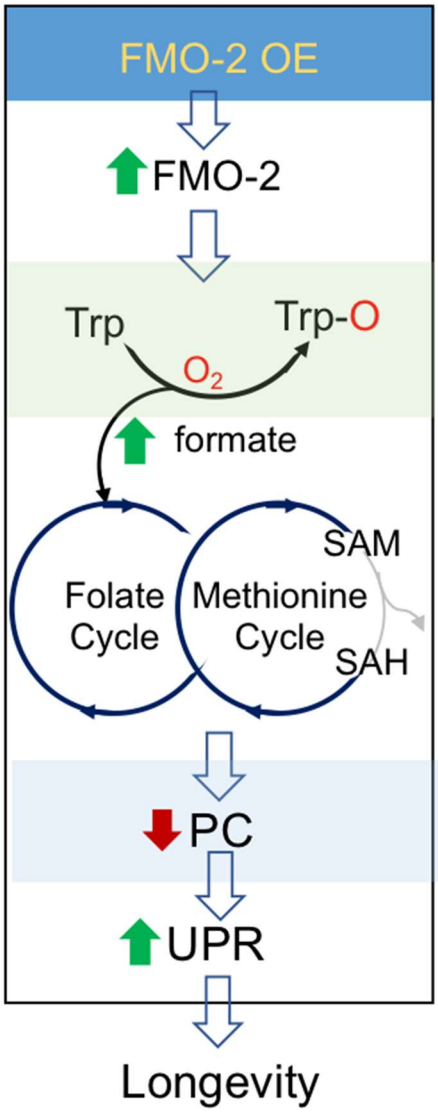

Figure 5.1: Overall Model

As shown above, I hypothesize that the induction of FMO-2 leads to an increase in the oxygenation of tryptophan, which then leads to the synthesis of formate. The synthesis of formate leads to the changes in OCM metabolic flux, which then suppresses the flux through methylation processes, leading to a reduction in phosphatidylcholine synthesis.

Reduction in phosphatidylcholine synthesis leads to the induction of the IRE-1-mediated UPR in the endoplasmic reticulum, which then promotes longevity and stress resistance in worms.

Future Directions

In science, we can never prove our hypotheses, but can only attempt to disprove them. It would be interesting to investigate the following avenues, in addition to optimizing some of the experiments presented thus far, to further attempt to disprove or modify the overall hypothetical model that I have presented above:

1. Determine the flux changes within tryptophan metabolism and one-carbon metabolism following *fmo-2* expression

   In Chapter III, I establish the connection between FMO-2, tryptophan metabolism, and one-carbon metabolism in regulating longevity in *C. elegans*. However, the state of the metabolic fluxes in these pathways following *fmo-2* expression is unclear. Therefore, assessing the flux changes due to *fmo-2* expression will be necessary to understand how *fmo-2* changes the internal fluxes of tryptophan metabolism and one-carbon metabolism. This could be done by exposing worms to isotope-labeled substrates of tryptophan metabolism and OCM, including tryptophan and methionine, and measuring the abundance level of their labeled-downstream products over a time course. This will allow for a more rigorous testing of the

hypotheses that 1) the overexpression of FMO-2 leads to increased tryptophan oxygenation that leads to an increase in formate synthesis and 2) an increase in formate synthesis leads to changes in OCM.

2. Determine the necessity of FMO-2 catalytic function

   A major assumption in my thesis is that the catalytic function of FMO-2 is necessary for its longevity regulation. FMOs have a conserved arginine group in their catalytic domain that is necessary for their oxygenation activity[5,6]. Therefore, a lifespan analysis using worms overexpressing *fmo-2* with an inactivating mutation in this residue will allow us to determine whether the catalytic activity of FMO-2 is indeed necessary for its longevity benefits.

3. Establish the connection between PC synthesis and UPR^{ER} induction downstream of FMO-2.

   As mentioned before, the work presented in Chapter IV is preliminary and does not fully investigate the connection between FMO-2, PC synthesis, and the UPR^{ER} induction. In addition to the experiments shown in Chapter IV, the levels of PC in FMO-2 OE should be measured to determine if overexpressing FMO-2 does indeed reduce PC levels. It should also be determined if knocking down the key genes involved in PC synthesis would confer lifespan extension, similar to what we observe for stress resistance against paraquat. This experiment would be a more direct way

of testing the hypothesis that FMO-2 interacts with key enzymes in the PC synthesis pathway to regulate longevity. In addition, a supplementation lifespan analysis with PC would allow for a direct testing of the hypothesis that reduced PC is in the same functional pathway as FMO-2. I would expect that supplementing with PC will abrogate the lifespan expansion in FMO-2 OE. Lastly, it should be determined if the UPR^{ER} is induced in FMO-2 OE and under reduced PC conditions (e.g., *pmt-1* or *ckb-2* RNAi knockdown) by comparing the ratio of IRE-1 and phosphorylated IRE-1 via western blot. It would also be interesting to test if supplementing the worms with substrates tested in Chapter IV will suppress the UPR^{ER} induction under these conditions via western blot. In sum, these experiments will help to determine whether overexpressing FMO-2 leads to reduced PC synthesis and the induction of UPR^{ER}.

4. Determine other downstream methylation reactions that are involved in the FMO-2-mediated longevity regulation

While I focused on phospholipid synthesis in Chapter IV, there are many other methylation reactions that are dependent on SAM, and a recent study suggest that some of these other methylation processes are also involved in longevity regulation[7]. This makes it plausible that FMO-2 affects longevity through other methylation processes as well. It will be interesting to screen these relevant processes to test the hypothesis that FMO-2 acts on multiple methylation processes to regulate longevity. It will also be interesting to consider how different methylation processes interact

with one another to regulate longevity (i.e. Is there a preferential donation of methyl group to specific metabolites? If so, what is the mechanism?).

Implications and Speculations

In addition to the future directions I propose above, there are other interesting questions to be addressed, but currently lack the data to pursue in the near future. Interestingly, *fmo-2* expression downstream of dietary restriction is transient[3]. This suggest that there is a feedback inhibition of *fmo-2* expression, possibly to conserve energy or nutrients. This is consistent with the previous observation that FMO-2 OE worms have slight developmental delay compared to their wildtype counterpart[8]. However, even though the *fmo-2* induction is transient, the animals are long-lived, suggesting that *fmo-2* may act as a metabolic "switch" to initiate a change in the metabolome that is more permanent. Considering that tryptophan, an essential amino acid, is a substrate of FMO-2, it is possible that the constitutive activation of FMO-2 reduces availability of tryptophan for other metabolic processes. This could lead to growth delay and therefore require a feedback inhibition to conserve tryptophan. Thus, I hypothesize that after FMO-2 is induced under an environmentally stressful condition, such as dietary restriction, it activates the UPR^{ER}, but is inhibited once a more permanent and nutrient-economic "switch" is activated. A good candidate for this switch is serine, another major substrate of OCM that has been implicated in longevity regulation, whereby exogenous supplementation of serine extends worm lifespan[9]. Serine can enter OCM through gluconeogenesis, which is significantly affected by the tricarboxylic acid (TCA) cycle[10].

The TCA cycle and mitochondrial respiration interact closely with the ER through mitochondria-associated membranes (MAMs)[11]. To my knowledge, there is little known about the connection between the UPR, mitochondria and serine level, but I speculate the following: upon its induction, FMO-2 activates the UPR^{ER}. The induction of UPR^{ER} leads to unspecified changes in the mitochondria, which in turn promotes gluconeogenesis, which then increases the level of serine entering OCM, leading to a similar metabolic changes as the initial *fmo-2* induction, thus forming a metabolic loop from OCM to the UPR^{ER} to TCA, back to OCM. Once this loop is formed, *fmo-2* will no longer be necessary to modify OCM and thus can be inhibited to conserve tryptophan. The idea presented here is highly speculative and requires further hypothesis generation and investigation. However, if such a loop does exist, it would suggest that FMOs have a more ancient role than simply metabolizing xenobiotic substrates, in particular, serving as a metabolic switch to regulate metabolism to respond to environmental stress. Considering the broad effect that FMO-2 has on endogenous metabolism under stressful conditions, it is unlikely that this function is an incidental role of FMOs. Instead, they may have evolved to regulate endogenous metabolism to better respond to stress, thereby also extending lifespan as a side effect. It would be interesting to look at the role of other FMOs to test this hypothesis.

The finding that FMO-2 plays an important role in modifying endogenous metabolism to regulate longevity has important implications under multiple contexts. As mentioned in Chapter I, FMOs are known to be involved in xenobiotic metabolism, where they oxygenate foreign substrates to increase their solubility across the membrane[3].

However, given their conserved nature, it is likely that FMOs share a more ancient role than simply detoxifying xenobiotic substrates, such as regulating endogenous metabolism to influence longevity. While their effects on endogenous metabolism have been reported previously[3], the molecular mechanisms of their activity are not well-studied. My work identifies the first endogenous substrate for *C. elegans* FMOs, tryptophan. My work also suggests FMO-2 is a regulator of an important metabolic network, OCM, which is downstream of multiple longevity pathways, including insulin signaling and dietary restriction[12]. The previous work on the role of OCM in longevity regulation focused mainly on specific intermediate metabolites and genes within OCM[12–14]. However, my work also focuses on identifying the upstream and downstream metabolic effectors of OCM, namely tryptophan and phospholipid metabolisms. While these pathways were previously studied under the context of aging[15,16], this is the first time that these seemingly independent pathways have been linked together in their mechanism of longevity regulation. My work suggests that similar to the activation of kinases and transcription factors, perturbations in a single metabolite or a metabolic enzyme can bring about a multitude of downstream changes that can drastically affect physiology. Moreover, my work identifies another longevity-inducing metabolite within tryptophan metabolism, formate, that will be of interest to those studying the metabolic role of in this pathway, particularly in the aging field. It is important to note that the work presented here may not be constrained to worm physiology. Considering the conservation of FMOs across taxa and the role of mammalian FMOs in regulating conserved metabolic pathways[3], it is likely that the mechanisms I discuss here under the context of *C. elegans* will be translatable to human health. Thus, it is possible that

the pathways, metabolites, and genes discussed in my thesis could be used as therapeutic targets in the future and will play an important role in Geroscience going forward and will therefore be a continued model of study in the Leiser Lab and beyond going forward.

References

1. Ziegler DM. An overview of the mechanism, substrate specificities, and structure of FMOs. In: *Drug Metabolism Reviews*. ; 2002. doi:10.1081/DMR-120005650

2. Krueger SK, Williams DE. Mammalian flavin-containing monooxygenases: Structure/function, genetic polymorphisms and role in drug metabolism. *Pharmacol Ther*. 2005. doi:10.1016/j.pharmthera.2005.01.001

3. Rossner R, Kaeberlein M, Leiser SF. Flavin-containing monooxygenases in aging and disease: Emerging roles for ancient enzymes. *J Biol Chem*. 2017. doi:10.1074/jbc.R117.779678

4. Beydoun S, Choi HS, Dela-Cruz G, et al. An alternative food source for metabolism and longevity studies in Caenorhabditis elegans. *Commun Biol*. 2021;4(1). doi:10.1038/s42003-021-01764-4

5. Cho HJ, Cho HY, Kim KJ, Kim MH, Kim SW, Kang BS. Structural and functional analysis of bacterial flavin-containing monooxygenase reveals its ping-pong-type reaction mechanism. *J Struct Biol*. 2011;175(1):39-48. doi:10.1016/j.jsb.2011.04.007

6. Adali O, Carver GC, Philpot RM. The effect of arginine-428 mutation on modulation of activity of human liver flavin monooxygenase 3 (FMO3) by imipramine and chlorpromazine. In: *Experimental and Toxicologic Pathology*. Vol 51. Elsevier GmbH; 1999:271-276. doi:10.1016/S0940-2993(99)80004-9

7. Lim C-Y, Lin H-T, Kumsta C, et al. SAMS-1 coordinates HLH-30/TFEB and PHA-4/FOXA activities through histone methylation to mediate dietary restriction-induced autophagy and longevity. *Autophagy*. May 2022:1-17. doi:10.1080/15548627.2022.2068267

8. Leiser SF, Miller H, Rossner R, et al. Cell nonautonomous activation of flavin-containing monooxygenase promotes longevity and health span. *Science (80-)*. 2015. doi:10.1126/science.aac9257

9. Liu YJ, Janssens GE, McIntyre RL, et al. Glycine promotes longevity in caenorhabditis elegans in a methionine cycle-dependent fashion. *PLoS Genet*.

2019. doi:10.1371/journal.pgen.1007633

10. Reid MA, Allen AE, Liu S, et al. Serine synthesis through PHGDH coordinates nucleotide levels by maintaining central carbon metabolism. *Nat Commun*. 2018;9(1):1-11. doi:10.1038/s41467-018-07868-6

11. Malhotra JD, Kaufman RJ. ER stress and Its functional link to mitochondria: Role in cell survival and death. *Cold Spring Harb Perspect Biol*. 2011;3(9):1-13. doi:10.1101/cshperspect.a004424

12. Annibal A, George Tharyan R, Fides Schonewolff M, et al. Regulation of the one carbon folate cycle as a shared metabolic signature of longevity. doi:10.1038/s41467-021-23856-9

13. Hansen M, Hsu A-L, Dillin A, Kenyon C. New Genes Tied to Endocrine, Metabolic, and Dietary Regulation of Lifespan from a Caenorhabditis elegans Genomic RNAi Screen. Kim S, ed. *PLoS Genet*. 2005;1(1):e17. doi:10.1371/journal.pgen.0010017

14. Cabreiro F, Au C, Leung KY, et al. Metformin retards aging in C. elegans by altering microbial folate and methionine metabolism. *Cell*. 2013. doi:10.1016/j.cell.2013.02.035

15. Castro-Portuguez R, Sutphin GL. Kynurenine pathway, NAD+ synthesis, and mitochondrial function: Targeting tryptophan metabolism to promote longevity and healthspan. *Exp Gerontol*. 2020;132:110841. doi:10.1016/j.exger.2020.110841

16. Hou NS, Gutschmidt A, Choi DY, et al. Activation of the endoplasmic reticulum unfolded protein response by lipid disequilibrium without disturbed proteostasis in vivo. *Proc Natl Acad Sci U S A*. 2014;111(22):E2271. doi:10.1073/pnas.1318262111